ISTANBUL TECHNICAL UNIVERSITY ★ EURASIA INSTITUTE OF EARTH SCIENCES

LATE HOLOCENE HIGH RESOLUTION MULTI-PROXY CLIMATE AND ENVIRONMENTAL RECORDS FROM LAKE VAN, EASTERN TURKEY

Ph. D. THESIS

Funda BARLAS ŞİMŞEK
(601062002)

Climate and Marine Sciences

Earth System Science

Thesis Advisor: Prof. Dr. M. Namık ÇAĞATAY

NOVEMBER 2015

İSTANBUL TEKNİK ÜNİVERSİTESİ ★ AVRASYA YER BİLİMLERİ ENSTİTÜSÜ

VAN GÖLÜ'NÜN GEÇ HOLOSEN'DEKİ YÜKSEK ÇÖZÜNÜRLÜKLÜ İKLİM VE ÇEVRESEL KAYITLARI

DOKTORA TEZİ

Funda BARLAS ŞİMŞEK
(601062002)

İklim ve Deniz Bilimleri Anabilim Dalı

Yer Sistem Bilimi Programı

Tez Danışmanı: Prof. Dr. M. Namık ÇAĞATAY

KASIM 2015

Funda BARLAS ŞİMŞEK, a Ph.D. student of ITU Eurasia Institute Of Earth Sciences student ID 601062002, successfully defended the dissertation entitled "LATE HOLOCENE HIGH RESOLUTION MULTI-PROXY CLIMATE AND ENVIRONMENTAL RECORDS FROM LAKE VAN, EASTERN TURKEY", which she prepared after fulfilling the requirements specified in the associated legislations, before the jury whose signatures are below.

Thesis Advisor : **Prof. Dr. M. Namık ÇAĞATAY** ....
İstanbul Technical University

Jury Members : **Prof. Dr. Namık YALÇIN** ....
İstanbul University

Prof. Dr. Nüzhet DALFES ....
İstanbul Technical University

Assoc. Prof. Dr. K. Kadir KELEŞ ....
İstanbul Technical University

Assoc. Prof. Dr. Erol Sarı ....
İstanbul University

Date of Submission : 20 October 2015
Date of Defense   : 26 November 2015

To my grandmother and grandfather,

"The important thing is not to stop questioning. Curiosity has its own reason for existing. One cannot help but be in awe when he contemplates the mysteries of eternity, of life, of the marvelous structure of reality. It is enough if one tries merely to comprehend a little of this mystery every day. Never lose a holy curiosity."

Albert Einstein (1879-1955), Physicist

FOREWORD

"A person who never made a mistake never tried anything new" (Albert Einstein). As a physicist working on climate was new and interesting for me.

x

TABLE OF CONTENTS

ABBREVIATIONS

AD	**:** Anno Domini
AMS	**:** Accelator Mass Spectrometry
AR	**:** Ahlat Ridge
ARC	**:** Acoustic Rolling Contact
BP	**:** Before Present
CIC	**:** Constant Initial Concentration
CRS	**:** Constant Rate of Supply
DACP	**:** Dark Age Cold Period
EDS	**:** Energey Dispersive Spectroscopy
E	**:** Evaporation
GI	**:** Greenland Interstadial
GD	**:** Gamma Density
HPGe	**:** High Purity Germanium
IAEA	**:** International Atomic Energy Agency
ICDP	**:** International Continental Scientific Drilling Program
LMM	**:** Late Maunder Minimum
LIA	**:** Little Ice Age
LSC	**:** Liquid Scintillation Counter
MAR	**:** Mass Accumulation Rate
MWP	**:** Medieval Warm Period
MS	**:** Magnetic Susceptibility
MSCL	**:** Multi Sensor Core Logger
NB	**:** Northern Basin
NCR	**:** Non-Contact (Electric) Resistivity
NH	**:** Northern Hemisphere
NIST	**:** National Institute of Standards and Technology
NAO	**:** North Atlantic Oscillation
OM	**:** Organic Matter
P	**:** Precipitation
RWP	**:** Roman Warm Period
S/N	**:** Signal to Noise ratio
SR	**:** Sedimentation Rate
TC	**:** Total Carbon
TDIC	**:** Total Dissolved Inorganic Carbon
TIC	**:** Total Inorganic Carbon
TOC	**:** Total Organic Carbon
TON	**:** Total Organic Nitrogen
XRF	**:** X-Ray Fluorescence
VPDB	**:** Vienna Pee Dee Belemnite standard
YD	**:** Younger Dryas

LIST OF TABLES

LIST OF FIGURES

LATE HOLOCENE HIGH RESOLUTION MULTI-PROXY CLIMATE AND ENVIRONMENTAL RECORDS FROM LAKE VAN, EASTERN TURKEY

SUMMARY

Lake Van is the largest alkaline lake in the world characterized by varved sediments. It is located in eastern Anatolian plateau of Turkey. This study highlights the use of a multi-proxy approach toward understanding paleoenvironmental changes and sedimentation processes in Lake Van. We specifically focuse on climate records of the last 3500 years at centennial resolution. Compare the results with other studies in Anatolia, Near East and Europe.

This study uses multi-proxy analyses of four interface sediment cores from different parts of the Lake. The multi-proxy data include ostracod counts, μ-XRF elemental, total organic (TOC) and inorganic carbon, C-N elemental and stable isotopes. For the age model of the core, we use radionuclide (^{210}Pb and ^{137}Cs) analysis and varve counting. Accelerator Mass Spectrometry (AMS) ^{14}C dates from total organic carbon (TOC) indicates large differences with the corresponding varve ages, suggesting significant reservoir ages, which range from 1.2 to 3.8 ka BP.

Double energetic window method by LSC which relies on the direct determination of ^{210}Pb without waiting for the in growth of ^{210}Po from ^{210}Pb was used to construct the past environmental conditions of Lake Van in eastern Turkey. The results show that the sedimentation rate varies significantly among the four study sites, ranging between 0.3 and 0.7 mm.year^{-1}.Varve counting of annually laminated sediments of Lake Van using digital X-ray radiographic images provided another means of dating the cores. Our study shows that varve counting method detects and counts fine-scale laminae, and produces robust varve ages that are comparable with independently determined ^{210}Pb and ^{137}Cs ages for the upper part of the core.

All multi-proxy parameters including ostracods population, C/N ratio, stable isotope values, organic matter, Ti/Ca ratio showed 16 consistent periods varying between 100 and 350 years corresponding to alternation of cold/dry and warm/wet periods during the last 3500 years. The Lake Van climate records are conformable with the Lake Nar and the Sofular speleothem records as well as the European historical climate periods including Roman Warm Period (RWP), Dark Age Cold Period (DACP), Medieval Warm Period (MWP) and Little Ice Age (LIA), indicating teleconnections with the North Atlantic system.

μ-XRF heavy metal profiles along the Lake Van cores show antropogenic inputs since 1960s. A significant increase occurred in metals such as Zn, Pb, Ni, and Co in the last 30-60 years in Lake Van cores. Especially increases in Zn and Pb in the upper parts of the cores indicate that important agricultural and industrial pollution began in the 1960s.

VAN GÖLÜ'NÜN GEÇ HOLOSEN'DEKİ YÜKSEK ÇÖZÜNÜRLÜKLÜ İKLİM VE ÇEVRESEL KAYITLARI

ÖZET

Doğu Anadolu Yüksek Platosu'nda yer alan Van Gölü, 607 km^3 hacmi ve 3,570 km^2 lik alanı ile dünyanın en büyük 4. kapalı gölü ve en büyük soda gölüdür. Derinliği 460 m ve su seviyesi deniz seviyesinden 1648 m yükseklikte olan gölün suları, yüksek pH değeri (9.8) ve %24'lük tuzluluk oranına sahiptir. Gölün yıllık lamina (varv) yapılı çökel istifi, bölgede yüksek çözünürlüklü iklim ve çevresel değişimlerin arşivini oluşturmaktadır.

Bu tez kapsamında, Van Gölü'nde çökel karotlarında özellikle son 3500 yıldaki iklimsel ve çevresel değişim kayıtları incelenmiştir. Çalışmadan elde edilen iklim kayıtları; Anadolu, Yakın Doğu ve Avrupa'dan elde edilmiş kayıtlarla karşılaştırılarak tartışılmıştır.

Tez çalışması, Van Gölü'nün farklı bölgelerinden alınan ve uzunlukları 0.75 ile 1.30 m arasında değişen toplam dört karotta değişik kimyasal ve fiziksel analizler ile yapılmıştır. Çok Sensörlü karot tarayıcısı (Multi Sensor Core Logger, MSCL) ile 5 mm çözünürlükte manyetik duyarlılık, yoğunluk ve porozite ölçümleri yapılmış, μ-XRF karot tarayıcısı ile 0.5 mm çözünürlükle 15 element taranmıştır. Sediment örnekleri 0.5-1 cm aralıklarla örneklenerek toplam inorganik (TIC) ve toplam organik karbon (TOC) analizleri yapılmıştır. 0.5-1 cm aralıkla sediment örnekleri 63 μm elek kullanılarak yıkanıp elenmiş elek-üstü malzemede binoküler mikroskop altında ostrakod tanımları yapılmıştır. En uzun çökel karotu boyunca sürekliliği olan ostrakod çeşidi ve sayıları belirlenerek kavkıları toplanmış ve kavkı ve çökel örneklerinin toplam (bulk) karbonat fraksiyonunda duraylı oksijen ve karbon analizleri yapılmıştır. Ayrıca karotun çökel örneklerinin organik madde fraksiyonunda elementel C ve N analizleri yapılmıştır.

Van Gölü sediment karotlarının kronostratigrafisi için değişik yöntemler kullanılmıştır. Kronostratigrafinin ana yöntemleri ^{210}Pb radyoizotopik tarihlendirme ve varve sayımı olmakla birlikte; bu iki yönteme ek olarak ^{137}Cs tarihlendirme ve tefrakronoloji yöntemleri de kullanılmıştır. Ayrıca, yüksek TOC değerleri içeren seviyelerde organik karbondan elde edilen AMS radyokarbon yaşları, varve yaşları ile karşılaştırıldığında gölün 1.2 ile 3.8 bin yıl arasında değişen ^{14}C rezervuar yaşına sahip olduğu saptanmıştır.

^{210}Pb analizleri Sıvı Sintilasyon Sayım Sistemi kullanılarak Çift Enerji Pencere Yöntemi (Double Energetic Window Method) ile gerçekleştirilmiştir. Bu yöntem ^{210}Pb izotopunun 17 keV'lik β enerjisini kullanmaktadır. Yöntemin en büyük avantajı örneklerin alınır alınmaz analiz edilebilmesidir. ^{210}Pb tarihlendirme, ^{210}Pb'un kız radyoizotopu olan ^{210}Po'un 5.30 MeV'deki alfa enerjisinden yararlanılarak da yapılabilmektedir. Ancak bu çalışmada kullanılan yöntemden farklı olarak, çevreden gelen ve sediment örneklerinin içinde olması beklenen ^{210}Po radyoizotoplarının ^{210}Pb radyoizotopları ile dengeye gelmesi için en az 5 yarı ömür (yaklaşık 2 yıl) beklemek gerekmektedir. CRS (Constant Rate of Supply) modeli ile

yapılan tarihlendirme sonuçlarına göre Van Gölü'nün sedimanlarının sedimantasyon hızı gölün değişik karotlarında 0.3 ile 0.7 mm.yıl^{-1} arasında, kütle birikim hızları ise 0.3-0.60 kg.m^{-2}.yıl^{-1} değerleri arasında değişmektedir. Sedimantasyon ve kütle birikim hızlarındaki bu değişkenlik, gölün değişik noktalarındaki farklı sediment akılarına bağlıdır. Sediment akılarındaki bu farklılıklar, gölün topografyasındaki farklılıklara, göl yatağı litolojisine, farklı bölgelerdeki drenaj özelliklerine ve ayrıca bölgeye göre değişim gösteren antropojenik aktivitelere bağlı olarak açıklanabilmektedir.

Bir fizyon ürünü olan ^{137}Cs izotopunun çökel karotları boyunca aktivite dağılımları HpGe Gama Sayım Sistemi ile 671 keV'deki gama enerjisi kullanılarak incelenmiş ve 1950-1963 yıllarındaki nükleer silah denemeleri sonucunda ve 1986 yılında meydana gelen Çernobil Nükleer santral kazası sonucu çevreye yayılan ^{137}Cs radyoizotopunun varlığı tespit edilmiştir.

Van Gölü sediment karotlarının yaşlandırılması için kullanılan ana yöntemlerden biri olan varv sayımı, bir algoritma ile yıllık laminalı (varv) yapıdaki karotların sayısal X-ışını radyografi görüntülerinden yapılır. Bu çalışmada kullanılan varv sayım yöntemi ile elde edilen yaş verileri, karotların 7.5 cm lik üst kısımları için (100-150 yıl) radyoizotopik (^{210}Pb ve ^{137}Cs) tarihlendirme yöntemlerinden elde edilen yaş verileri ile büyük bir uyum içerisindedir. Bu uyum göz önüne alınarak karotların yaş-derinlik modelleri varv sayım yöntemi kullanılarak yapılmış ve böylece radyoizotopik yöntem ile 100-150 yıla kadar yaşlandırılabilen çökel karot istifleri uzunluklarına bağlı olarak 3500 yıla kadar yaşlandırılmıştır.

Geç Holosen süresince, Van Gölü çökel istifinde karbonatlardaki düşük oksijen-izotop değerleri, kış yağışının (kar) etkisinin bir sonucu olarak değerlendirilmektedir. Dağlara doğru yönelen nemi engelleyen yerel yaz doğulu rüzgarlarının erken oluşması ile meydana gelen "klasik" Akdeniz ikliminin, bölgede artan kış yağışlarının sebebi olduğu düşünülmektedir.

Ostrakod sayıları, C/N oranı, duraylı izotop değerleri, TOC-TIC değerleri ve Ti/Ca oranı gibi tüm çoklu belirteç (multi-proxy) verileri değerlendirilerek son 3500 yıldaki soğuk/kurak ve ılık/yağışlı dönemlerin değişimleri incelenmiştir. Tüm bu parametrelerin birlikte değerlendirilmesi sonucu söz konusu zaman aralığında 16 adet ardışık soğuk/kurak ve ılık/yağışlı dönem tespit edilmiş olup, bu dönemlerin uzunluğu 100 yıl ile 350 yıl arasında değişim göstermektedir. Günümüzden önce 3500-3300, 2900-2600, 2400-1800, 1600-1450, 1350-1050, 770-600, 500-350 ve 200-0 yılları arasında soğuk/kurak dönemlerin hakim olduğu öte yandan günümüzden önce 3300-2900, 2600-2400, 2300-2100, 1800-1600, 1400-1350, 1050-770, 600-500 ve 350-200 yılları arasında sıcak/yağışlı dönemlerin hüküm sürdüğü sonucuna varılmıştır.

Bu çalışmada elde edilen veriler ışığında Van Gölü iklim kayıtlarının özellikle Kuzey Atlantik iklim sistemi ile uyumluluğunu doğrulayan Roma Ilık Dönemi (RWP), Karanlık Çağ Soğuk Dönemi (DACP), Ortaçağ Ilık Dönemi (MWP) ve Küçük Buz Çağı dönemlerini içeren son 1800 yıllık verilerinin Nar Gölü (Orta Anadolu) çökel ve Sofular Mağarası (Kuzeybatı Anadolu) stalagmit kayıtları ile uyumlu olduğu görülmüştür. Bölgesel ölçekte, Van Gölü kayıtları İran'da bulunan Zeribar ve Mirabad göllerine ait düşük çözünürlüklü sediment ve İsrail'de bulunan Soreq Mağarası kayıtları ile de uyumludur.

Van Gölü çökel karotları boyunca elde edilen μ-XRF ağır metal profilleri 1960'lardan bu yana göle olan antropojenik girdileri göstermektedir. Van Gölü bölgesinde son 30-60 yılda Zn, Pb, Ni ve Co metallerinin önemli ölçüde arttığı saptanmıştır. Özellikle karotların üst kısımlarında çok belirgin olarak gözüken Zn ve

Pb zenginleşmesi 1960 yıllarında başlayan önemli tarımsal ve endüstriyel kirlenmenin bir göstergesidir. µ-XRF sayım sonuçları göz önünde bulundurularak dört karottaki ağır metal konsantrasyonları karşılaştırıldığında Gölde Van Şehri'nin batısından alınan karotta en yüksek ağır metal değerleri karotun üst kısımlarında görülmüştür. Bu sonuç ağır metallerin ana kaynağının antropojenik kirlenme olduğunu güçlü bir şekilde göstermektedir.

Son 60 yılı temsil eden, karotların üst kısımlarındaki metal birikimi Van'ın şehirleşme ve endüstrileşmesinin 1960'dan sonra daha hızlandığını doğrulamaktadır. Bu hızlanma Van Gölü kıyılarının her iki yakasında kara yolu ulaşımına açılmasının bir sonucudur. 1960'lardan itibaren sulama, hasat gibi tarımsal işlemlerde kullanılan tarım makineleri ve trafikteki araç sayısı artmıştır. Bu da araçlarda kullanılan yakıtın içeriğinde bulunan Pb salınımını artırmıştır. Bu salınım artışının sonuçları çalışılan karotlarda belirgin Pb anomalisinin gözlenmesine neden olmuştur. 2000'li yıllarda kurşunsuz yakıtın kullanılmaya başlamasıyla bu anomali değişerek doğal seviyelere gelmiştir. Öte yandan tarımsal faaliyetlerde kullanılan gübrenin içeriğinde bulunan Zn, direkt olarak ya da nehirler aracılığıyla metal kirliliğine katkıda bulunmuştur. Ayrıca genel olarak yollarda artan trafik metal kirliliğinin önemli sebeplerindendir.

1. INTRODUCTION

1.1 The Holocene Climate

Climate is one of the important elements of the geographical environment, and hence has an important control on human life. The changes in environmental conditions resulting from the naturally and anthropogenically influenced climate changes and evolution of climate in general are very important from both scientific, social and economic points of view.

Although the climate of the Holocene (11,750 cal yr B.P. to the present) has sustained the growth and development of modern society, there is surprisingly limited systematic knowledge from different parts of the Earth about climate variability during this period. Many paleoclimate studies over the last decade have highlighted the extreme or rapid climate fluctuations of the last glacial interval. If we are to understand the background of natural variability underlying anthropogenic climate change, however, it is important to concentrate on climate of the more recent past.

It is remarkable that little is known about the causes of climatic changes during the Holocene, which is most familiar of all geologic periods. Solar variability, volcanicity, tropospheric aerosols and carbon dioxide, among other factors, have been invoked to produce climate change, but no clear lines of evidence have been developed. Little Ice Age (LIA), Medieval Warm Period (MWP), and Bond cycles are significant changes in the historical period determined by the climate of the world. In recent years the existence of the human impact on greenhouse gas emissions and global warming has been the subject of discussion.

Although there is no consensus regarding the time when the Little Ice Age observed, the most common opinion is that it occurred in between 700-100 years before present (BP) (Muller and McDonald, 2000; Mann, 2002). While there is evidence that many other regions outside Europe exhibited periods of cooler conditions, expanded glaciations, and significantly altered climate conditions, the timing and nature of

these variations are highly variable from region to region, and the notion of the Little Ice Age as a globally synchronous cold period has all but been dismissed (Bradley and Jones, 1993; Mann et al., 1999). If defined as a large-scale event, the Little Ice Age must instead be considered a time of modest cooling of the Northern Hemisphere, with average temperatures dropping by about 0.6 °C during the 15th–19th centuries (Bradley and Jones, 1993; Jones et al., 1998; Mann et al.,1998, 1999). Significant records of the Late Maunder Minimum (LMM) (300-200 years BP) the coldest period of the LIA, were found in Black Sea sediments (Çağatay et al., 2005; Güngör and Çağatay, 2007). Just before the LIA, Medieval Warm Period was observed in between 1050-570 years BP. The temperature was 0.5-0.8 °C higher than the average temperature of 1950 in Europe during this period (Bradley et al., 2003). Welfare and production increased and the Dark Age Cold Period (DACP) ended in Europe. This positive period ended suddenly, with a climate process which was seen in storms and floods. While they were observed in and around the North Atlantic, global scale of these events is still debated (Raymaond et al., 2003; Bradley et al., 2003). Immediately after the Dark Age Cold Period (1500-1000 years BP), a temperate period was experienced in Europe.

Bond events are North Atlantic climate fluctuations occurring every ≈1,470 ± 500 years throughout the Holocene (Bond et al., 1997). Eight such events have been identified, primarily from fluctuations in ice-rafted debris. Bond events may be the interglacial relatives of the glacial Dansgaard–Oeschger events, with a magnitude of perhaps 15–20% of the glacial-interglacial temperature change. According to studies found in North Atlantic ice drift sediments, Bond events can be listed as follows (Bond et al., 1997):

~1.4 ka BP (1. Bond E.)- Migration Period

~2.8 ka BP (2. Bond E.)-Coldest Period of the Iron age

~4.2 ka BP (3. Bond E.)- 4.2 ky event

~5.9 ka BP (4. Bond E.)- 5.9 ky event

~8.1 ka BP (5. Bond E.)- 8.2 ky event

~9.4 ka BP (6.Bond E.)- Erdalen event of glacier activity in Norway, as well as with a cold event in China

~10.3 ka BP (7. Bond E.)

~11.1 ka BP (8. Bond E.)-transition from the Younger Dryas to the boreal.

1.2 The Holocene Climate of Turkey

The climate regime of Turkey is controlled by very different factors during summer and winter times. In summer, it is mainly influenced by the extentions of Indian monsoons into the Middle East (Raicich et al., 2003; Ziv et al., 2004). When these monsoons are more powerful, the climate becomes drier. However, during winter, Turkey's climate is mainly influenced by two teleconnections (Krichak et al., 2004; Türkeş and Erlat, 2009). First, the influence of the North Atlantic climate is felt through the westerlies blowing across the Mediterranean whose strength is altered with the North Atlantic Oscillation (NAO).   NAO's negative mode makes the westerlies stronger and this leads to a warmer and wetter environment in the Eastern Mediterranean region (Hurrell, 1995; Hurrell and Van Loon, 1997). Secondly, the East Atlantic/Western Russia pattern shows its effects with the spread of cold, continental air masses from the North (Barnston and Livezey, 1987; Kutiel and Benaroch, 2002). Its positive mode causes the climate to be cooler and drier.

Although, Turkey's climate is largely controlled by the dynamics explained above, they are not enough to explain the entire story. Mainly, three more major factors must be taken into consideration. First, Anatolia is surrounded by sea on three sides which causes warm and humid environment along its coastal areas. Second, the north and south coastal lines are cut from the inner parts of Anotolia by two mountain chains that block warm marine air reaching the central part. Third, the dry and cool continental air masses of the North are moistened while passing over the Black Sea and ascending over the North Anatolian mountains (Pontides), which eventually causes increased precipitation in the Black Sea region

Records of Holocene climate in and around Turkey have been recently increasing. The records have been mostly obtained from marine and lake deposits, tree rings and stalagmites. Paleoclimate studies were made in Central Anatolia (Lake Nar, Lake Tecer, Lake Akgöl), Eastern Anatolia (Lake Van and Lake Hazar), Blacksea region (Sofular and Ovacık caves) and Western Anatolia (Lake Gölhisar) (Fleitmann et al., 2009; Kuzucuoğlu et al., 2011; Roberts et al., 2008, 2011; Jones et al., 2006; Dalfes et al., 2006; Wick et al., 2003) (Figure 1.1). Holocene climate studies has gained

momentum in the last two decades, with most these studies mostly focused on Central and Eastern Anatolia.

Fleitmann *et al.* (2009) obtained high resolution records of the last 50.000 years BP by using the Speleothems stable isotope records obtained from Sofular and Ovacık caves in the western Black Sea Region (Figure 1.1). The authors compared their records with cave records from Hulu (China), Villars (France), Botuvera (Brasil), pollen records from Lago Grande di Monticchio (Italy), and ice core records from NGRIP (Greenland). From these comparisons, they were able to identify the Heinrich 1-5 and Younger Dryas events and Greenland Interstadial (GI) during the last glacial. Their stable isotope records showed that the GIs were characterized by wet and warm climate in northwest Anatolia.

Figure 1.1 : Map showing the location of sites from which Holocene climate records are obtained

Göktürk *et al.* (2011), describes the climate changes during the Holocene by using $\delta^{13}C$ isotopes from Sofular Cave speleotems. These changes were explained by comparing with different proxies (pollen, isotope, salinity) obtained from Jeita (Lebanon), Soreq (Israel), Qunf (Oman) caves and sediments from Lake Van, Lake Acıgöl, Aegean Sea, and Red Sea. Between ~9.6 and 5.4 ka BP, the Sofular record indicates a remarkable increase in rainfall amount and intensity, in the line with other paleoclimate studies in the Eastern Mediterranian.

Roberts et al., (2011) conclude in their study that during the period between 6 and 3 ka BP, literate, urban-based cultures and management emerged, initially in the valleys of the Nile, Euphrates and Tigris rivers and in the Levant and later in Anatolia and Greece. These changes in human culture were of the highest importance and they overlapped with a very significant oscillating trend from wetter to drier

climatic conditions. In the mid Holocene, climate and human agency combined to transform the landscape ecologies of the Eastern Mediterranean. The different components that make up the region's cultural environmental-system (vegetation, climate, etc.) can be reconstructed from a range of proxies (pollen, stable isotope, archeology, etc.).

Eastwood et al. (2007) obtained that stable isotope analysis of lacustrine authigenic calcites from Lake Gölhisar provide a valuable indicator of past climatic change through the Holocene for southwest Turkey. $\delta^{18}O$ records from Gölhisar as with lakes in similar environments from the eastern Mediterranean region, can consequently be interpreted in terms of past changes in the precipitation/evaporation balance.

Accordingly, between 6800 and 5200 years BP and in the Byzantine period (1650-500 BP- AD 300-1400) the rainy conditions than today has become more arid in the last 1300 years.

1.3 Previous Paleoclimate Records from Lake Van

The first international expedition to Lake Van in 1974 included sediment coring, hydrochemistry sampling and seismic surveys (Degens and Kurtman, 1978; Degens et al., 1984). During this expedition the bathymetric map of the lake was also constructed for the first time (Wong and Degens, 1978). As a result of these projects also it was emerged that Lake Van sediments consist of annually laminated (Kempe and Degens, 1978) which can be used for varve counting and reconstruction of climate changes. After that, two more expeditions occured in 1989 and 1990 comprised high resolution geochemical, geological, hydrochemical and biological researches. Especially, hydrochemistry of Lake Van was investigated in detail and microbiolites were mapped and sampled during this projects (Kempe et al.,1991; Kazmierczak and Kempe, 2003). The first varve record from the cores covered approximately the last 14 kyr (Landmann et al., 1996a; Wick et al., 2003) (Figure 1.2). However, the resolution of especially the last 3000 years of these records was inadequate. First pollen analysis were made to reconstruct climate history and vegetation (Van Zeist and Woldering, 1978). Also results of $\delta^{18}O$, $\delta^{13}C$, pollen and continous records of varve thickness obtained from these projects were used to

distinguish different climate phases during the Younger Dryas and the 3rd millennium (Lemcke, 1996; Landmann et al., 1996a,b).

Pollen records and stable isotopes proves the existence of rapid climate transitions (Wick et al., 2003).
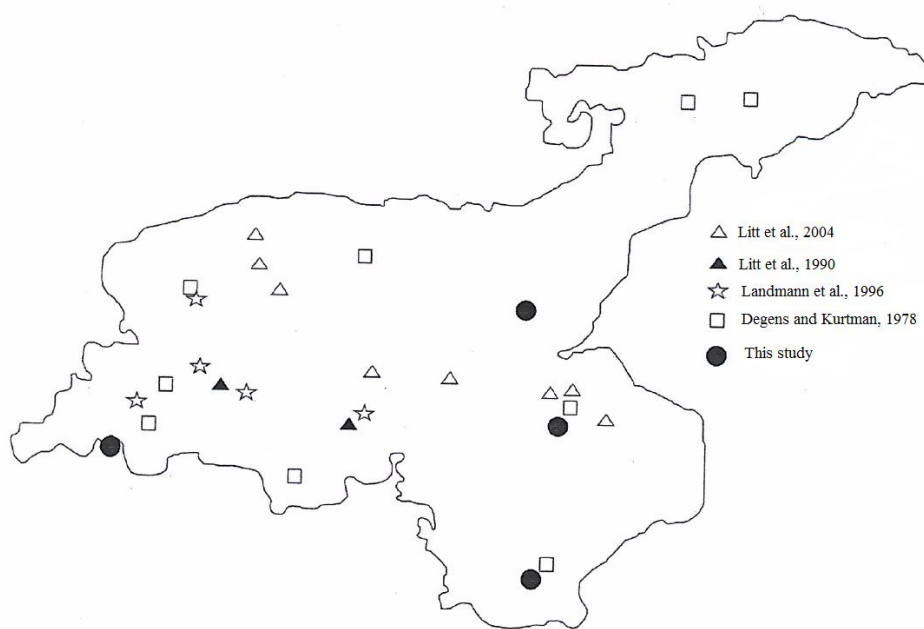
Figure 1.2 : Core locations of previous studies done in Lake Van.

In preparations for the International Continental Scientific Drilling Program (ICDP) "PALEOVAN" project, Litt et al. (2009) collected 50 seismic profiles to classify continuous undisturbed sedimentary sequences for potential ICDP locations and according to the seismic results, they cored 10 different locations to water depths of up to 420 m (Figure 1.3). This multi-disciplinary study involved measurements of magnetic susceptibility, physical properties, stable isotopes, XRF scans, pollen and spores. Also this study investigated the potential of "PALEOVAN" to create new results on the dynamics of lake level fluctuations, noble gas concentration in pore water of the lake sediment, history of volcanism and volcanic activities based on tephrostratigraphy, and paleoseismic and earthquake activities.
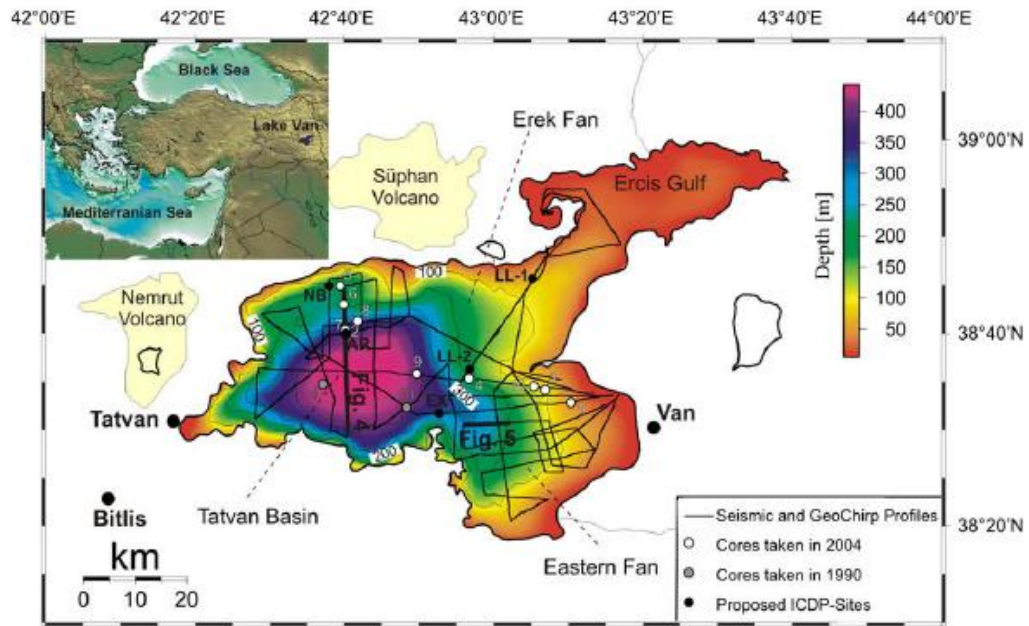
Figure 1.3 : Seismic lines (50 profiles, 850 km length) and 10 coring sites (site survey 2004, white circles). In addition, the map showing two locations of cores taken in 2004 (grey circles) and the proposed primary ICDP drill sites (black circles). NB:Northern Basin Site, AR:Ahlat Ridge Site; LL-1, LL-2: Lake Level Sites, EX:Extrusion Site. Available seismic profiles are shown as solid black lines.

Promoted by the potential of the sedimentary sequence for reconstructing the paleoecological and paleoclimate development of the Near East, a deep drilling operation was carried out in 2010 supported by the International Continental Scientific Drilling Program (ICDP).

Lake Van sediment cores from the Ahlat Ridge (AR) and Northern Basin (NB) drill sites of the ICDP Project are full of significant information about past environmental processes (Litt and Anselmetti, 2014). The drilled sedimentary sections were dated using different techniques such as climatostratigraphic alignment, varve chronology, teprostratigraphy, argon-argon single-crystal dating, radiocarbon dating, magnetostratigraphy, and cosmogenic nuclides (Stockhecke et al., 2014; Çağatay et al., 2014). These different dating techniques allowed a reliable and precise chronology of the 600 ka year-old Lake Van records, which covers six Glacial/Interglacial cycles, is obtained.

In the framework of the PALEOVAN project, a high-resolution paleomagnetic and rock magnetic study was carried out on a 149 m sedimentary sequence recovered from Ahlat Ridge in the deepest part of the Lake Van (Vigliotti et al., 2014). This study concludes that higher magnetic content with larger magnetic grain size

characterize glacial intervals when colder, windier and more arid conditions are associated with the Anatolian Plateau (Landmann et al., 1996a; Lemcke, 1996; Litt et al., 2014). The concentration of magnetic particles mimics detrital proxies (Ti, Al, K concentrations), determined from X-Ray Fluorescence (XRF) core scanning (Kwiecien et al., 2014), implying that magnetic concentration is controlled by detrital input rather than diagenetic alteration. The fidelity of the paleomagnetic record of Lake Van sediments is affected by low concentrations of magnetic minerals in some intervals and weak natural remanent magnetization intensities, as well as by the presence of tephra layers occurring throughout the sequence.

Lake Van's 600 ka pollen record documents the glacial and interglacial stages as well as the most evident interstadials with obvious increase of thermophilous oak and further arboreal polen types (Litt et al., 2014). Based on a comparison of multi-proxy sediment core records from Lake Van, Kwiecien et al. (2014) propose a depositional model explaining different patterns observed in all the proxies during the glacial terminations. It was hypothesized that the relative contribution of rain, snow and melt water recharging the basin plays an important role for hydrological conditions, producing and sustaining bottom-water anoxia and influencing isotopic composition of carbonates.

More than 1500 km of multi-channel seismic reflection profiles combined with the drilling data to provide significant insights into the sedimentary history of Lake Van over the past ~600 ka (Çukur et al., 2014). In addition, the higher sedimentation rate in the Northern basin is explained as due to the abundance of volcaniclastic mass-transport sediments accumulated in this basin.

Also the long cores of the ICDP project was analyzed for noble-gas in the pore water to determine the local terrestrial He-gradient as a function of depth within a sediment column of more than 200 m which yield first insight into the physical transport mechanism with regards to terrestrial fluid emission in the deep sediments of Lake Van (Tomonaga et al., 2014).

1.4 Aim and Scope

Although studies on Holocene climate in Turkey have increased considerably in recent years, there is still a need for high resolution and multi-proxy studies in different locations. This is especially true considering the geographical location and

the morphological characteristics of the country which cause significant climate variability. Moreover, part of the studies carried out so far lack the necessary resolution to decipher millenial and centennial scale climate events. This is also the case for Lake Van where although many studies have been carried out so far as summarized in section 1.3, much of these studies cover a much longer period than the Holocene and lack the resolution for detailed analysis of the Holocene climate variability.

As a paleoenvironmental archive, annually laminated sediments comprise high resolution proxies that can be used to study of climate changes. Due to their high resolution and containing long and continous proxy records of physical, chemical and biological parameters, annually laminated sediments provide one of the most detailed terrestrial archives for the study of paleoloimnology and rapid environmental changes including human impact. (Brauer et al., 2008). Annually laminated sediments can be used as not only high resolution proxy data but also provides an accurate dating method for a continuous and long timescale which is independent of radiocarbon reservoir problem. In other words precisely dated varve records provide detailed paleoclimatic records, which can be correlated with other climatic proxies (Brauer et al., 2008). In particular, closed-basin (terminal) lakes with no outlet and groundwater interaction are well-suited for such studies. Additionally, such lakes are very sensitive not only to climate changes and antropogenic impacts but also to rapid environmental changes which effects sedimentation processes.

The combination of climatic sensitivity and the presence of its annually laminated sediments makes Lake Van an appropriate candidate to study climate and environmental changes. Within the climatically sensitive region of eastern Anatolia, the Lake Van record represents a remarkable continental climate archive between the Black Sea, the Arabian Sea and the Red Sea (e.g. Roberts and Wright, 1993; Cullen and de Menocal, 2000; Lamy et al., 2006; Litt et al., 2009, 2011). Since Lake Van is hydrologically closed, the lake level and water chemistry are considerably sensitive to climatic changes. Namely, sedimentological evidence shows that lake level changes up to a few hundred meters during the last 20 ka which points out that the lake reacts considerably to alteration of the hydrological regime in reaction to climatic changes. (Landmann et al., 1996a; Çağatay et al., 2014; Çukur et al., 2014). Also the sediments of Lake Van are annually laminated for at least the last 14 kyr

(Kempe and Degens, 1978; Lemcke, 1996; Landmann et al., 1996b; Wick et al., 2003), which makes it ideal for high-resolution paleoclimate studies.

The aim of this PhD thesis is to construct highly resolved and well dated records of past climate using sediments collected from different parts of Lake Van in Eastern Turkey. Interpretation of these sedimentary records in terms of local, regional and larger scale climate dynamics is also an important objective. The late Holocene (last ~ 3000-3500 years in geological history) is the target time frame. Another aim is to investigate the environmental changes, including anthropogenic impacts, within this time frame.

For this purpose four interface cores with lengths up to 1.3 m were recovered from Lake Van in the year 2008 (Figure 2.1). These cores were analyzed for physical, geochemical, micropaleontological and stable- isotopic compositons.

The physical properties (gamma density and magnetic susceptibility) were analyzed using GEOTEK Multi Sensor Core Logger (MSCL). The μ-XRF elemental geochemical analysis were carried out using ITRAX XRF core scanner. The stable oxygen and carbon isotopes of bulk and and ostracod samples in one core were made using a Finnigan-MAT 252 isotope ratio mass spectrometer. Also the stable carbon and nitrogen isotope analysis of organic matter were performed by a continuous-flow gas-ratio mass spectrometer (Finnigan Delta PlusXL) coupled to an elemental analyzer (Costech). The same core that was analyzed for stable isotope ratios was also analyzed for ostracods using a binocular microscope. The chronology of the cores were obtained using radioisotopic methods and varve-counting. ^{210}Pb and ^{137}Cs analyses were performed by using Ultra Low Level Liquid Scintillation Counter (LSC), and HPGe coaxial well type detector respectively. Varve-counting method used in this study involves image analysis of digital X-ray radiographic images (Damcı and Çağatay, 2015). Attempts to date the bulk organic carbon in cores by Accelerator Mass Spectrometry (AMS) radiocarbon method was also used.

2. MATERIALS AND METHODS

2.1 Sediment Cores and Sampling Methods

Four cores with undisturbed tops were collected in summer of 2012 from four diferent sites in Lake Van (Figure 2.1; Table 2.1). Core V08G04 is located from offshore Gevaş, V08G08 from offshore Van, V08G11 from the entrance of Erciş Gulf and V08G16 from a small sublacustrine crater south west of the Tatvan Basin.

The cores were recovered using a water-sediment interface corer on a 4 m x 4 m portable platform fitted with 2.7 m heigh tripod (Figures 2.2 and 2.3). The cores were collected in 11 cm diameter PVC liners.fitted to the interface corer with 30 kg weight. The corer system generates a vacuum so that can it hold maximal 1-1.5 m long sediment core.
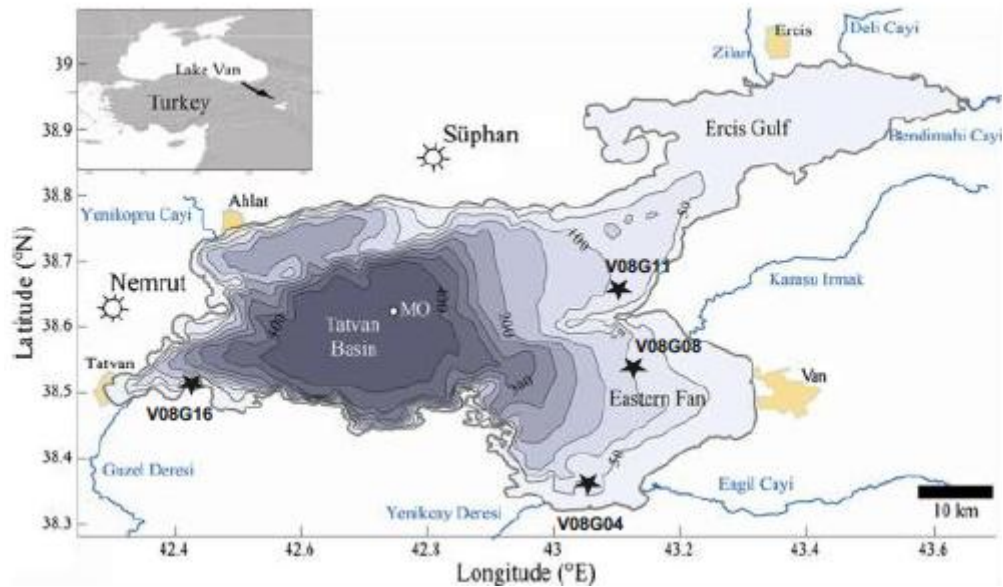
Figure 2.1 : Bathymetric map of Lake Van showing the location of coring sites.

Table 2.1 : Water depth, geographic coordinantes and length of the studied cores.

Core Name	Depth(m)	Latitude (N)	Longitude (E)	Core Length (m)
V08G04	70	38°20'56.8"	43°02'57.5"	1.30
V08G08	70	38°31'46.8"	43°09'04.7"	0.75
V08G11	86	38°40'15.3"	43°07'16.9"	0.90
V08G16	65	38°30'55.2"	42°25'35.2"	0.77

Figure 2.2 : Core sampling on a portable platform of ITU EMCOL.
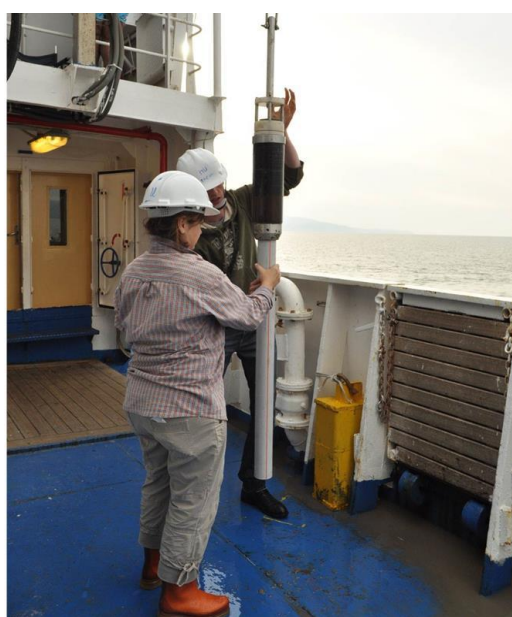
Figure 2.3 : Core sampling water /sediment interface corer of ITU EMCOL.

2.2 Analyses of Physical Properties Using Multi Sensor Core Logger (MSCL)

The physical properties of marine sediments have been widely used to understand the geological events as good indicators for the composition, microstructure, and environmental conditions during and after the depositional process (Kim et al., 2001). Measurements generally provide a rapid and nondestructive method for characterizing the nature and composition of long sedimentary sequences. Continuous physical properties records provide the basis for stratigraphy and core correlation, the first insight into core lithology, continuous data for time series analyses and a decision tool for determining the best subsampling strategy. Physical properties include gamma density, p-wave velocity, magnetic susceptibility and electrical resistivity. Most of these properties can be measured continuously and automatically, on whole or split cores placed horizontally or, when the sediment-water interface must remain undisturbed, vertically. A Geotek Multi sensor core logger (MSCL) located in İTÜ EMCOL's laboratories was used to analyze gamma density and magnetic susceptiblity of the split half cores at 5 mm resolution (Figure 2.4) (Weaver and Schultheis, 1990). The MSCL is equipped with gamma density, magnetic susceptibility, P-wave velocity and electric resistivity sensors. The analysis is done automatically using software based on "Windows" operating system prepared for this equipment. Core sections get pushed towards to the mounted sensors by an automatic pusher driven by a stepper motor with a user defined resolution. Each section gets measured as it passes the sensors. Stepper motor is controlled by computer which also controls the sensors, so that all the data including the length of each core section are correlated and saved automatically and also the sections can follow sequentially without breaking stream of data (webpage of Geotek MSCL, 2011).
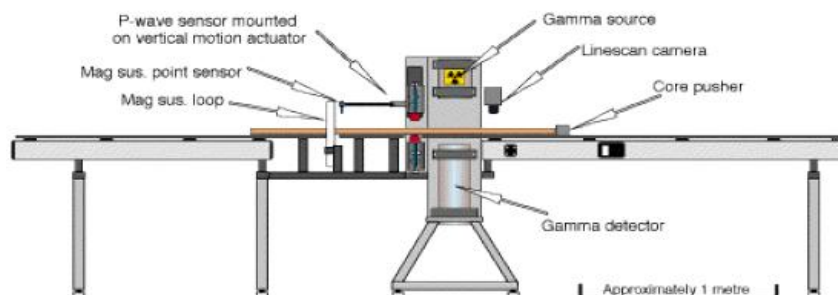
Figure 2.4 : Geotek MSCL used for the analysis of physical properties in Lake Van cores.

Different sensors of the MSCL are calibrated using standads provided by the manufacturer (Weaver and Schultheis, 1990). According to the calibration measurements, graphs and formulas are created by the software, and these data are used for the core analysis until the equipment is turned off. Created calibration file and formulas are used to evaluate the raw data. During the measurements for this study, half sediment core samples are used with a resolution of 5 mm. The main measurements of Geotek MSCL are briefly summarized below (webpage of Geotek MSCL, 2011):

1. Temperature: Both the temperature of the room and the cores can be measured with $0.01^{\circ}C$ sensitivity by a PRT probe. Temperature data is used for calibration files.

2. Gamma Density (GD): A gamma ray source and a detector are mounted on instrument in which core sections pass through the centre of them. A beam of collimated gamma rays are emitted from Cs-137 source and these emitted gamma rays − photons − pass through the core and meet the detector. By measuring the number of transmitted gamma photons that pass through the core unattenuated the density of the core material can be determined. Calibration for this measurement is done with a cylindrical piece of aluminium of varying thickness surrounded completely by water in a sealed liner which is the same type of liner of cores.

3. Core Sample Thickness: There are two sensors in motion with a mechanic spring mounted on P-wave sensor. As the sample passes these sensors move horizontally and measures the thickness with 0.01 mm sensitivity.

4. P-wave Velocity: Measurements of almost any composition cores are obtained by the Acoustic Rolling Contact (ARC) transducers. This system is operated for core section measurements and its centre frequency is 230 kHz. The ARC transducer uses an active transducer element with a material which combines high coupling with relatively low acoustic impedance. Precise repeatable timing measurements can be obtained with the high signal to noise (S/N) ratio resulting from the use of the lower frequency and good coupling with the wide bandwidth. Large contact area and lower frequency provide improved S/N enabling accurate velocity measurement even through coarse sand.

5. Non-Contact (Electric) Resistivity (NCR): A transmitter coil induces electrical currents in the core which are inversely proportional to the resistivity. This way a high frequency magnetic field in the core is induced as a part of NCR technique. Along the core of approximately 2 cm, resistivities between 0.1 and 10 ohm-meters can be measured at spatial resolutions. Calibration for this measurement is done by measuring the different percentage salt-water solutions in a sealed liner which is the same type of liner of cores.

6. Magnetic Susceptibility (MS): Magnetic susceptibility is the degree of magnetization of a material in response to an applied magnetic field. In the sensor there is an oscillator circuit which produces a low intensity, non-saturating, alternating magnetic field. Any material having a magnetic susceptibility causes a change in the oscillator frequency when it gets closer of the sensor. The electronics convert this pulsed frequency information into magnetic susceptibility values. For whole core sections Bartington loop sensor (MS2C) and for split cores Bartington point sensor (MS2E) can be used. Calibration for this measurement is done by measuring a single standard sample of a stable iron oxide which has been tested and analyzed by the manufacturer (The Bartington). The magnetic susceptibility sensor is electronically set to measure this standard sample.

2.3 Geochemical Methods

2.3.1 X-Ray fluorescence (XRF) analysis

X-Ray fluorescence analyses provide high-resolution records of trace elemental concentrations within the sediment. The variation in concentrations of certain metal species such as iron, manganese and calcium are a result of changes in hydrological processes, climate, and ecology (Boyle, 2001). X-Ray fluorescence core scanning is commonly used to reconstruct paleo-environments in both marine and lacustrine sediments in addition to identifying diagenetic processes (Ashley and Driese, 2000; Peterson et al., 2000; Haug et al., 2001; Bahr et al., 2005; Peterson and Haug, 2006; Löwemark et al., 2011). Accurate interpretations of trace elemental concentrations in lacustrine deposits require a sedimentary, hydrological, and geochemical context of the region.

µ-XRF elemental analysis of the cores were carried out using ITRAX Core Scanner at ITU-EMCOL laboratories. ITRAX Core Scanner allows automatic

characterization of up to 1.5 m long cores using the optical imaging in three colour bands, X-ray radiography and X-ray fluorescence – energey dispersive spectroscopic (XRF-EDS) analysis at 200 µm resolution along he entire core length (Croudace et al., 2006).

An intense X-ray beam, focused through a flat, capillary waveguide, is used to irradiate samples in order to enable both micro radiography and major and trace element analysis. This instrument is a flat beam X-ray scanner providing micro-radiographic images and elemental profiles of sediment half cores. The principle of operation is based on the simultaneous acquisition of micro density (radiography) and micro compositional variations (XRF) using two separate X-ray detection systems (Figure 2.5). X-ray transmission image information is recorded to display the samples chemical and density features as a radiographic image. Optical image displays the sample surface at high resolution. XRF, radiographic, and optical measurements are obtained without disturbing the sample and are performed without contact to the sample surface   (Croudace et al, 2006).

Depending on the requirements; user can define the duration of the analyses as short as 1 second per point or longer at each step. In case of Lake Van cores 10 second counting time per point was used for high accuracy and precision. The step by step analyses together build up element profiles that show the changes in composition throughout the sample. Analyses reaching ppm sensitivity in a second for wide range of elements from Al to U can be obtained with Itrax Core Scanner. Analyses reaching ppm sensitivity in a second for wide range of elements from Al to U can be obtained with Itrax Core Scanner.

Figure 2.5 : Front view of the Itrax core scanner with open hoods.

The instrument is controlled from a central computer and user can control the system by a graphical interface based on Windows XP Platform where standard operation procedures can be monitored. There is a second program called Q-Spec which interacts with the interface is used for both and on the fly analysis of XRF spectral data and refining the X-ray spectral analysis after scanning (Croudace et al, 2006).

Itrax achieves to keep the sample detector distance constant as reliable XRF analyses require, by using a laser system to measure the topography of the sample surface. The detector moves vertically adjusting itself according to the topographic scan data previously obtained. Count rates of up to 200,000 cps can be processed by digital signal processing which provides energy dispersive spectrometry. During this study, all the core sections are measured with Itrax Core Scanner with an optical image resolution of 0.1 mm pixel^{-1}, and X-ray analysis with a step size of 0.5mm, counting for 10 seconds at each step with the selected elements of Al, Si, P, S, Cl, Ar, K, Ca, Ti, V, Cr, Mn, Fe, Ni, Cu, Zn, As, Se, Br, Rb, Sr, Y, Zr, Nb, Pd, Sn, I, Ba, Ce, W, Pb, U, Th. Evaluation of the raw data is obtained by Q-Spec program using USGS standards for marine samples.

2.3.2 Total organic and inorganic carbon analysis

Secular and spatial changes in the total organic carbon (TOC) of lake sediments can indicate changes or differences in benthic secondary productivity, pelagic primary productivity, and organic matter flux into the lake from terrestrial systems (Palacios-Fest et al., 2005). Similarly, total inorganic carbon (TIC) studies can be used to study differences in biogenic carbonate (shell material) distribution.

Shimadzu TOC/TIC Analyzer is used to obtain total organic carbon and inorganic carbon in the sediment samples. Discrete sediment samples from cores at 0.5 cm, 1cm and 5 cm were dried using oven at about 60°C over night. Dried samples were grinded down to finest size using an agate mortar and pestle for the analysis. About 50 mg sample was weighed for the anlysis. First, Total Carbon (TC) analyzed by total combustion of the sample at 900°C and measurement of the evolved carbon dioxide, Then, Total Inorganic Carbon (TIC) was determined by treating the sample with 85% phosphoric acid at 200°C in the closed chamber of the instrument and measuring the amount of CO_2. The TOC percentage was calculated using Total carbon (TC) – total inorganic carbon (TIC) = TOC equation. For the calibration of

total carbon analysis, potassium hydrogen ftalat [C6H4(COOK)(COOH)] with 204.22 molecule weight and 47.05 weight percentage was used. Calibration curves for total carbon were constructed by burning 10, 20 and 40 mg of potassium hydrogen ftalat. For the total inorganic carbon analysis, sodium hydrogen carbonate (NaHCO$_3$) with 1200 molecule weight and 14.28 weight percentage was used. Calibration curves for total inorganic carbon were constructed by burning 20, 40 and 80 mg of carbonate. These analyses has better than 1% precision at 95% confidence level.

2.3.3 Carbon-Nitrogen elemental analysis

The type and amount of sedimentary organic matter (OM) can be used to reflect past fluctuations in lakes' productivity and terrestrial inputs linked to climate-induced environmental changes (Leng and Marshall, 2004; Meyers, 1997; Talbot and Johannessen, 1992). Indeed, land-derived OM has C/N ratio higher than 14–20, while phytoplankton and aquatic macrophytes exhibit C/N ratios between 4 and 10 (Meyers and Teranes, 2001).

For C/N analysis six samples from different levels of core V08G04 including those sampled for radiocarbon dating were selected. Dried samples (60 °C) were treated with 30% HCl to remove inorganic carbon from the sediment samples, and HCl was removed from the samples several washing the sample with distilled water and centrifugation. C/N analysis of the dried and powdered samples was performed by a Thermo Finnigan Flash EA 1112 Series CHNS-O elemental analyzer at the chemistry laboratory of the Institute of Marine Sciences and Management at İstanbul University. This elemental analyzer consists of four components: Chromotography column, adsorption filters, reactors, and auto sampler.

Carbon and nitrogen elemental analysis was carried out by burning 15-20 mg carbonate free sample tin capsule at 950 to 1000 °C. Helium was used as carrier gas and oxygen was used as burning gas in this instrument. The combustion gas mixture was driven through an oxidation catalyst (WO$_3$) zone, then through a subsequent copper zone which reduces nitrogen oxides and sulphuric anhydride (SO$_3$) eventually formed during combustion on catalyst reduction to elemental nitrogen and sulphurous anhydride (SO$_2$) and retains the oxygen excess. The resulting four

components of the combustion mixture were detected by a Thermal Conductivity detector in the sequence N_2, CO_2 and H_2O.

2.4 Micropaleontological Methods (Ostracod Analysis)

Ostracods have some particular characteristics that make them suitable for paleoclimatic and paleoenvironmental studies. In particular it is remarkable that their moults take place in a discrete period of time and the ions that build the shells are directly taken from the host water (Xia et al., 1997a; b; Von Grafenstein et al., 1999; Tütken et al., 2006). Consequently through a geochemical approach it is possible to obtain reliable information about the environment in which they grew. Ostracods' importance is more evident in those setting in which there is a lack of other organisms such as foraminifers e.g., lake systems.

For ostracod analysis sediment cores are sampled as 1 cm half slice (10 cm^3) in every 5 cm. Samples were sieved through 63 μm mesh size with low pressure water and then dried in the oven about two days. Dried samples were labeled and bottled after weighing again. Ostracods were identified and counted using a binocular microscope, Paleontology Laboratory of the Department of Geological Engineering at ITU. About 15-20 ostracods are collected for stable isotope analysis at the Department of Geosciences Isotope Geochemistry Laboratory of the University of Arizona.

2.5 Chronological Analyses

2.5.1 ^{210}Pb analysis using liquid scintillation counter

The chronology of the upper part of Lake Van cores were obtained by ^{210}Pb analysis using liquid scintillation. In the method, ^{210}Pb is directly measured by liquid scintillation counter (LSC) without waiting for ^{210}Pb to reach equilibrium with ^{210}Bi, saving analysis time (Barlas Şimşek and Çağatay, 2014). It is expected that this method can be used for the rapid measurement of ^{210}Pb also in environmental samples.

2.5.1.1 Radiochemical procedure

Figure 2.6 schematizes the steps of the radiochemical procedure. The method is based on the sequential determination of ^{210}Pb and ^{210}Po using Sr-resin (Eichrom) (Kim et al., 2008). The weighed dried sediment sample (1g) was digested using an acid mixture (HNO$_3$, HF and HCl) in microwave oven after adding Pb carrier (30mg). After adding 0.1 g H$_3$BO$_3$ the digested solution was evaporated three times with 65% HNO$_3$ to remove the HF. The residue was dissolved in 30 mL of 2 mol L^{-1} HCl and then loaded onto a Sr-resin column. The columns were rinsed with 100 mL of 2 mol L^{-1} HCl and 25 mL of 6 mol L$^-$1 HNO$_3$ to remove interfering elements. Polonium was eluted with 60 mL of 6 mol L^{-1} HNO$_3$ and then ^{210}Pb was eluted with 60 mL of 6 mol L^{-1} HCl (Vajda et al., 1997).

After separation, the Pb fraction was evaporated, the residue was dissolved, oxalic acid was added to form a Pb-oxalate precipitation, the precipitate was filtered and dissolved with 1 mL 6 mol L^{-1} HNO$_3$. Following the chemical procedure an aliquot of the dissolved sample (1 mL) is mixed with 14 mL of scintillation cocktail (Insta-Gel Plus, Perkin Elmer) in a 20 mL container vial and the sample activity is determined using a liquid scintillation spectrometer (Perkin Elmer Quantulus 1220). The chemical recovery was determined by gravimetry. The counting efficiency was evaluated with a known activity of ^{210}Pb standard solution after the chemical procedure above was applied to this solution which is in secular equilibrium with the progeny ^{210}Bi and ^{210}Po (Kim et al., 2008).
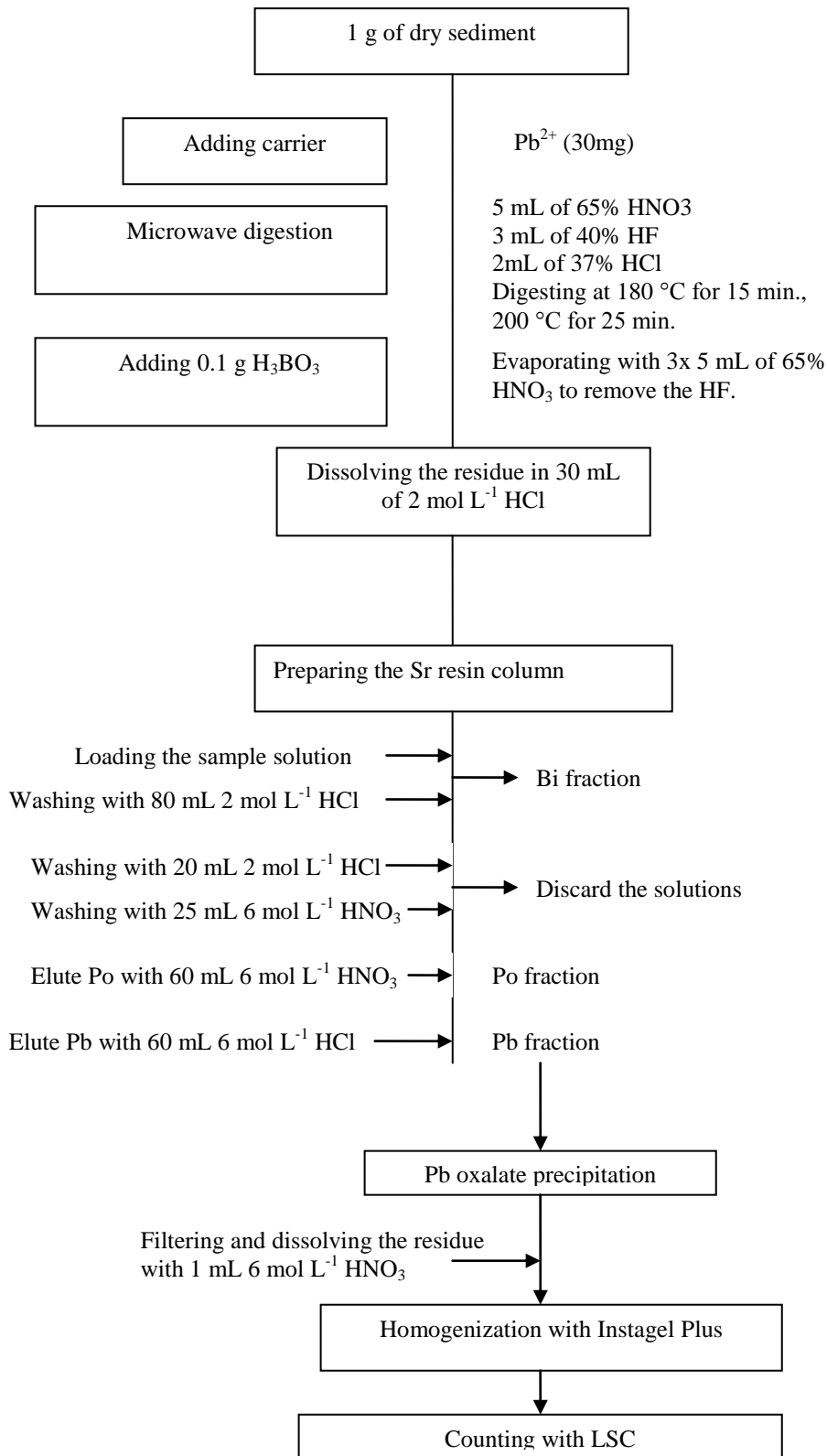
Figure 2.6 : Radiochemical procedure scheme for ^{210}Pb analysis with LSC.

2.5.1.2 Counting procedure with LSC

The activity concentration of ^{210}Pb was determined by LSC (1220 Quantulus Ultra Low Level Liquid Scintillation Counter) (Figure 2.7) adjusted to the low energy mode and low bias with double energetic window method (Vajda et al., 1997). The complexity of the ^{210}Pb decay scheme, which includes low energy beta particles from ^{210}Pb and high energy beta particles from ^{210}Bi, as well as alpha particles from ^{210}Po, makes difficult the calibration of the detector for a proper ^{210}Pb counting. However after radiochemical separation, double energetic window method enable us the successful determination of this radionuclide. In this method two counting windows should be adjusted, due to the overlapping of the beta spectra of ^{210}Pb and ^{210}Bi. Counting windows are shown in Figure 2.8. Window A is set from channel 120 to 320 and window B is set from channel 320 to 410.
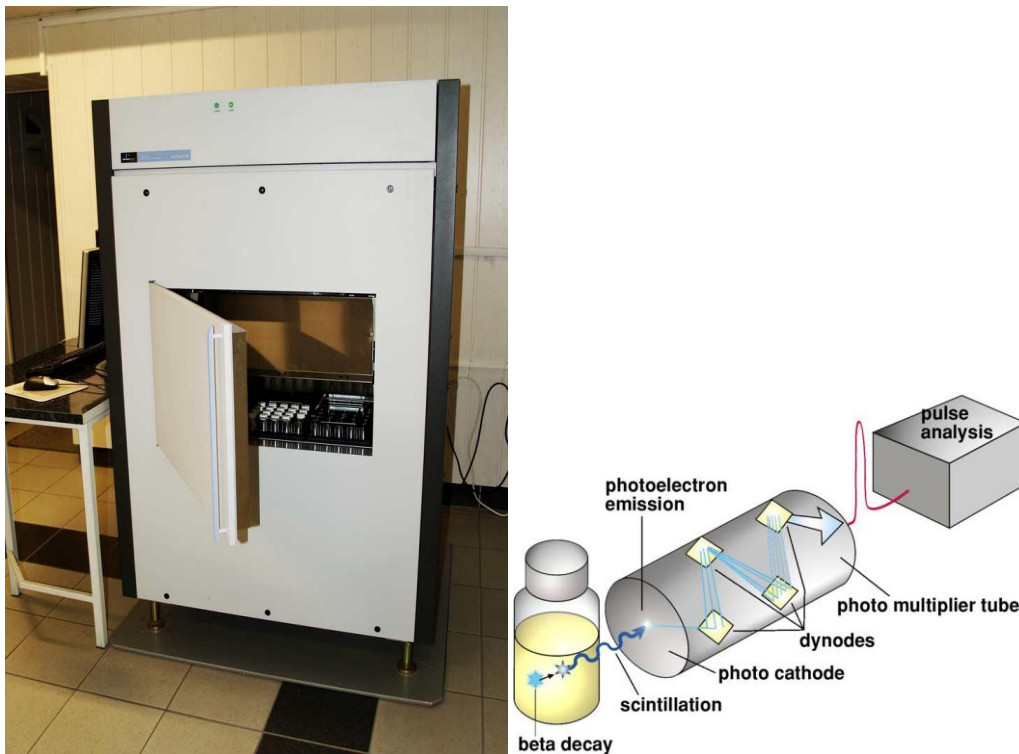
Figure 2.7 : 1220 Quantulus ultra low level liquid scintillation counter.
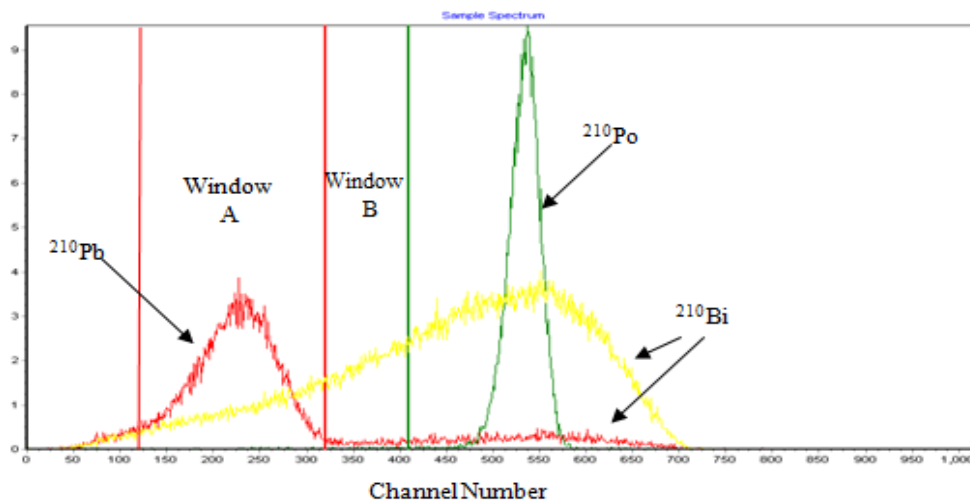
Figure 2.8 : Beta spectra of of ^{210}Pb, ^{210}Bi, and ^{210}Po.

For determination of the accuracy and the precision of the results repeated analysis of the International atomic energy Agency IAEA-434 reference material with known activity was carried out. The calculated results and the reference values are shown in Table 2.2 and Figure 2.9.
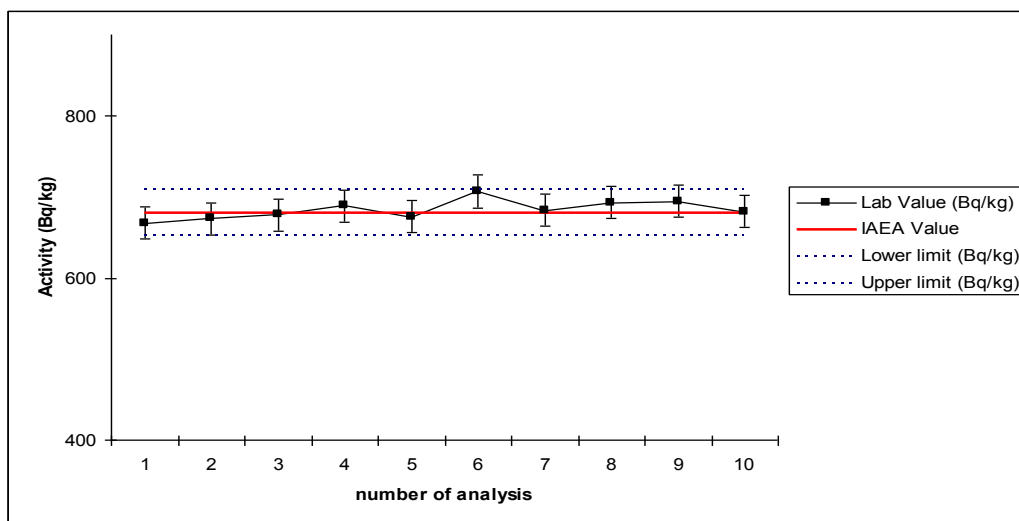
Figure 2.9 : Control chart for relative bias of ^{210}Pb determination in IAEA-434 referance material: Measured activity concentration of ^{210}Pb (Bq/kg) is plotted against the number of replicates (k=1).

Table 2.2 : Example repeatability test results for IAEA 434 reference material.

IAEA-434	Lab Value± 1σ (Bq/kg)	IAEA Value (Bq/kg)	Lower Limit (Bq/kg)	Upper Limit (Bq/kg)
1. Analysis	668±26	680	651	709
2. Analysis	673±27	680	651	709
3. Analysis	678±27	680	651	709
4. Analysis	689±30	680	651	709
5. Analysis	676±30	680	651	709
6. Analysis	707±30	680	651	709
7. Analysis	684±31	680	651	709
8. Analysis	693±31	680	651	709
9. Analysis	695±30	680	651	709
10.Analysis	682±31	680	651	709

2.5.2 ^{137}Cs and ^{226}Ra analysis with gamma spectrometry

^{226}Ra and ^{137}Cs were measured in aliquots of dry sediment weighing 10-20 g, using direct gamma counting with gamma-spectrometer equipped with High Purity Germanium (HPGe) coaxial well type detector (Ortec Model) having 2.1 keV resolution in the energy ^{60}Co 1332 keV. ^{226}Ra was measured by the 351 keV emission of its daughter isotope ^{214}Pb (with a correction for losses of the intermediary gaseous isotope ^{222}Rn).

^{137}Cs was measured by its emissions at 661 keV. Detector efficiency was determined by counting a National Institute of Standards and Technology (NIST) traceable mixed liquid gamma standard (Isotope Products Labs). The background corrected counts were then analyzed with the GESPECOR software, which uses Monte Carlo simulations to correct for self-absorption and coincidence-summing effects (Sima et al., 2001). Minimum detectable activity was calculated at 0.004 Bq for ^{137}Cs and 0.040 Bq for ^{226}Ra.

2.5.2.1 ^{210}Pb and ^{137}Cs age modelling (Geochronology)

Chemical structures as well as radionuclide concentrations in the bottom sediment cores are the source of valuable information about the physicochemical processes occurring in water ecosystems. Particularly, the determination of concentration of some pollutants and specific activity of the natural radionuclide ^{210}Pb in profiles of bottom sediment cores allows determining the history and sources of pollution in different environments (Gelen et al., 2003).

Dated environmental archives, such as sediment cores, corals and tree rings, are widely used to reconstruct past environmental ecosystems conditions. In particular, ^{210}Pb has been used for dating of undisturbed sediment cores, to study climate and environmental changes during the last 100-150 years. The establishment of accurate chronologies of sedimentation is used for dating and also for determining sediment accumulation rates (Appleby and Oldfield, 1983).

^{210}Pb is a naturally occurring radionuclide in the ^{238}U decay series (Figure 2.10), and of importance in environmental sciences (Tokieda et al., 1994). It has a physical half life of 22.3 years and decays to ^{210}Bi by beta emission. It is present in the atmosphere as a result of the decay of ^{226}Ra in the earth's crust to the rare gas ^{222}Rn with a half life of 3.8 days, which in turn decays via a series of short-lived daughters to ^{210}Pb (Figure 2.10).

$$^{238}U \rightarrow \rightarrow \rightarrow {}^{226}Ra \rightarrow {}^{222}Rn \rightarrow {}^{218}Po \rightarrow {}^{214}Po \rightarrow {}^{214}Bi$$

$$\downarrow$$

$$\downarrow$$

$$^{206}Pb \leftarrow {}^{210}Po \leftarrow {}^{210}Bi \leftarrow {}^{210}Pb \leftarrow {}^{214}Po$$

(stable)   (22.3y)
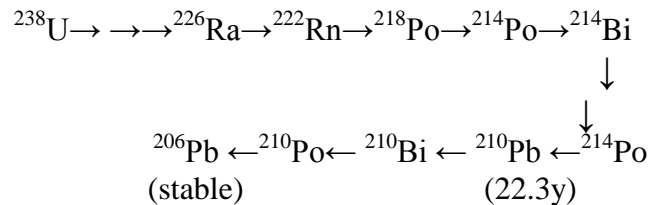
Figure 2.10 : Decay scheme of ^{226}Ra and its daugthers.

^{210}Pb enters a lake or reservoir either directly as rain or indirectly in run-off from the catchment. A subsequent source of ^{210}Pb in the water column is from the decay of ^{222}Rn in solution, which may or may not be provided by ^{226}Ra. ^{210}Pb is deposited at the mud/water interface by sedimentation and exchange processes and becomes integrated into the sediment column. Figure 2.11 shows the various routes of entry of ^{210}Pb to a fresh water body.
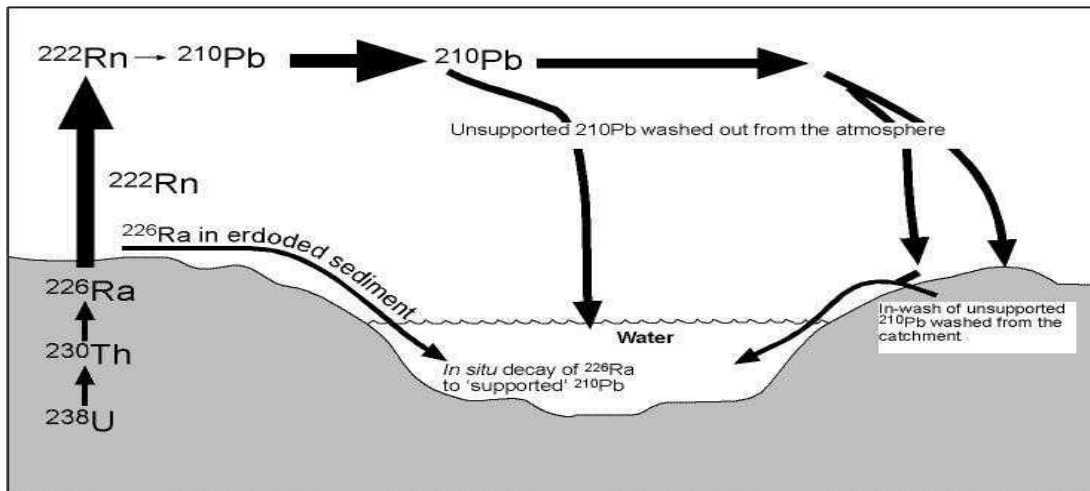
Figure 2.11 : Potential sources of ^{210}Pb in marine sediments (after Oldfield and Appleby, 1984).

^{226}Ra is also appear in the sediment as part of the erosive contribution of particulate matter from the catchment. ^{210}Pb formed in the sediment by decay of ^{226}Ra is referred to as supported ^{210}Pb, which is usually expected to be in equilibrium with the ^{226}Ra. ^{210}Pb in excess of the supported activity is termed the unsupported ^{210}Pb, and is considered to be derived predominantly from atmospheric input.

As long as the input of ^{210}Pb to a water body and its residence time are reasonably constant and there is no critical migration of ^{210}Pb within the sediment, the concentration of unsupported ^{210}Pb will decrease as a function of depth because of radioactive decay. It is possible by applying the law of radioactive decay to decreasing concentration of ^{210}Pb with depth, to calculate the age of the sediment at any prospects. In order to do this, certain assumptions describing the delivery of ^{210}Pb to the sediment must be identified, which clarify the validity of the chronology.

The total ^{210}Pb activity follows an exponential decay with depth, assuming a uniform sedimentation rate over a 150-year period. However, because of anthropogenic and environmental effects, this is not often the situation. Several models for ^{210}Pb analysis have been developed using the radioactive decay equation. Model selection depends on environmental conditions, sediment processes including sediment focusing and sediment stability (e.g., bioturbation, erosion, deposition). To select a model for ^{210}Pb sediment chronology, a historic knowledge of the sampled sediment is required.

The decay of this atmospherically derived ^{210}Pb provides a measure of the rate of deposition of the sediment column. In the absence of sediment mixing, two models are commonly used to derive age-depth correlations in sedimentary profiles. The constant rate of supply (CRS) model (Appleby and Oldfield, 1978) assumes that sedimentation rate and sediment compaction change throughout the core and automatically corrects for these parameters, while the constant initial concentration (CIC) model (Goldberg, 1963; Krishnaswamy et al., 1971) assumes that sedimentation rate is constant in the area under study and requires that the depth of the sediment column be corrected for compaction before the method be applied. Both models assume no postdepositional migration of ^{210}Pb and a constant flux of ^{210}Pb$_{exc}$ at the sediment-water interface.

Concentration and flux relate to each other by the equation (2.1)

$$C = \frac{F}{r} \qquad (2.1)$$

where r is the mass accumulation rate. By assuming a constant flux of ^{210}Pb^{ex}c at the sediment-water interface and constant sedimentation rate, the CIC model fixes the concentration of ^{210}Pb$_{exc}$ at the surface. If no physical processes alter the amount of ^{210}Pb$_{exc}$ in the surface sediments, the activity of ^{210}Pb$_{exc}$ declines down the sedimentary profile according to its natural radioactive decay (2.2):

$$C_{(x)} = C_{(0)} \exp(-\lambda t) \qquad (2.2)$$

where C is the ^{210}Pb$_{exc}$ concentration per mass of dry sediment (Bq kg^{-1}) at the sediment-water interface ($C_{(0)}$) and at depth x ($C_{(x)}$), λ is the decay constant of ^{210}Pb (0.03114 yr^{-1}), and t is the age of the sediment at depth x. Because the age of the sediment is a function of sedimentation rate (R) (cm yr^{-1}) and depth (x) (cm), equation (2.2) takes the form:

$$C_{(x)} = C_{(0)} * \exp(-\frac{\lambda}{R} * x) \qquad (2.3)$$

From this point, there are at least three different ways of calculating sedimentation rate using the CIC model. Graphically, the semi logarithmic plot of ^{210}Pb$_{exc}$ concentration against depth is predominantly linear and the mean sedimentation rate

is taken from the ratio of the decay constant of ^{210}Pb to the slope of the line (CIC with no compaction correction and constant sedimentation rate). If compaction plays an important role in the study site the slope of this line decreases towards the top of the core as a result of reduced compaction at surface, assuming no physical mixing and no change in accumulation rate has taken place. The effects of compaction can be eliminated from the CIC model by expressing depth in terms of cumulative dry mass of sediment (m) (g cm^{-2}):

$$Drybulkdensity(DBD)_{(x)} = (1 - \phi_{(x)})\rho_{sed} \qquad (2.4)$$

$$m = \sum(DBD_{(x)} * T_{(x)}) \qquad (2.5)$$

where ϕ is the porosity at depth x; ρ_{sed} is the density of the sediment at depth x and T is the thickness of the sediment layer. Equation (2.3) now takes the form (Hughen et al., 1996):

$$C_{(x)} = C_{(0)} * \exp(-\frac{\lambda}{r}m) \qquad (2.6)$$

r, the mass accumulation rate (g cm^{-2} y^{-1}), is calculated by the ratio of the decay constant of ^{210}Pb to the slope of the line of the semi logarithmic plot of ^{210}Pb$_{exc}$ concentration against cumulative dry mass, and sedimentation rate (R) as a function of depth is calculated by (Hughen et al., 1996) (CIC with compaction correction):

$$R = \frac{r}{(1 - \phi)\rho_{sed}} \qquad (2.7)$$

A third way of calculating sedimentation rate with the CIC model is by simply applying Equation (2.2) to the data (CIC with no compaction correction and variable sedimentation rate). Since $C(0)$ is the ^{210}Pb$_{exc}$ concentration per mass of dry sediment (Bq kg^{-1}) at the sediment-water interface and $C(x)$ is the ^{210}Pb$_{exc}$ concentration of the layer under investigation, then t, the age of the sediment at depth x, can be calculated for each depth. Because this method does not fit a regression line through the data, calculated sedimentation rates vary with depth and yield scattered results.

In the CRS model, the initial concentration of ^{210}Pb$_{exc}$ and the sediment accumulation rate vary with time, but their product remains constant and equals the flux of ^{210}Pb$_{exc}$ that reaches the sediment-water interface. The constant flux assumption implies a constant residue of ^{210}Pb$_{exc}$ within the sediment column. Equation (2.2) then takes the form:

$$A_{(x)} = A_{(0)} \exp(-\lambda t) \tag{2.8}$$

Where $A(x)$ is the residual ^{210}Pb$_{exc}$ in the core below depth x (Bq m^{-2}), and $A(0)$ is the entire ^{210}Pb$_{exc}$ inventory below the sediment-water interface. Because measurements are rarely made on every sample from a core, the midpoint procedure is applied in most cases. The residual ^{210}Pb$_{exc}$ for each sediment layer is calculated by multiplying ^{210}Pb$_{exc}$ concentration ($C(x)$) by cumulative dry mass (m), using the trapezium rule described by Appleby (2001). The age of each sediment layer can be calculated by rearranging Equation (2.8),

$$t = \frac{1}{\lambda} \ln\left(\frac{A_{(0)}}{A_{(x)}}\right) \tag{2.9}$$

and the mass accumulation rate at time t from(Appleby, 2001).

$$r = \frac{\lambda A_{(x)}}{C_{(x)}} \tag{2.10}$$

Whatever the model used, ^{210}Pb based chronologies must be confirmed by independent methods (Smith, 2001). Generally, ^{210}Pb dates are confirmed using ^{137}Cs profiles, when the ^{137}Cs profiles are sufficiently good (Appleby and Oldfield, 1983). In other words in order to reduce the number of model-determined answers, an independent time marker, such as ^{137}Cs, can be input to the model. ^{137}Cs (half-life 30.2 years) is a man-made radionuclide occurring in the global fallout of debris from nuclear weapons tests during the 1950s and 1960s.

In the northern hemisphere the deposition reached a considerable level until 1954 and increase rapidly later. In 1958 it was noticed a decrease and it was followed by an increase because of the restarting of the testing. After the agreement from 1963, the ^{137}Cs deposition reduced, but at the beginning of the 70's it increased again, due

to the states which did not sign the agreement. Also the most important sources of this radionuclide is fallout from the Chernobyl accident in 1986 which have caused the existence of this radionuclide in the marine environment. Due to the insignificance of loss by vegetation uptake (Ritchie and McHenry, 1990), ^{137}Cs is absorbed by organic matter in the top soil and concentrated there.

^{137}Cs has been widely used as an important tracer in soil erosion and sediment delivery investigations. It has also been used to obtain environmental changes and human effects in soils during the last 30–50 years (Ritchie and McHenry, 1990).

2.5.3 AMS radiocarbon (^{14}C) analysis

In general, organic matter from 0.5 to 40 thousand years ago (ka) can be dated with radiocarbon (e.g. Libby, 1955; Walker, 2005). ^{14}C, a radioactive isotope of carbon, is continually produced in the upper atmosphere due to the cosmic rays removing a proton from ^{14}N and promptly reacting with free-oxygen to produce ^{14}CO$_2$, which is included in plants by photosynthesis (Bjorck and Wohlfarth, 2001). A consistent amount of ^{14}C is found in all living organisms because ^{14}CO$_2$ is well mixed in the troposphere and organisms permanently take up ^{14}CO$_2$ into their tissues. When an organism dies, the ^{14}C in the tissues stops being refilled and radioactively decays back to ^{14}N with a half-life of 5730 years (Bjorck and Wohlfarth, 2001). Impotant amount of organic matter can be found in lake sediments and used for radiocarbon dating. Hard water effects and old carcon sources (Cohen, 2003) can cause some erros therefore to prevent such errors, a piece of a plant which grew in equilibrium with the atmosphere should be used for dating. Additionally, organic matter in the sediment must have been accumulated promptly, or else it would have decomposed, which allows to apply the age of the organic matter to the age of the sediment layer.

Measurements counting the amount of ^{14}C of the materials give an uncalibrated age result. For this study, ^{14}C dating of bulk organic carbon in selected samples is made at the Arizona University NSF Radiocarbon facility, using Accelerator Mass Spectrometry (AMS) method. ^{14}C ages obtained from the analysis were calibrated to calendar age by using *Calib Radiocarbon Calibration Execute Version 6.0 html* (Reimer et al., 2009).

2.6 Varve Counting Method

Varve-counting method used in this study involves image analysis of analogue and digital X-ray radiographic images. The method is based on step-wise counting of light and dark grey scale bands (lamina) along a laminated core using its radiographic image (Damcı and Çağatay, 2015).

The grey scale colour variation in the digital X-radiographic images cores along their length is controlled by the density variations in the sediment, provided that the sediment core has a uniform thickness along its length and a monochromatic X-ray of uniform energy is used during the radiographic core imaging. Hence, a core with a laminated structure with each lamina having different proportions of detrital silicate minerals and biological organic and inorganic materials would be represented by mm to sub-mm thick light and dark gray bands of different density in the radiographic images. Commonly, two or more lamina are deposited in a cyclic seasonal pattern that makes up an annual varve. According to sediment trap and scanning electron microscopic studies, the varve structure of the Lake Van sediments, consists of three laminae: an organic-rich lamina deposited in winter, a silt dominated detrital mineral-rich lamina in spring, and a carbonate-rich white laminae in summer (Kempe et al., 2002; Huguet et al., 2011; 2012; Stockhecke et al., 2012; 2014).

60 μm resolution digital X-ray radiographic images of the Lake Van cores were obtained directly from a 1 cm-thick U-channel prepared vertically to the laminations, using Itrax XRF core scanner coupled with a digital X-ray radiographic set up (Croudace et al., 2006). Such a thin (≤1 cm thick) U-channel vertical to the laminations avoids multiple counting of the same lamina, in case the lamina are perfectly vertical to the length of the core, and provide a more clear and symmetrical digital image of individual lamina.

The algorithm developed by Damcı and Çağatay (2015) and used in this study detects each maximum and minimum gray-scale value in the radiographic image along the core length. Detection of each lamina with a clear signal along the core length is based on the fact that the smallest lamina thickness should include at least three pixels on the radiographic image. So, the pixel size should be one-third of the lamina thickness.

2.7 Stable Isotope Analysis

2.7.1 Oxygen and carbon isotope analysis of bulk carbonate and ostracods

Stable oxygen ($\delta^{18}O$) and carbon ($\delta^{13}C$) isotope ratios are among the most frequently used proxies in palaeoclimate studies, allowing for instance the reconstruction of past changes in temperature, hydrology or vegetation cover (McKenzie, 1985; Schwalb, 2003; Leng and Marshall, 2004). Stable isotope techniques can be applied both to sediments and fossils, such as foraminifers, ostracods, molluscs, and other vertebrates. Ostracods' significance is more evident in those settings in which there is a lack of other organisms such as foraminifers, e.g., lake systems. The $CaCO_3$ shells of the organisms used in interpreting the history of environment can be used for stable isotope analysis.

Isotopic compositions ($\delta^{18}O_{VPDB}$ and $\delta^{13}C_{VPDB}$) of the bulk carbonates were determined by using both sediment samples and microsamples of single carbonate components (ostracod valves) of core V08G04.

Sampling, washing and drying procedures of ostracods used for stable isotope analysis were made non-destructively. Hydrogen peroxide and splicer were not used. All samples were washed with 63 μm sieve, and rinsed with distilled water, then dried in the oven for two days. The only existing ostracod *Limnocythere inopinata* was used for the isotope analysis. Depending on the size of the ostracods, 10-15 pieces were selected for the nalysis .

Stable isotopes were determined with a Kiel III carbonate preparation device attached to a Finnigan-MAT 252 isotope ratio mass spectrometer in the Arizona University Isotope Geochemistry Laboratory. Powdered bulk samples were treated with dehydrated phosphoric acid under vacume at 70 °C. The isotope ratio measurement was calibrated based on repeated measurements of NBS-19 and NBS-18. All data are reported in the standard delta notation against the Vienna Pee Dee Belemnite standard (VPDB). The precision of the method was ±0.1 ‰ for $\delta^{18}O$ and ±0.06 ‰ for $\delta^{13}C$ (1 σ).

2.7.2 Stable carbon and nitrogen isotope analysis of organic matter

The carbon and nitrogen stable-isotope composition of autochtonous sedimentary organic matter (OM) can also be used to reconstruct changes in aquatic productivity

rates and sources of nutrients (Bertrand et al., 2009). This is because of through periods of improved aquatic productivity, lacustrine algae specially consumes the dissolved light carbon isotope (^{12}C) while doing photosynthesis. The improved uptake of $^{12}CO_2$ by aquatic organisms results in the production and the sedimentation of ^{13}C-poor OM that is with more negative $\delta^{13}C_{org}$ ($^{13}C/^{12}C$ ratio) values (Meyers and Teranes, 2001). Lower $\delta^{13}C$ values of sedimentary OM can also reproduce increased arrival of terrestrial OM into the lake, or better dissolved CO_2 supply to the lake water due to a reduction in the seasonal ice cover or changes in the lake trophic levels (Harwart et al., 1999; Teranes and Bernasconi, 2005). Also both concentrated and longer lake stratification and enhanced photosynthesis by marine plants and algae may also effect the δ^{15}Norg composition of lacustrine OM (Lu et al., 2010; Xu et al., 2006).

In this study, six samples from core V08G04, including those selected for AMS radiocarbon dating, were selected for δ^{13}C ‰ and δ^{15}N ‰ analyses. The samples were treated with HCl to eliminate the carbonate fraction. The dried and homogenized carbonate-free samples were analysed at the Environmental Isotope Laboratory of Arizona University. δ^{15}N and δ^{13}C, as well as carbon and nitrogen content were measured on a continuous-flow gas-ratio mass spectrometer (Finnigan Delta PlusXL) coupled to an elemental analyzer (Costech). Standardization is based on acetanilide for elemental concentration, NBS-22 and USGS-24 for d^{13}C, and IAEA-N-1 and IAEA-N-2 for δ^{15}N. Precision of the method is better than $\pm$ 0.10 for δ^{13}C and $\pm$ 0.2 for δ^{15}N (1 sigma), based on repeated measurement internal standards.

3. STUDY AREA

3.1 Geological Setting and Bathymetry of Lake Van

Lake Van is the world's largest soda lake. It is, situated in the East Anatolian Highlands of Turkey (43°E and 38.5°N) at an altitude of 1648 m (Kempe, 1977; Kempe et al., 1991). By volume of 607 km^3, it is the fourth-largest terminal lake in the world, extending for 130 km in WSW-ENE direction and having a surface area of 3570 km^2. The average and maximum water depths of the lake are 171 m and 460 m respectively (Degens and Kurtman, 1978; Landmann et al., 1996a; Lemcke, 1996).

Lake Van area is located near the boundary of the Eurasian and the Afro-Arabian continental plates. The Lake Van area is characterized by recent volcanism and hydrothermal activity and active tectonics (Degens and Kurtmann, 1978; Kipfer et al., 1994; Şengör et al., 2003). On its northern shore lies the complex volcanic mass of the Süphan, which rises to an elevation of 4434 m (Blumenthal et al., 1964). The Nemrut volcano is located 15 km west from the western lake shore, with its top reaching 3050 m above sea level today. The eastern half of the huge Nemrut caldera is filled with eruptive volcanic material, leaving the western half to be occupied by a caldera lake of crystal-clear, blue water.

The long axis of Lake Van, trending approximately east-west, is about 70 km in length. Near the eastern edge, this axis branches. The main part extends northeastwards for almost 60 km, while the southwesterly branch measures only about 30 km before the lake shore is extended. The drainage basin of Lake Van lies within the tectonic unit of the Anatolides- Taurides. These are metamorphic massifs in which intermontane flysch basins change with young volcanics. To the south of the lake is the Bitlis Massif (Altınlı, 1964; MTA Inst., 1961), of Paleozoic age. The northern boundary of the Bitlis Massif is distinct by an active over thrust, along which the Massif is thrust onto the Muş Basin to the north. The Muş Basin appropriate extends over a distance of 250 km in an east-west direction. It is up to 85

km wide, and is filled with about 10 km of Cretaceous and Tertiary clastic sediments (Figure 3.1).
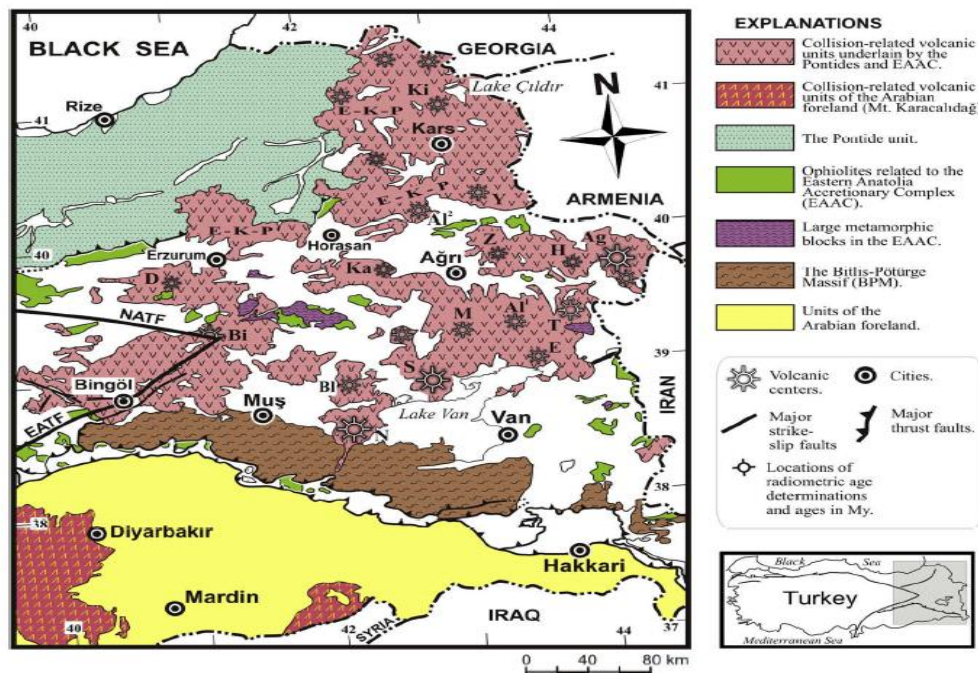
Figure 3.1 : Geological map of Lake Van (Keskin, 2007).

The bathymetry of the lake is depicted in Figure 3.2. Three district physiographic provinces can be recognized: shelf, slope and basin (Wong and Degens, 1978). Instantaneously offshore is the lacustrine shelf, which is narrow and weakly developed to the north, south and west. In contrast, almost the whole eastern half of the lake may be categorized as a shelf. Here, the shallow (average 20 m) Erciş Gulf situated in the northest, while the Erek and Eastern Fans, cut up by immersed fluvial valleys, control the residual area.

The sublacustrine slope is narrow and steep along the southern shores of the lake, suggesting that it may be the sub-lake unit of a large, east-west-trending fault scarp. By comparison, the eastern and western slopes are wide, and benches are developed between the depths of 300 to 400 m, which can be interpreted as submerged terraces. Near Deveboynu Peninsula are several depressions and shoals.

The lake basin province is separated by combining Erek-Eastern Fans into a large, quasi-circular Tatvan basin, which averages 445 m in depth, and a slightly shallower, much smaller Deveboynu basin. The maximum depth of 451 m was recorded at a point 16 km southwest of Adilcevaz near the northern edge of this province.
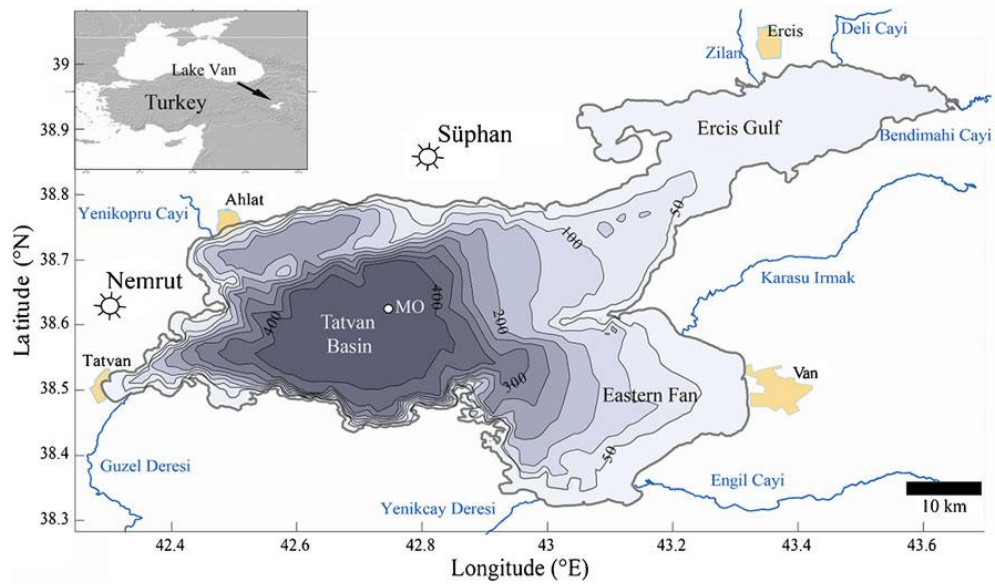
Figure 3.2 : Bathymetric map of Lake Van (Huguet et al., 2011).

To its northwest, the Tatvan Basin is separated from the ~410 m-deep small Ahlat subbasin and 260 m-deep Northern basin (NB) by the NEE-trending Ahlat and Northern ridges having elevations of 300-370 m and 75-200 m below the present lake level, respectively (Çukur et al., 2014)

3.2 Water Chemistry

The extreme alkalinity (152 meq L^{-1}) and salinity (21.6 ‰) of Lake Van is the result of chemical weathering of the surrounding volcanic rocks, hydrothermal activity, and evaporation (Kadıoğlu et al., 1997).

The water volume of Lake Van and the dissolved ion concentrations are dominated by the ratio of water influx by precipitation and rivers to water loss by evaporation. Having been a closed lake for about last 600 ky (Litt et al., 2014) and thus the absence of outflows has caused the accumulation of salts in Lake Van and an increase in salinity to present day value of 21.6 ‰ (Reimer et al., 2009) (Table 3.1). The major cation, Na, is balanced by chloride, carbonate and bicarbonate (Kempe et al., 1991). Generally, the lake is characterized by an Na-CO_3-Cl-(SO_4)-chemistry that derived from the incessant loss of calcium as carbonate and magnesium in the form of Mg-silica-rich mineral phases (Reimer et al., 2009). As a result, the lake water behaves like an alkaline buffer solution, leading to a very high pH value of 9.8.

Free oxygen is existing in the whole water body although the concentration decreases the value below 1 mg L^{-1} in the near bottom layers (Reimer, 2009). However, the lake waters below 300 m became unoxic after the water level rise in 1990s (Kipfer et al., 1994; Peeters et al., 2000; Reimer et al., 2009; Stockhecke et al., 2012). In summer lake's surface temperature is about 20-23 °C whereas in winter it sometimes decreases under 0 °C. (Kempe and Degens, 1978).

The water chemistry and stable isotope ratios (D/H and $^{18}O/^{16}O$) are uniform throughout the water column, except close to river outlets (Kempe et al., 1978). In view of the considerable flux of inflowing and outgoing water, one must invoke a rapid mixing mechanism. The content of heavy metals is around normal levels for natural waters. Only lead is present at a high concentration (15 ppb) (Kempe et al., 1978).

Table 3.1 : Hydrological parameters of the Lake Van surface water (from Thiel et al., 1997).

Parameter	Value	Explanation
Na^+	339 meq L^{-1}	(1)
K^+	10.8 meq L^{-1}	(1)
Mg^{2+}	8.9 meq L^{-1}	(1)
Ca^{2+}	0.2 meq L^{-1}	(2)
Cl$^-$	161 meq L^{-1}	(1)
Alkalinity	152 meq L^{-1}	(1)
SO_4^{-2}	49.1 meq L^{-1}	(1)
PO_4^{-2}	3.7 µmol L^{-1}	(2)
Salinity	21.6 ‰	(1)
pH	9.8	(1)
O_2	7.5 mg/L	(2)
Temperature	18 to 5 °C	(3)

(1) average 0-30 m, 1990; increase with depth
(2) average 0-30 m, 1990.
(3) 1990; decrease with depth.

3.3 Climatic Features

The climate in eastern Anatolia, including the Lake Van region, is strongly influenced by changes in the position of the westerly jet stream, the extension of the subtropical low-pressure belt and Siberian high-pressure area (Akçar and Schlühter, 2005; Litt et al., 2009; Wick et al., 2003). The lake's position at the junction of the

atmospheric south-western jet stream and northern branch of the Subtropical High makes it climatically sensitive (Figure 3.3). The jet stream influences the cyclone tracks which provides moisture from Mediterranean air masses during winter. The position of the Subtropical High effects the southward extension of the dry continental air masses of northeastern Europe and Asia (La Fontaine et al., 1990; Akcar and Schlüchter, 2005).

The local climate of Lake Van area is continental and it is characterized by strong seasonality, expressed as warm, dry summers in July and August with mean temperatures exceeding 20 °C, and cold winters from December to February with mean temperatures below 0 °C. Mean annual temperature in Lake Van is about 8.8°C. Due to the high salinity, only rarely ice forms on the lake surface. Cold, dry air masses coming from high northern latitudes acquire moisture on passing over the Mediterranian Sea, reaching Lake Van from the south-west. These south westerly winds cause precipitation during autumn, winter and spring, whereas in summer, continental air masses originating from low latitudes result in dry conditions (Roberts and Wright, 1993). Highest precipitation in the catchment area of approximately 16000 km^2, occurs between March and May, and between October and December. Although the annual precipitation rate is highly variable according to the exact location, averages are in between 400 and 700 mm (Schweizer, 1975). Main input of lithogenic material into Lake Van occurs from April to June during spring rain and snow melt. The natural vegetation is steppe, prevailed by sub-euxinian oak forest (Wick et al. 2003). However, there is barely any natural vegetation left, which is largeley replaced by agricultural land.
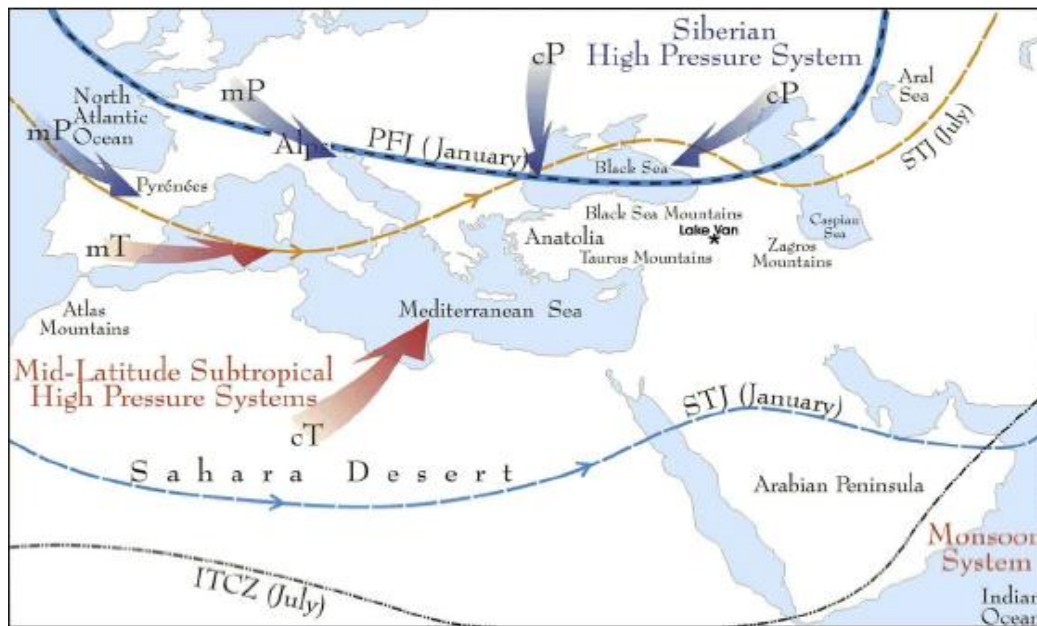
Figure 3.3 : Geol Lake Van and the mean position of the Polar Front Jet (PFJ), Subtropical Jet (STJ) and Intertropical Convergence Zone (ITCZ) in winter and summer in the Mediterranean Region, and High Pressure System that influence the climate of the Eastern Mediterranean Region. cP: Continental Polar Air Mass; mP: Marine Polar Air Mass; mT: Marine Tropical Air Mass; cT: Continental Tropical Air Mass (after Akcar and Schlüchter, 2005; modified from Wigley and Farmer, 1982).

3.4 Ecology

Very little data exit about the biological life in Lake Van. Due to the extreme chemical composition of the water, the lake shows low biodiversity. There is, for example, only one specially adapted fish species in the lake (Danulat and Kempe, 1992). Although some species of phytoplankton have been recorded in the lake including cyanobacteria, flagellates, diatoms, green algae and brown algae and some species of zooplankton including Rotatoria, Cladocera and Copepoda (Danulat and Selçuk, 1992). Many groups which are widespread in normal marine or limnic environments are lacking (Gessner, 1957). According to Gessner (1957), diatoms and cyanobacteria are important members of the phytoplankton, whereas the zooplankton appears to be dominated by copepods (Hauer,1957) and ciliates (Gessner, 1957).

3.5 Water Level Changes of Lake Van

Lakes are natural, inland water bodies which react to atmospheric, meteorological, geological, hydrological and astronomical effects. Therefore, the behavior of natural lakes involves information about these driving events occurring in the lake's drainage basin and he surrounding region. The effects of different factors which influence the hydraulic balance of a drainage area are combined by stream flow data; likewise, lake-water level fluctuations represent the end result of the complex interaction of the various water balance factors. These factors are the flow of incoming or outgoing river and streams, direct precipitation onto the lake surface and the groundwater exchange. In addition, some other factors such as precipitation over the lake drainage area, evaporation from the lake surface, wind velocity, humidity, temperature and other meterological factors can play important roles in lake water level fluctuations.

Some lakes in semi-arid regions are closed with no outlet. Large lakes can change the precipitation over and around the free water surface. Concurrent measurements of all the components influencing lake water level fluctuations are complex and measurements for the application of hydrological water balance equations are not enough for many large natural lakes in the world.

Lake Van is the world's fourth closed basin lake with no natural outlets. Anually 4.2 km^3 of water is lost by evaporation from the lake surface (Kadıoğlu et al., 1997). This situation is compensated by both the long-term averages of annual surface runoff and precipitation amounts of 2.5 km^3 and 1.7 km^3, respectively The fluctuations in water level are completely dependent on the natural variability of the hydrological cycle and any long term climatic changes which affect the drainage area (Kadıoğlu et al., 1997).

Generally, annual water fluctuations in Lake Van have a definite increase starting from January and ending in June with a decrease in the water level. During the period 1944-2010 each year water level increases from January to June and decreases afterward. Also it is also evident that the lake level increased quite rapidly from 1987 onwards (Figure 3.4). Although the long-term lake level average is at 1648 m above the sea level, it reached 1650 m by the year 1987. The lake level fluctuations have yearly amplitudes of between 40–60 cm depending on climatic

conditions. Degens and Kurtman (1978) calculated the average annual amplitude as 49.7 ± 18 cm for the period 1944–1974. During he annual fluctuations, the total water volume of the lake changes about 1.5 %. However, the values from 1944 to 1994 have average and standard deviation values of 136.8 cm and 70.8 cm, respectively (Sen *et al*., 1999). Comparison of these two periods shows increases of 275% and 383% in the mean lake level and amplitude, respectively, as a result of a rise in lake water level 1974, perhaps caused by a change in climate in the area. Consequently, the region has become more humid with more precipitation but less evaporation (Altunkaynak et al.,2003).
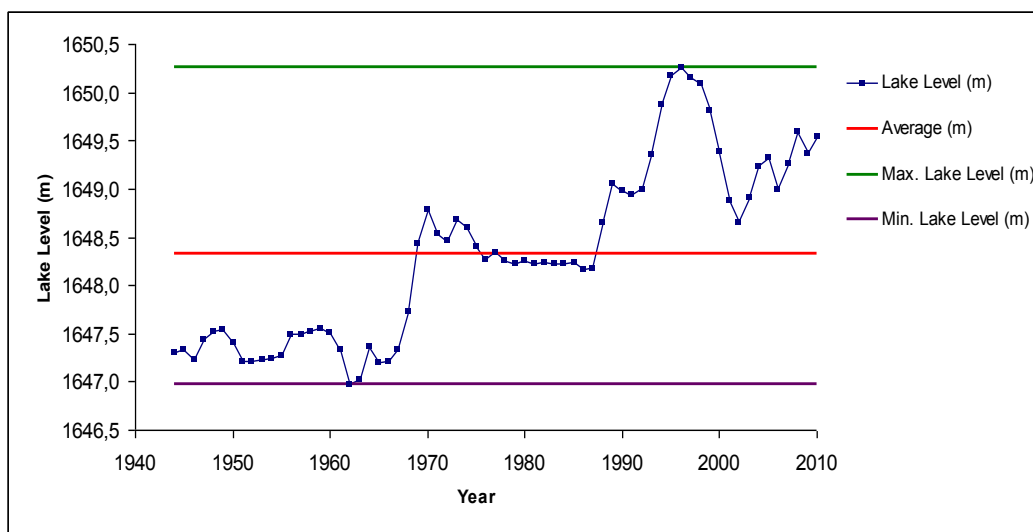
Figure 3.4 : Lake Van level fluctuation record from 1944 to 2010 (DSİ, 2010).

In addition, historical evidence show that Lake Van had experienced high levels during the late 1880s (Sieger, 1888). The level fluctuations were in the order of few meters during this period. Sun-spot activity was considered as a possible cause of water level changes in Lake Van during 1944-1974 (Kempe et al.,1978), As shown in Figure 3.5 there is a close agreement between the trends of lake level change and sun spots. Both curves have a frequency of about 11 years, which implies that the solar activity effected the overall water balance of Lake Van during the period, with increased solar activity corresponding to increase in the water level of the lake with about a one year delay. Such kind of increase in the sun-spot activity probably caused unstable weather conditions, resulting in larger cloud cover and increased precipitation.
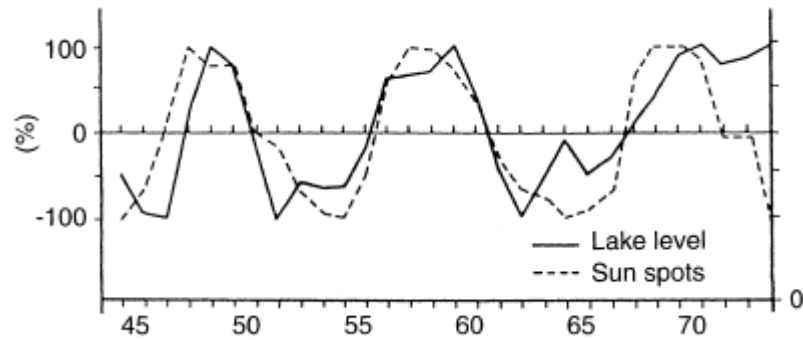
Figure 3.5 : Relation between lake level and sun-spots during 1944-1974 period.

However, it is clear from Figure 3.5 that close to the end of the 1944-1974 period curves deviate from each other, signifying that the lake level fluctuation was no longer depended on the number of sun-spots, and some other climate related factors should be considered (Kempe et al.,1978).

3.6 Level Fluctuations and Climate During The Past 18000 Years

The following lines of evidence have been used to reconstruct the climatic history and lake level fluctuations of the Lake area over the past 18,000 years: (i) dated coastal terraces (Schweizer, 1975; Valeton, 1978; Kempe et al. 2002; Kuzucuoğlu et al., 2010;), (ii) distinct submerged wavecut benches at different depths (Wong and Degens, 1978; Wong and Fınckh, 1978), (iii) presence of hard layers showing evidence of supratidal conditions (Khoo et al., 1978), (iv) varve patterns and related sediment structures (Kempe, 1977; Landmann et al., 1996a), (v) ^{18}O and ^{13}C contents of authigenic carbonates (Schöll, 1978; Lemcke and Sturm, 1997; Çağatay et al., 2014), (vi) distribution of organic carbon in sediments (Schöll, 1978; Çağatay et al., 2014), (vii) carbonate mineralogy (Landmann et al., 1996a; Çağatay et al., 2014), (viii) seismic stratigraphy (Çukur et al., 2014; Çağatay et al., 2014), and (ix) palynological data (Van Zeist and Woldring, 1978). The major results will be summarized here.

Around 18,000 years B.P. at the beginning of deglaciation, the Lake Van level rised at its highest, i.e. 72 m above present (1720 m above present sea level) (Landmann et al., 1996b). The stable isotope record of carbonates from the uppermost terrace shows (Schöll, 1978) that the lake must have been frozen most of the year,

preventing the winter-convection. It is possible that reducing conditions became established at depth.

For the next 8000 years, temperatures increased gradually in agreement with the isotope pattern of ice cores (Dansgaard et al., 1971). Probably the lower terraces are an indication of the warming trend during the interstadials, e.g. the Bolling and Allerod. The carbonates in these lower terraces are still indicative of a water stand higher than today, but they clearly indicate that winter convection was already existed. Pollen data from the oldest lake sediments (10,000 years B. P.) show that herbaceous pollen types are dominant, in particular that of Chenopodiaceae (Van Zeist and Woldring, 1978). Landmann et al (1996a and 2011) claim that Lake Van was evaporated to almost dryness during about 14 ka BP. Later studies carried out within the framework of he ICDP PaleoVan project showed however, that although there was some lake level lowering around 14 ka BP, complete dryness did not take place in Lake Van (Litt et al., 2009, 2011; Stoeckhe et al., 2014; Çağatay et al., 2014).

During the Younger Dryas (YD) cold period (12.8-11.5 ka BP Dansgaard et al., 1993; Gulliksen et al., 1998; Kirby et al., 2002), faintly laminated clay silt with some event deposits were deposited at the Northern Basin site. Geochemical and minerological proxy records point to a cold and dry climate, high detrital influx and evaporite regression of the lake level (Çağatay et al., 2014). Also depending on the humidity and temperature received from the calculations, Lemcke and Sturm (1997) modelled the YD lake levels to be 45 to 90 m lower than the modern level.

The most dramatic events in the Holocene Lake Van history are the rapid lowering of lake level at about 10,000 years BP and the rise between 7000 and 6000 B. P. From about 10,000 to 6500 years BP the pollen record indicates a steppe vegetation. Chenopodiaceae, Ephedra and Artemisia played consecutively an important part (Van Zeist and Woldring, 1978) ; not temperature, but low humidity was the limiting factor for tree growth.

Degens et al. (1978) explain that minor changes in the relationship : air temperature, evaporation and river run off will cause a rapid lowering or rise in lake level. Another deciding factor is the morphology of the Tatvan basin with its steep sides. Since the lake responds to changes in climate simply by a changing of its

surface area, a reduction of this area beyond the -200 m isobath can only be achieved by a rapid lowering of the lake level. The same holds true when the lake surface area has to be increased in response to climatic changes. The morphometric pattern of the lake therefore appears to play an important role. Also they attribute the rapid lowering at about 10 ka BP and that during 14 ka BP (Landmann et al., 1996a, 2011) to the morphometric structure of the lake rather than to a dramatic change in climate. The climate continued in the dry, temperate regime that prevailed in the Lake Van region for several thousand years.

The turning point in the direction of forest vegetation was around 6500 years B.P. This is reflected in the rapid rise in lake level at this time and the subsequent gradual ascent towards the present. Again, the morphometric pattern of the lake floor had a decisive influence. This time, however, the significant increase in humidity as recorded in the pollen data for the time period 6400 to 3400 years B.P. (Van Zeist and Woldring, 1978) had only a minor effect on water depth. The lake surface could areally expand over a wide range without significantly altering the water depth. There was a dry period around 3 ka BP and low lake levels in Lake Van in other lakes in the near east (Litt et al., 2009, 2012).

The climate of the past 3000 years must have been relatively moist. The decline in oak pollen over the past 1000 to 2000 years may point to deforestation in the Lake Van region. The activity of man is also reflected in the increase in Plantago and Juglans polen percentages (Van Zeist and Woldring, 1978).

Archeologists suggest (Jacobi, 1960) that between 875 and *585* years B.P. (Kingdom of Urartu) the lake level stood higher by a few meters. It is believed that the stones of the fortress walls on the Rock of Van had been transported on water by rafts.

4. RESULTS AND INTERPRETATIONS

4.1. Introduction

This chapter presents the lithostratigraphic descriptions and micropaleantological, geochemical, isotopic and chronostratigraphic analyses of cores V08G04, V08G08, V08G11, and V08G16 recovered from Lake Van (Figure 4.1). As previously explained in Section 2.1, these cores were obtained from offhore Gevaş, offshore Van, entrance of the Erciş Gulf north of the Çarpanak Peninsula, and a small sublacustrine crater south west of the Tatvan Basin, respectively. The water depths of the core range from 65 to 86 m, and the core lengths from 0.75 m to 1.30 m (Table 2.1).
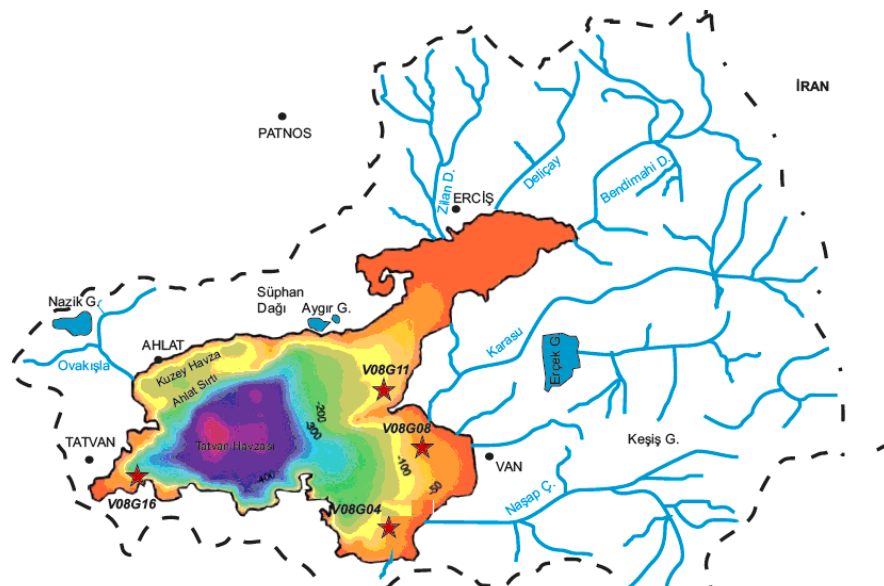
Figure 4.1 : Bathymetric and drainage area of Lake Van showing core locations.

Cores V08G04 and V08G08 were located in the same basin, east of Lake Van. Core V08G04 was collected in 70 m water depth and 5 km away from the center of Gevaş town, and 4 km away from the nearest shoreline. The core is also located 6.4 km away from the mouth of the Engil River, which is the second biggest river flowing into Lake Van.

Core V08G08 was collected in 80 m depth and 13 km away from the city center of Van. The nearest river flowing through this sampling location is Karasu River, and this location is about 8 km away from the entrance of the river.

Core V08G11 is located in the Erciş Basin, north of the Çarpanak Ridge and Island. Core V08G16 was collected in a small sublacustrine crater south west of the Tatvan Basin, which is related to the basaltic İncekaya volcanism dated ~80 ka BP (Sumita and Schmincke, 2013). There is no significant stream inflow into the crater location.

4.2 Lithostratigraphy and Micropaleontology

Core V08G04

This 1.30 m long gravity core was taken from 70 m water depth offshore from the mouth of Engil River (38°20'56.8"N, 43°02'57.5"E) (Figure 4.1). This is the longest core in this study. Lithological log of the core is given in Figure 4.2. Laminated structure of the core can be seen clearly in the optical and X-ray radiographic images. Although core V08G04 shows no sharp lithological change thoroughout the core, it consists of changes in color.

The top 5 cm of the core consists of watery mud (fluffy layer). From 5 cm to 20 cm of the core, the color changes progressively from dark to light beige. From 20 cm to 48 cm, beige to greenish brown mud with brown laminae can be seen. 48-49 cm interval is dark gray laminated band with thin beige lamina. Although 62-68 cm interval of the core is beige to brown faintly laminated mud, major part of the core from 49 cm to 80 cm, is reddish brown strongly laminated mud. From 80 cm to 106 cm, the color of mud changes into beige to brown with beige and brown laminae. Below 106 cm until the end of the core (130 cm) sediments are reddish brown to beige, laminated and banded mud having predominantly brown color.

The core includes only one ostracod species *Limnocythere inopinata* (Figure 4.3). The number of the octracods (*L. inopinata*) varies along the depth of the core, decreasing drastically between the interval from 95 cm to 120 cm (Figure 4.4).
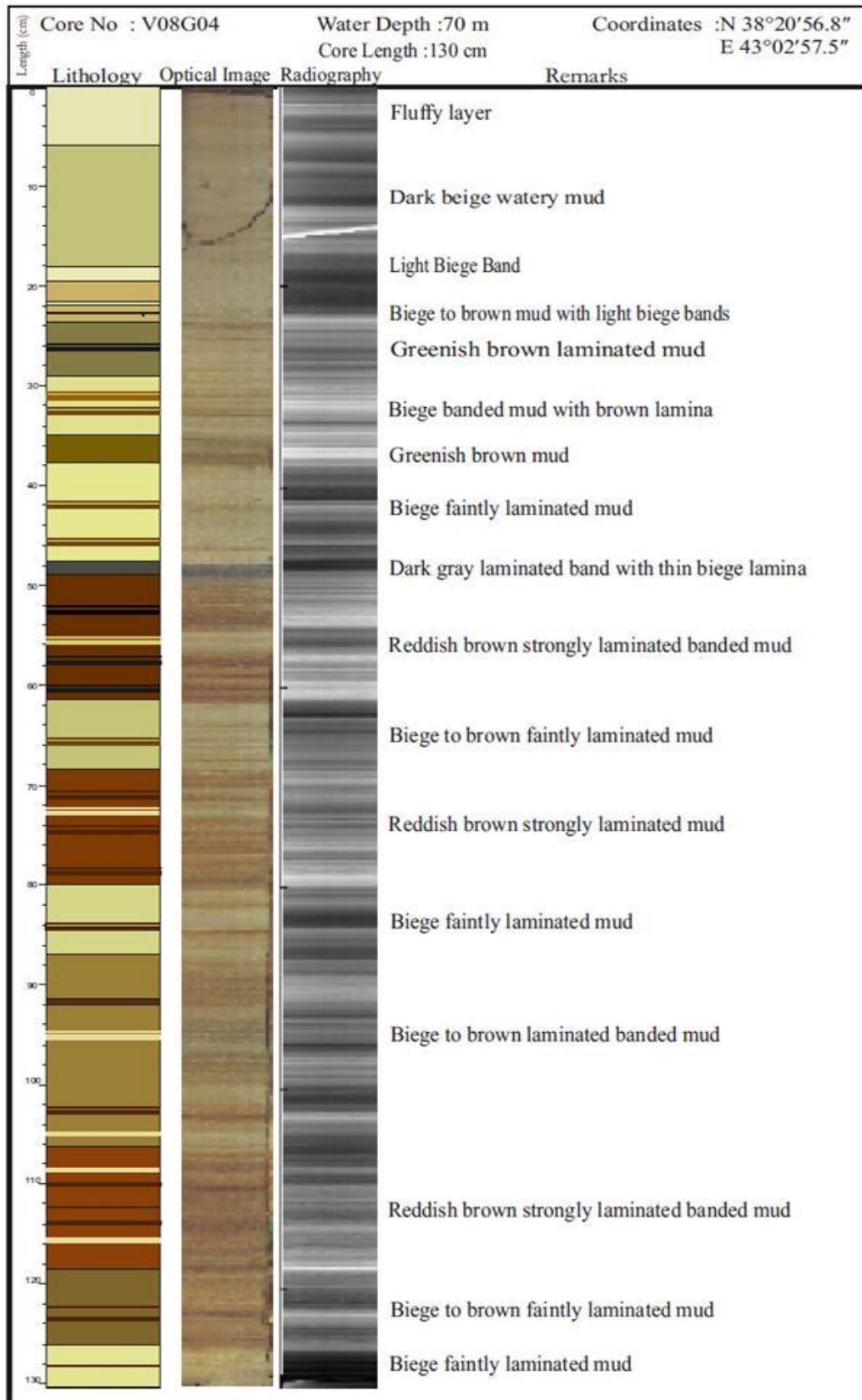
Figure 4.2 : Lithological description, optical and radiographic images of core V08G04.
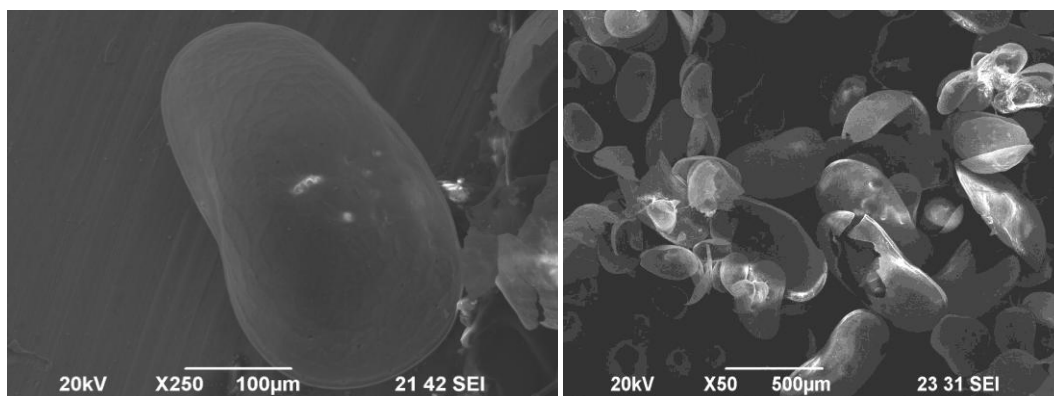
Figure 4.3 : Electron microscope (SEM) images of *Limnocythere inopinata* in core V08G04.
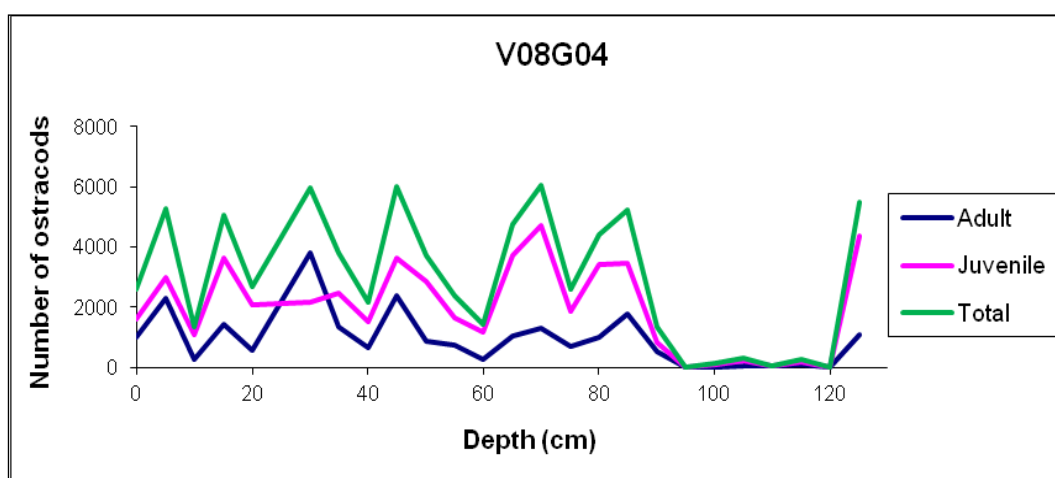
Figure 4.4 : Number of octracods (*L. inopinata*) per 10 cm^3 in core V08G04.

Core V08G08

This 0.75 m long gravity core was recovered from 70 m water depth offshore the city of Van (38°31'46.8"N, 43°09'04.7"E) (Figure 4.1). Lithological description of the core is presented in Figure 4.5. The laminated nature of core section can be seen clearly in the radiographic image. The top 6 cm of the core consists of watery mud. From 6 cm to 20 cm of the core, beige to brown laminated mud is present, with its lower boundary marked by the presence of a 1 cm thick gray lamina. The interval between 21cm and 40 cm is beige and beige to brown laminated and banded mud. Below 40 cm until the end of the core at 75 cm, the colour of the laminated and banded mud becomes darker, reddish brown and dark brown.

This core includes only one species of ostracoda which is *Limnocythere inopinata* (Figure 4.3). The number of the octracods (*L. inopinata*) are commonly low ranging

within a few hundred, except for 20 cm core depth at which the numbers increase to about 11,000 (Figure 4.6).
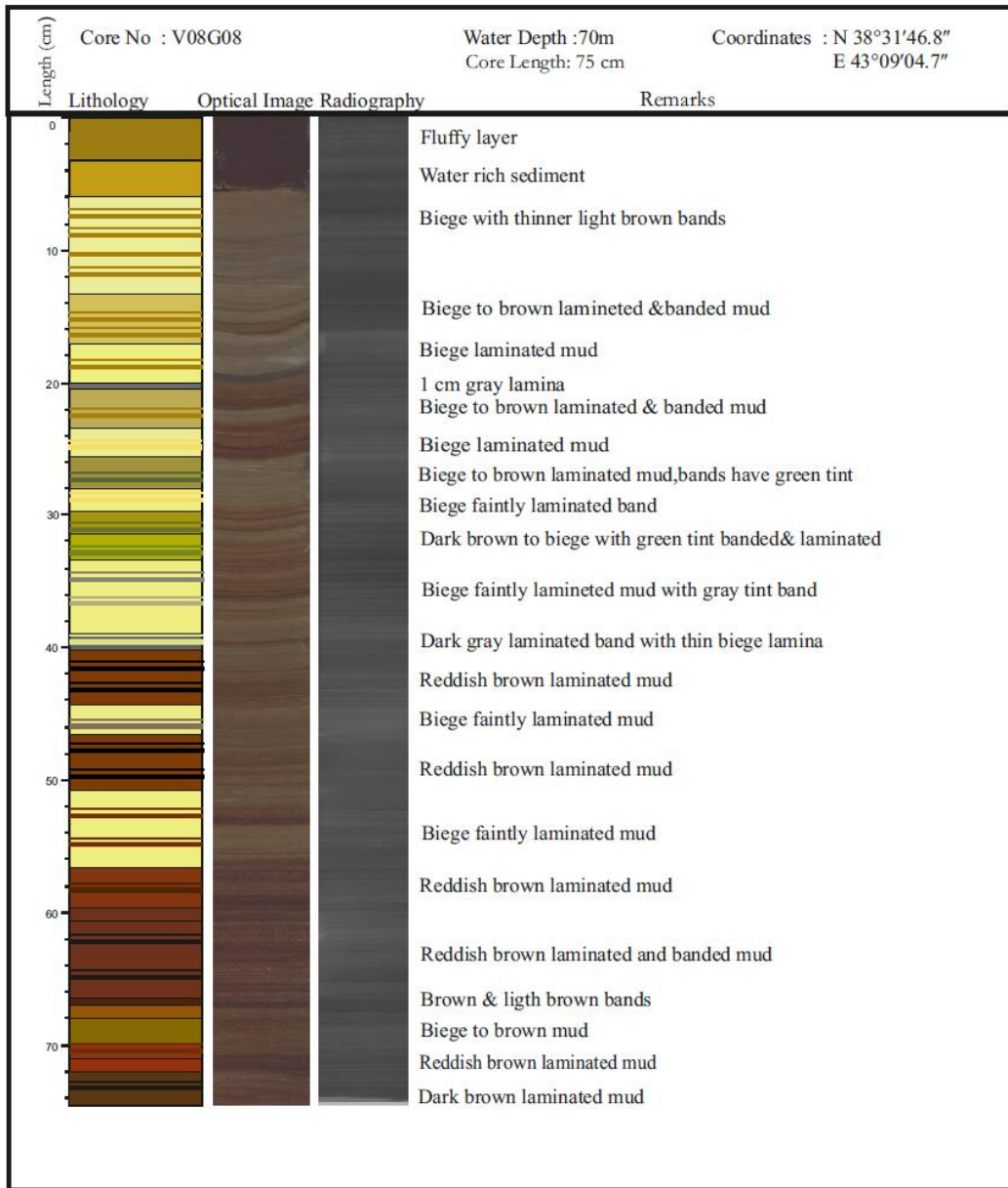
Figure 4.5 : Lithological description, optical and radiographic images of core V08G08.
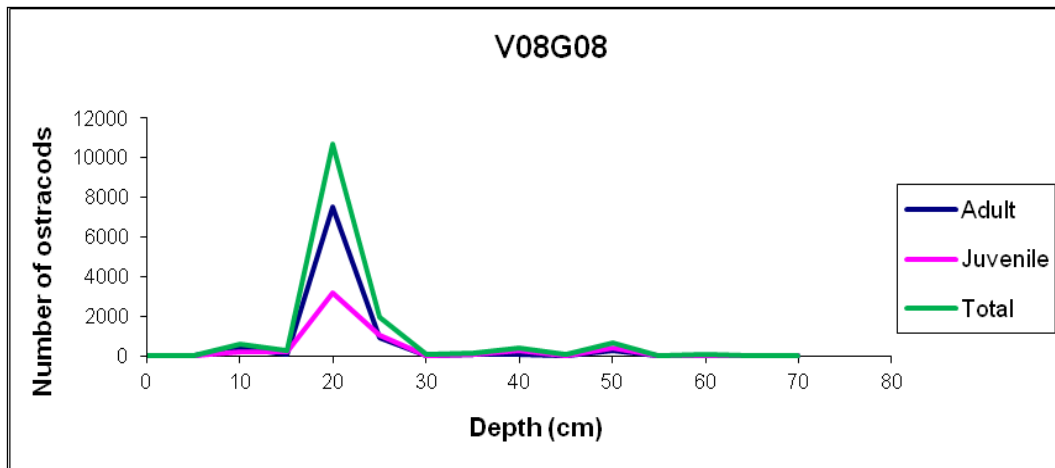
Figure 4.6 : Number of octracods (*L. inopinata*) per 10 cm^3 in core V08G08.

Core V08G11

This 0.90 m long core was taken from 86 m depth north of the Çarpanak Peninsula in the Erciş Gulf, Lake Van (38°40'15.3"N, 43°07'16.9"E) (Figure 4.1). Lithological description of the core is presented in Figure 4.7. The top 3 cm of the core consists of dark gray watery mud. From 3 cm to 9.5 cm of the core brown faintly laminated mud can be seen. Between 9.5-12 cms there is a beige to brown laminated band. From 12 cm to 19.5 cm brown faintly laminated mud is present. Below the brown laminated unit between 19.5 cm and 28 cm a reddish brown mud with dark gray laminae is observed. The underlying unit between 28 cm and 37.5 cm is a gray tinted biege and brown laminated mud. Between 37.5- 45.5 cm interval, there is brown laminated mud with dark gray laminae. From 45.5 cm to 75 cm green to brown, brown and reddish brown faintly laminated mud is observed. Between 75 cm and 80 cm gray faintly laminated mud is present. In the basal part of the core starting from 80 cm to base of core (90 cm) dark brown laminated mud is observed.

Similar with the other cores, core V08G11 includes only one species of ostracoda, *Limnocythere inopinata*, throughout the core. The number of the octracodas (*L. inopinata*) varies between 100 and 800 (Figure 4.8). The maximum ostracod abundance occurs at 17 cm core depth.
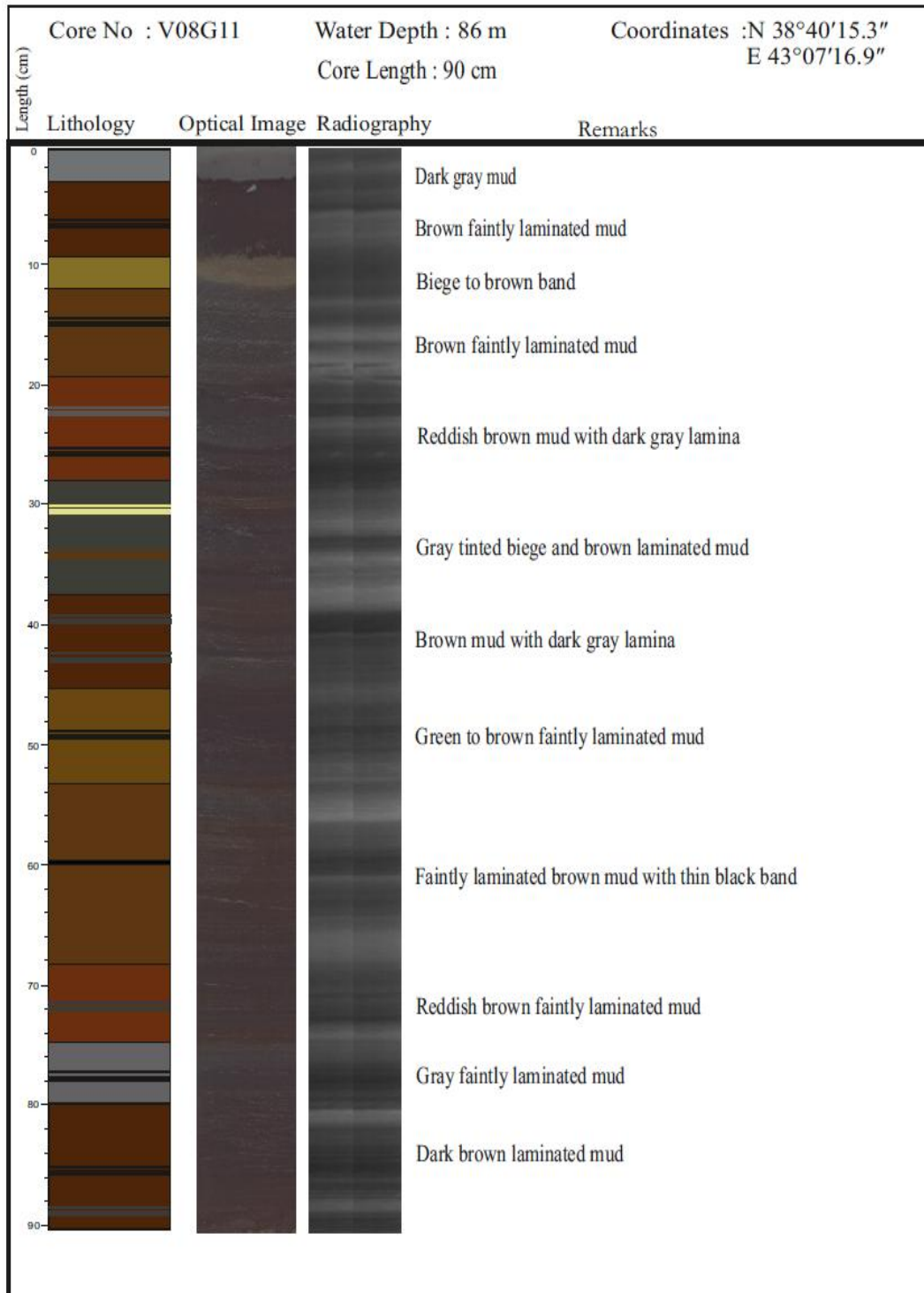
Figure 4.7 : Lithological description, optical and radiographic images of core V08G11.
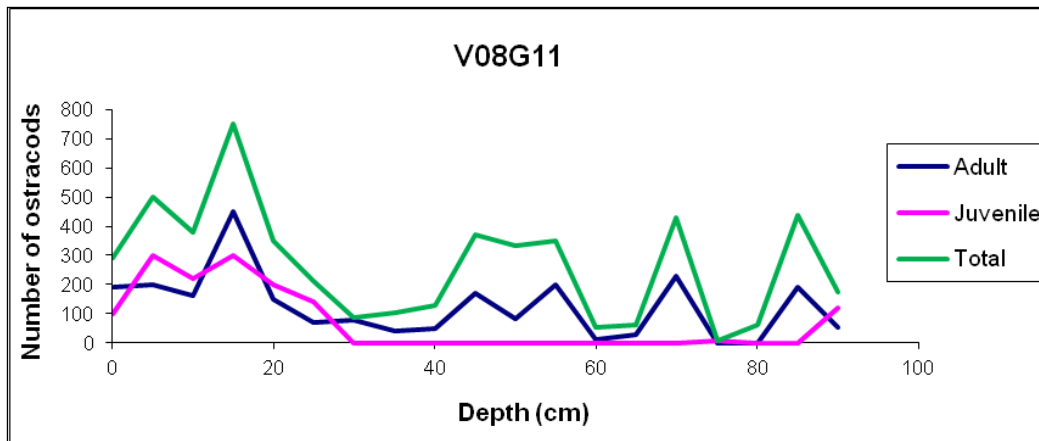
Figure 4.8 : Number of octracods (*L. inopinata*) per 10 cm^3 in core V08G11.

V08G16

Core V08G16 is 0.77 m long. It was recovered from 65 m water depth in a small crater south west of the Tatvan Basin (38°30'55.2"N, 42°25'35.2"E) (Figure 4.1). Lithological description of the core is presented in Figure 4.9. The top 6.5 cm of the core consists of fluffy layer with brown faintly laminated mud. From 6.5 cm to 14.5 cm reddish brown mud with beige laminae is observed. Between 14.5 and 16 cm, the core consists of a dark brown band without any distinct laminations. Different from the other cores, this core contians a 5 mm thick tephra layer between 19.5-20 cms. From 16 cm to 46 cm, of the sediments are mainly brown, and brown to green, faintly laminated mud. The core interval from 46 cm to the base of the core at 77 cm, consists of reddish brown to brown, laminated mud. Compared to the other three cores, this core is darker in color and the varves do not show significant changes throughout the core.

The core contains only one ostracoda species *Limnocythere inopinata*. The number of the octracodas (*L. inopinata*) ranges from less than 100 to 11,000 along the core length (Figure 4.10). The maximum numbers are observed at ~17 cm, 40 and 52 cm.

Length (cm)	Core No : V08G16	Water Depth :65 m	Coordinates :N 38°30′55.2″
		Core Lenght : 77 cm	E 42°25′35.2″
	Lithology	Optical Image Radiography	Remarks

Fluffy layer with brown faintly laminated mud

Reddish brown mud with biege lamina

Dark brown band without lamination

Thin black tephra

Laminated and banded brown mud

Brown to green faintly laminated mud

Reddish brown laminated mud

Brown laminated mud

Figure 4.9 : Lithological description, optical and radiographic images of core V08G16.
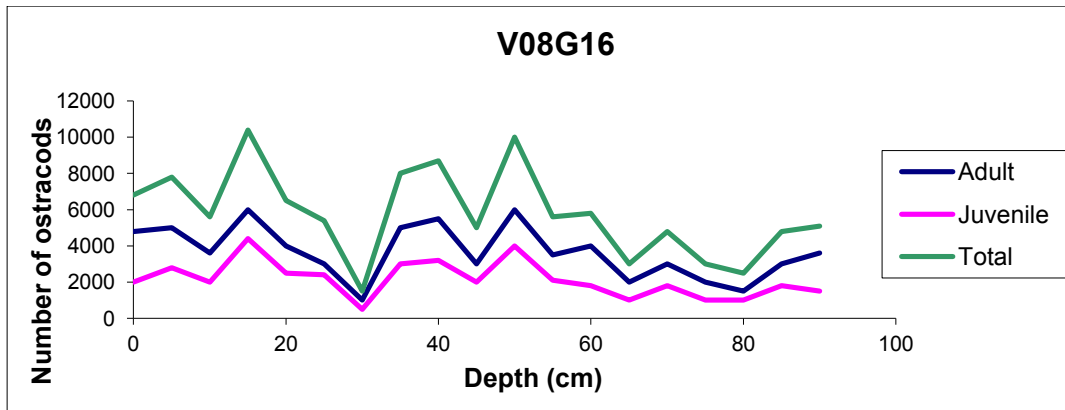
Figure 4.10 : Number of octracods (*L. inopinata*) per 10 cm³ in core V08G16.

4.3 Geochronolgy of Lake Van Sediments

In order to extract climate-related information from lake sediments, it is essential to establish a reliable chronology. The geochronology of Lake Van sediments determined by different techniques is presented in this section.

4.3.1 Geochronology of Lake Van sediments using [210]Pb-^{137}Cs dating: sedimentation (SR) and mass accumulation rates (MAR)

The excess (unsupported) ^{210}Pb, which is used for age calculation, was determined by the subtraction of the supported [210]Pb (obtained from [226]Ra with HPGe measurements) from the total [210]Pb (obtained from LSC measurements). The supported ^{210}Pb of each core, V08G04, V08G08, V08G11 and V08G16, has little or no variation with depth. The average of supported ^{210}Pb for each core was calculated as 21 Bq/kg[-1], 15 Bq/kg[-1], 18 Bq/kg[-1], 12 Bq/kg[-1] respectively.

On the other hand the profiles of unsupported ^{210}Pb of each core, especially in their upper parts, showed significant variation with depth (Figure 4.11). Based on this variation, the sediment age, sedimentation rates and mass accumulation rates were determined by the CRS model. This model is the most widely accepted model, which is predominatly characterized by constant direct atmospheric fallout (Appleby et al. 1990).
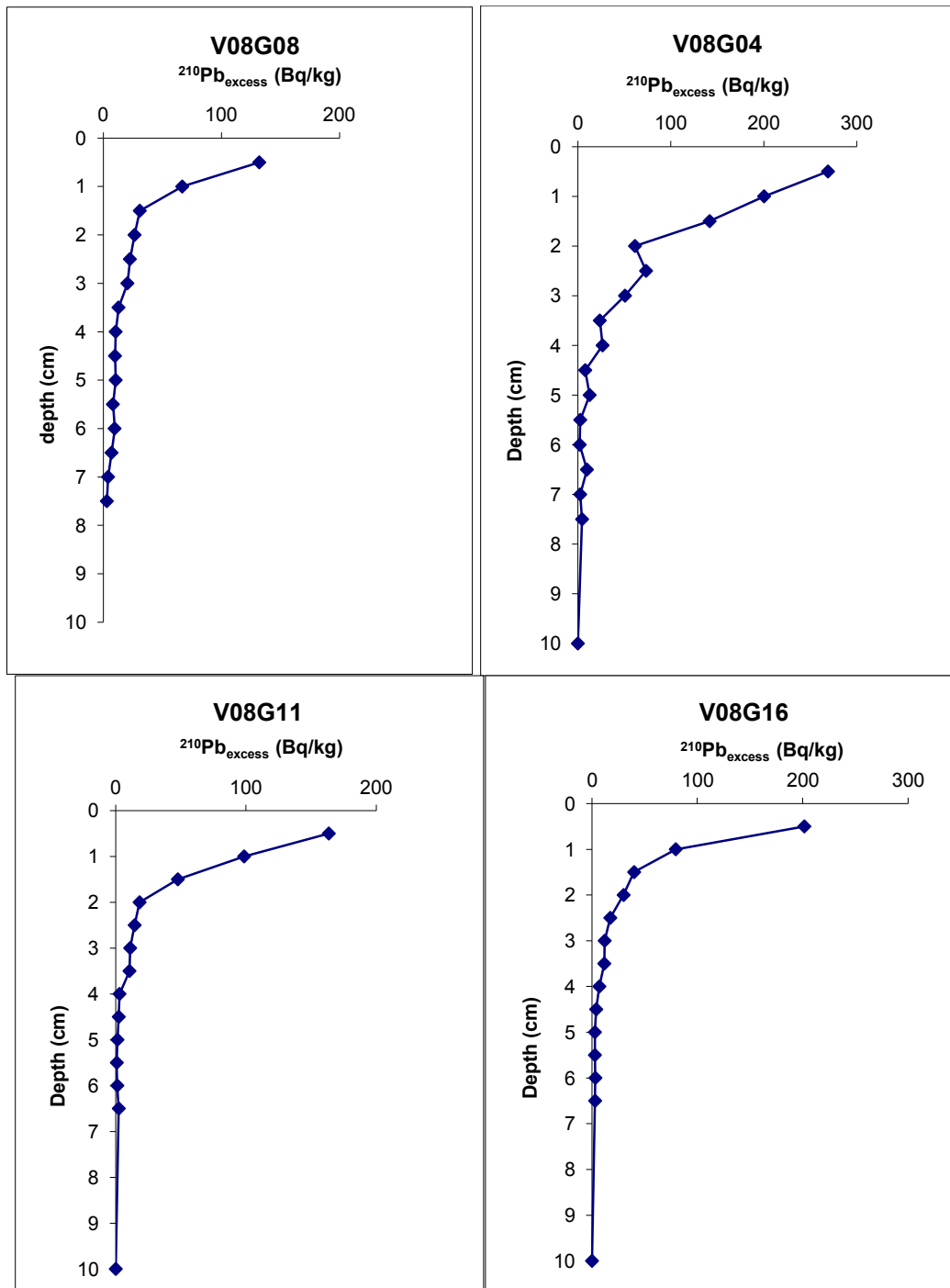
Figure 4.11 : Depth profile of unsupported (excess) ^{210}Pb in sediment samples of each core.

The results of calculations using CRS model for the ages, sedimentation and mass accumulation rates for the cores V08G04, V08G08, V08G11, and V08G16 are presented in Table 4.1, Table 4.2, Table 4.3, and Table 4.4, respectively.

Table 4.1 : Analysis data using CRS model to calculate the age, sedimentation and mass accumulation rates for upper part of core V08G04.

Depth (cm)	Porosity	Total ^{210}Pb (Bq.kg^{-1})	Supported ^{210}Pb (Bq.kg^{-1})	Unsupported ^{210}Pb (Bq.kg^{-1})	Estimated year	Date (year)	Sedimentation Rates (SR) (mm.y^{-1})	Mass Accumulation Rates (MAR) (kg.m^{-2}.y^{-1})
0-0.5	0,70	290,13	21	269,13	4,61	2003	0,54	0,39
0.5-1	0,72	221,33		200,33	16,94	1991	0,52	0,37
1-1.5	0,72	162,79		141,79	30,11	1978	0,50	0,36
1.5-2	0,75	82,43		61,43	44,18	1964	0,45	0,34
2-2.5	0,77	94,37		73,37	54,48	1954	0,46	0,32
2.5-3	0,75	71,71		50,71	61,68	1946	0,49	0,33
3-3.5	0,71	44,58		23,58	72,12	1936	0,49	0,34
3.5-4	0,70	47,59		26,59	84,49	1924	0,47	0,34
4-4.5	0,73	28,93		7,93	98,06	1910	0,46	0,33
4.5-5	0,73	33,70		12,70	109,11	1899	0,46	0,33
5-5.5	0,70	23,55		2,55	117,96	1890	0,47	0,34
5.5-6	0,68	23,01		2,01	128,99	1879	0,47	0,35
6-6.5	0,69	30,74		9,74	133,76	1874	0,49	0,37
6.5-7	0,71	23,50		2,50	149,68	1858	0,47	0,36
7-7.5	0,68	25,55		4,55	177,56	1830	0,42	0,33

Table 4.2 : Analysis data using CRS model to calculate the age, sedimentation and mass accumulation rates for upper part of core V08G08.

Depth (cm)	Porosity	Total ^{210}Pb (Bq.kg^{-1})	Supported ^{210}Pb (Bq.kg^{-1})	Unsupported ^{210}Pb (Bq.kg^{-1})	Estimated year	Date (year)	Sedimentation Rates (SR) (mm.y^{-1})	Mass Accumulation Rates (MAR) (kg.m^{-2}.y^{-1})
0-0.5	0,71	147,15	15	132,15	3,10	2005	0,68	0,60
0.5-1	0,69	81,88		66,88	12,64	1995	0,65	0,57
1-1.5	0,71	45,91		30,91	25,93	1982	0,58	0,49
1.5-2	0,70	41,47		26,47	33,17	1975	0,60	0,52
2-2.5	0,69	37,51		22,51	39,03	1969	0,64	0,56
2.5-3	0,70	35,41		20,41	45,87	1962	0,65	0,57
3-3.5	0,74	27,84		12,84	53,49	1955	0,65	0,55
3.5-4	0,73	25,46		10,46	59,22	1949	0,68	0,56
4-4.5	0,71	24,90		9,90	64,17	1944	0,70	0,58
4.5-5	0,68	25,45		10,45	70,05	1938	0,71	0,60
5-5.5	0,67	23,11		8,11	79,49	1929	0,69	0,60
5.5-6	0,69	24,56		9,56	91,94	1916	0,65	0,57
6-6.5	0,72	22,00		7,00	108,16	1900	0,60	0,52
6.5-7	0,74	19,00		4,00	131,75	1876	0,63	0,54
7-7.5	0,73	18,00		3,00	161,05	1847	0,64	0,56

Table 4.3 : Analysis data using CRS model to calculate the age, sedimentation and mass accumulation rates for upper part of core V08G11.

Depth (cm)	Porosity	Total ^{210}Pb (Bq.kg^{-1})	Supported ^{210}Pb (Bq.kg^{-1})	Unsupported ^{210}Pb (Bq.kg^{-1})	Estimated year	Date (year)	Sedimentation Rates (SR) (mm/year)	Mass Accumulation Rates (MAR) (kg.m^{-2}.y^{-1})
0-0.5	0,67	150,15	18	132,15	10,56	1997	0,44	0,49
0.5-1	0,70	84,88		66,88	26,11	1982	0,38	0,37
1-1.5	0,69	48,91		30,91	44,41	1964	0,34	0,32
1.5-2	0,70	44,47		26,47	63,61	1944	0,31	0,30
2-2.5	0,69	40,51		22,51	77,73	1930	0,32	0,30
2.5-3	0,68	38,41		20,41	88,95	1919	0,34	0,32
3-3.5	0,69	30,84		12,84	102,42	1906	0,34	0,33
3.5-4	0,68	28,46		10,46	119,74	1888	0,33	0,32
4-4.5	0,69	27,90		9,90	140,35	1868	0,32	0,31
4.5-5	0,71	28,45		10,45	152,44	1856	0,33	0,31
5-5.5	0,71	26,11		8,11	163,29	1845	0,34	0,32
5.5-6	0,68	27,56		9,56	171,63	1836	0,35	0,33
6-6.5	0,66	25,00		7,00	184,79	1823	0,35	0,33

Table 4.4 : Analysis data using CRS model to calculate the age, sedimentation and mass accumulation rates for upper part of core V08G16.

Depth (cm)	Porosity	Total ^{210}Pb (Bq.kg^{-1})	Supported ^{210}Pb (Bq.kg^{-1})	Unsupported ^{210}Pb (Bq.kg^{-1})	Estimated year	Date (year)	Sedimentation Rates (SR) (mm/year)	Mass Accumulation Rates (MAR) (kg.m^{-2}.y^{-1})
0-0.5	0,69	213,48	12	201,48	10,82	1997	0,46	0,44
0.5-1	0,72	91,48		79,48	26,14	1982	0,38	0,33
1-1.5	0,68	52,00		40,00	42,92	1965	0,35	0,32
1.5-2	0,69	42,00		30,00	57,98	1950	0,34	0,32
2-2.5	0,68	29,36		17,36	70,42	1938	0,36	0,33
2.5-3	0,70	24,00		12,00	84,01	1924	0,36	0,33
3-3.5	0,70	23,64		11,64	95,29	1913	0,37	0,34
3.5-4	0,73	19,00		7,00	108,58	1899	0,37	0,33
4-4.5	0,75	16,00		4,00	121,33	1887	0,37	0,32
4.5-5	0,72	14,76		2,76	130,24	1878	0,38	0,33
5-5.5	0,70	14,78		2,78	139,07	1869	0,40	0,34
5.5-6	0,69	15,25		3,25	150,87	1857	0,40	0,35
6-6.5	0,70	14,97		2,97	174,23	1834	0,37	0,33

The sediments layers of 7-7.5 cm in core V08G04 , 7-7.5 cm in core V08G08 (cm), 6-6.5 cm in core V08G11 , and 6-6.5 cm in core V08G16 were dated to represent the year 1830, 1847, 1823, and 1834, respectively. The sedimentation rates for core V08G04, V08G08, V08G11, and V08G16 are variable between 0.42-0.54 mm.y^{-1},

0.58-0.71 mm.y^{-1}, 0.31-0.44 mm.y^{-1}, and 0.34-0.46 mm.y^{-1} respectively. These values are comparable with the average annual sedimentation rate of 0.5 mm.y^{-1} in Lake Van found by Landmann et al. (1996a). MAR values for core V08G04, V08G08, V08G11, and V08G16 range between 0.33-0.39 kg.m^{-2}.y^{-1}, 0.49-0.60 kg.m^{-2}.y^{-1}, 0.30-0.49 kg.m^{-2}.y^{-1}, 0.32-0.44 kg.m^{-2}.y^{-1} respectively.

The results of the study showed that the highest sedimentation and mass accumulation rates belongs to the core V08G08 (0.6-0.7 mm.year^{-1}). This is probably due to anthropogenic activities in the provincial city of Van as well as the river input with a relatively large drainage area.

^{137}Cs results were also used as an independent method to confirm our ^{210}Pb models. A good age agreement obtained between the ^{137}Cs activity results and ^{210}Pb dates calculated by the CRS model.

The activity profile of ^{137}Cs (Figure 4.12) in the four different cores in Lake Van show a good correlation with the corresponding ^{210}Pb ages, according to the history of atmospheric deposition of radionuclides derived from nuclear weapons testing and the Chernobyl accident. The first detection of ^{137}Cs in the sediment cores corresponds to around 1953, which closely matches the early 1950s increase in total fission yields from the explosions (Carter and Moghissi, 1977). The yield and number of nuclear detonations per year peaked in 1962, resulting in extensive deposition of radionuclides in the Northern Hemisphere in 1963, the year the nuclear weapons Limited Test Ban Treaty was signed (Carter and Moghissi, 1977; Appleby, 2001). The elevated amounts of radioactivity released in the 1960s were recorded in the Lake Van sedimentary record.

The downcore profile of ^{137}Cs also reveals a peak in activity closer to the surface ^{210}Pb-dated at around 1986. The timing of this peak is consistent with fallout resulting from the release of radioactivity that followed the Chernobyl NP reactor accident in Ukraine. At some European sites, the deposition of Chernobyl ^{137}Cs provided another datable horizon in the sediments, characterized in some cases by an even greater inventory than that resulting from the bomb tests (Dominik and Span, 1992; Ehlers et al., 1993; Callway et al., 1996; Gevao et al., 1997).
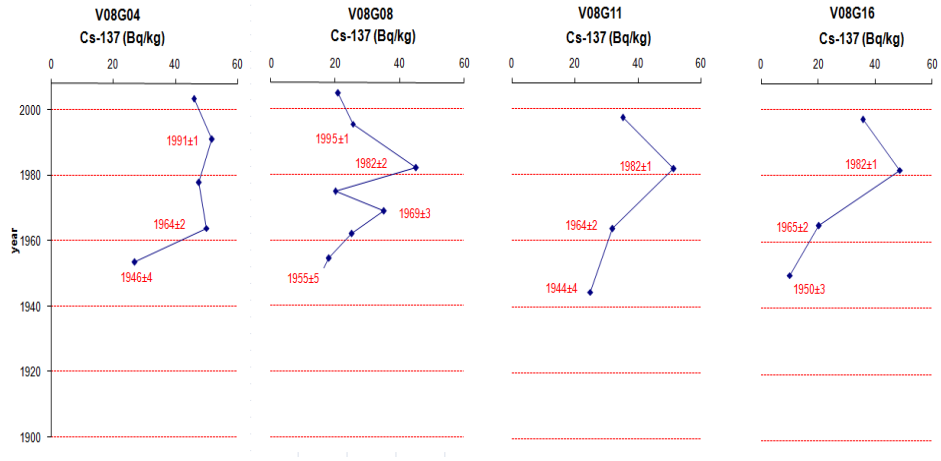
Figure 4.12 : The activity profile of ^{137}Cs in four different cores in Lake Van.

4.3.2 Varve counting and the age model

Varve counting using the radiography and the algorithm developed by Damcı and Çağatay (2015) in the Lake Van cores was used as an independent dating method. Figure 4.13 shows the varve counting results of core V08G04. According to results of varve counting process, core V08G04 which is 1.30 m in length has a total of 11644 laminae, representing about the last 3500 years. The 0.75 m long Core V08G08 has a total of 5614 laminae, deposited during the last 1800 years. Core V08G11 is 0.90 m long and has a total of 7780 laminae, corresponding to a record of about 2600 years. Finally, 0.77 m long core V08G16 includes 5890 laminae and represents the last 1900 years. Figure 4.14 shows the radiographic images and approximate ages of the all cores.
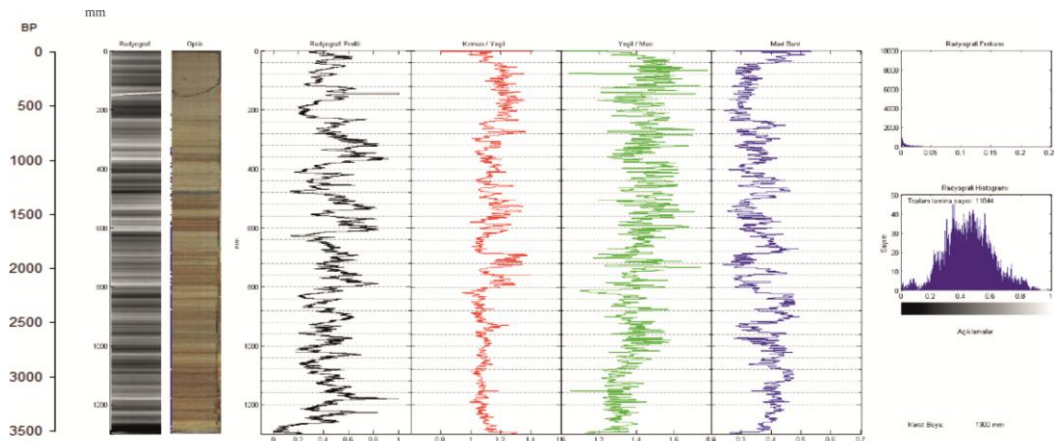
Figure 4.13 : Varve counting results of core V08G04**.**
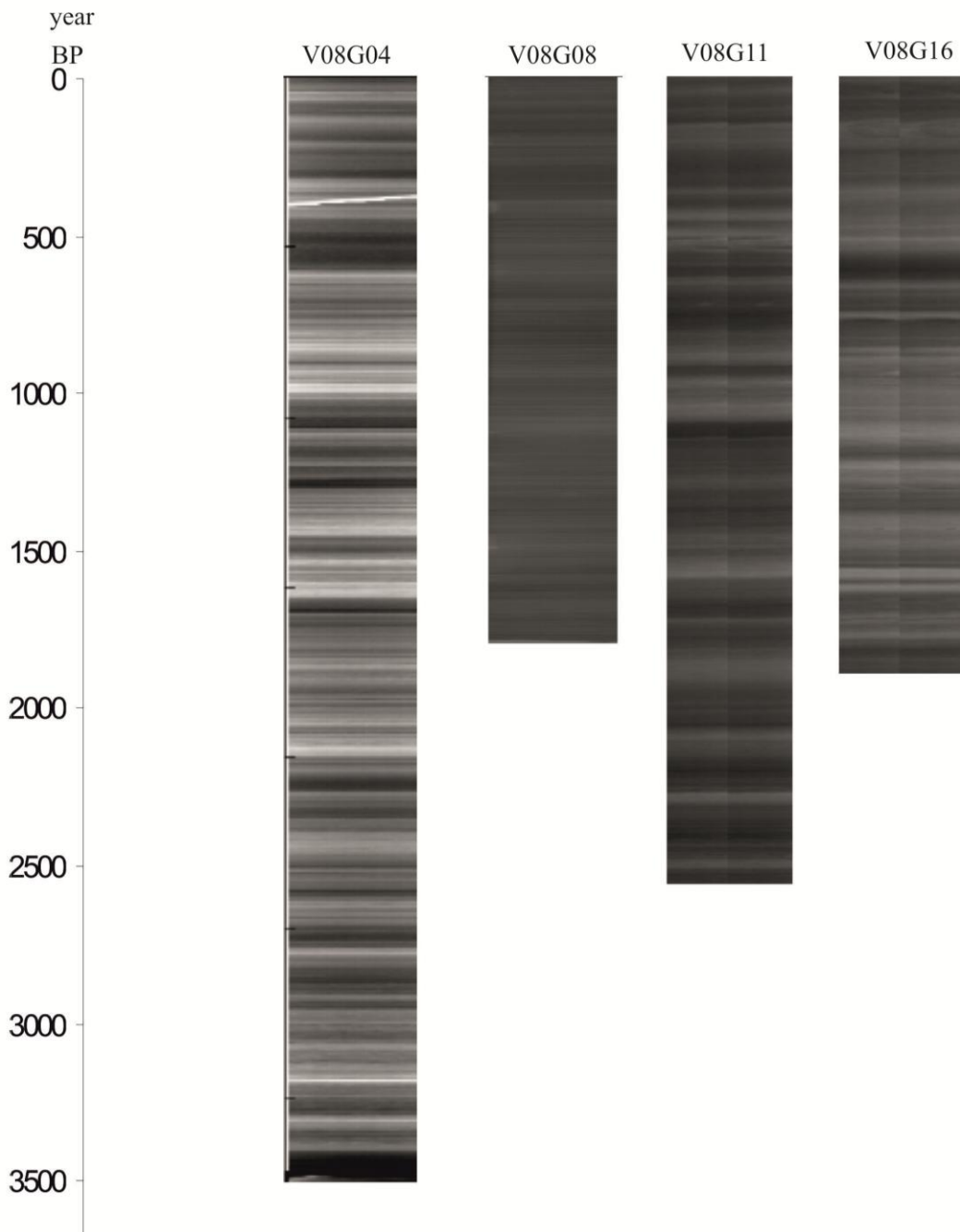
Figure 4.14 : Radiographic images and approximate ages of all cores.

A good agreement is obtained between the varve counts and ^{210}Pb dates calculated by the CRS model, validating radionuclide dating technique for the upper 7-8 cm of the Lake Van sedimentary column (Figure 4.15 and Tables 4.5-4.8). We could have used the varve chronology alone to date the entire sedimentary sections in our Lake Van cores. However our initial goal was to apply the ^{210}Pb technique to date recent sediments and use the varve counting to extend the chronology beyond the limit of the ^{210}Pb method (100–150 yr). Therefore, CRS model ages were used to date the

uppermost 7-8 cm of the sediment column, while the varve chronology was applied for the rest of the sediment cores . The use of varve counts instead of the CRS model in the top 7-8 cm of the core does not change the age estimates significantly, as can be seen in Tables 4.5-4.8. Increasing uncertainity values (k=1) of ^{210}Pb ages through downcore caused by the decreasing ^{210}Pb activity concentrations towards the lower parts of the core (Tables 4.5-4.8).

Considering the very good agreement between varve counting and radionuclide (^{210}Pb and ^{137}Cs) dating methods (Figure 4.13 and Tables 4.5-4.8), the varve counting method was used with confidence for the age-depth model of the cores, which allowed to extend the age dating beyond the limits of the radionuclide techniques (up to 150 years) (Figure 4.16). The varve age-depth model indicates a uniform sedimentation rates about 0.34 mmy^{-1} for the last 3500 years BP, 0.37 mmy^{-1} for the last 1800 years BP, 0.34 mmy^{-1} for the last 2600 years BP, and 0.38 mmy^{-1} for the last 1900 years BP for cores V08G04, V08G08, V08G11, and V08G16 respectively.

However, there are some slight increases before 2800 years BP, 1300 years BP, 2000 years BP, and 1400 years BP for cores V08G04, V08G08, V08G11, and V08G16 respectively. (Figure 4.16).

Table 4.5 : Comparison of ^{210}Pb (CRS model) and varve chronologies for core V08G04.

Depth (cm)	CRS Model (^{210}Pb) Date	Varve Date
0-0.5	2003±0	2002±0.1
0.5-1	1991±1	1994±0.1
1-1.5	1978±2	1979±0.2
1.5-2	1964±2	1965±0.3
2-2.5	1954±3	1951±0.4
2.5-3	1946±4	1942±0.5
3-3.5	1936±5	1930±0.6
3.5-4	1924+6	1919±0.7
4-4.5	1910±10	1900±0.8
4.5-5	1899+11	1889±1.0
5-5.5	1890±12	1878±1.1
5.5-6	1879±13	1865±1.2
6-6.5	1874±13	1857±1.3
6.5-7	1858±15	1842±1.4
7-7.5	1830±18	1811±1.5

Table 4.6 : Comparison of ^{210}Pb (CRS model) and varve chronologies for core V08G08.

Depth (cm)	CRS Model (^{210}Pb) Date	Varve Date
0-0.5	2005±0	2003±0.0
0.5-1	1995±1	1998±0.1
1-1.5	1982±2	1985±0.2
1.5-2	1975±3	1978±0.2
2-2.5	1969±3	1971±0.2
2.5-3	1962±4	1956±0.3
3-3.5	1955±5	1948±0.3
3.5-4	1949±6	1938±0.4
4-4.5	1944±7	1930±0.4
4.5-5	1938±8	1927±0.4
5-5.5	1929±10	1915±0.5
5.5-6	1916±12	1900±0.5
6-6.5	1900±15	1879±0.5
6.5-7	1876±15	1850±0.6
7-7.5	1847±18	1816±0.6

Table 4.7 : Comparison of ^{210}Pb (CRS model) and varve chronologies for core V08G11.

Depth (cm)	CRS Model (^{210}Pb) Date	Varve Date
0-0.5	1997±0	2000±0.0
0.5-1	1982±1	1984±0.1
1-1.5	1964±2	1970±0.1
1.5-2	1944±4	1952±0.2
2-2.5	1930±5	1937±0.2
2.5-3	1919±6	1926±0.2
3-3.5	1906±8	1916±0.3
3.5-4	1888±11	1895±0.5
4-4.5	1868±14	1879±0.6
4.5-5	1856±15	1870±0.8
5-5.5	1845±18	1858±1.0
5.5-6	1836±19	1845±1.3
6-6.5	1823±20	1834±1.6

Table 4.8 : Comparison of ^{210}Pb (CRS model) and varve chronologies for core V08G16.

Depth (cm)	CRS Model (^{210}Pb) Date	Varve Date
0-0.5	1997±0	1997±0.0
0.5-1	1982±1	1987±0.1
1-1.5	1965±2	1975±0.1
1.5-2	1950±3	1963±0.1
2-2.5	1938±4	1948±0.2
2.5-3	1924±6	1933±0.3
3-3.5	1913±7	1923±0.3
3.5-4	1899±9	1908±0.4
4-4.5	1887±10	1896±0.5
4.5-5	1878±12	1879±0.7
5-5.5	1869±14	1866±0.9
5.5-6	1857±15	1848±1.0
6-6.5	1834±19	1833±1.3
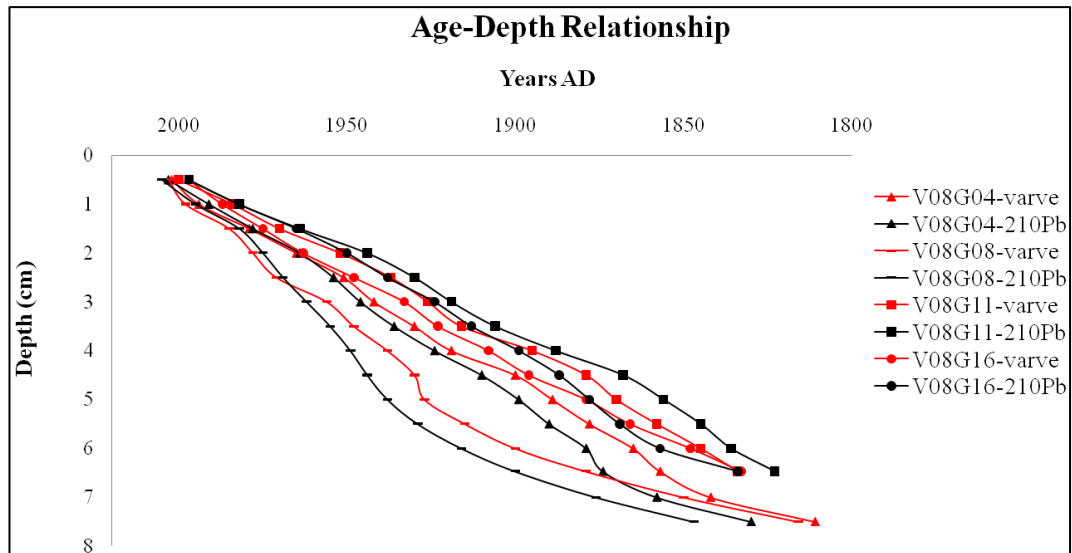
Figure 4.15 : ^{210}Pb and varve based age-depth model for upper part of cores V08G04, V08G08, V08G11, and V08G16.
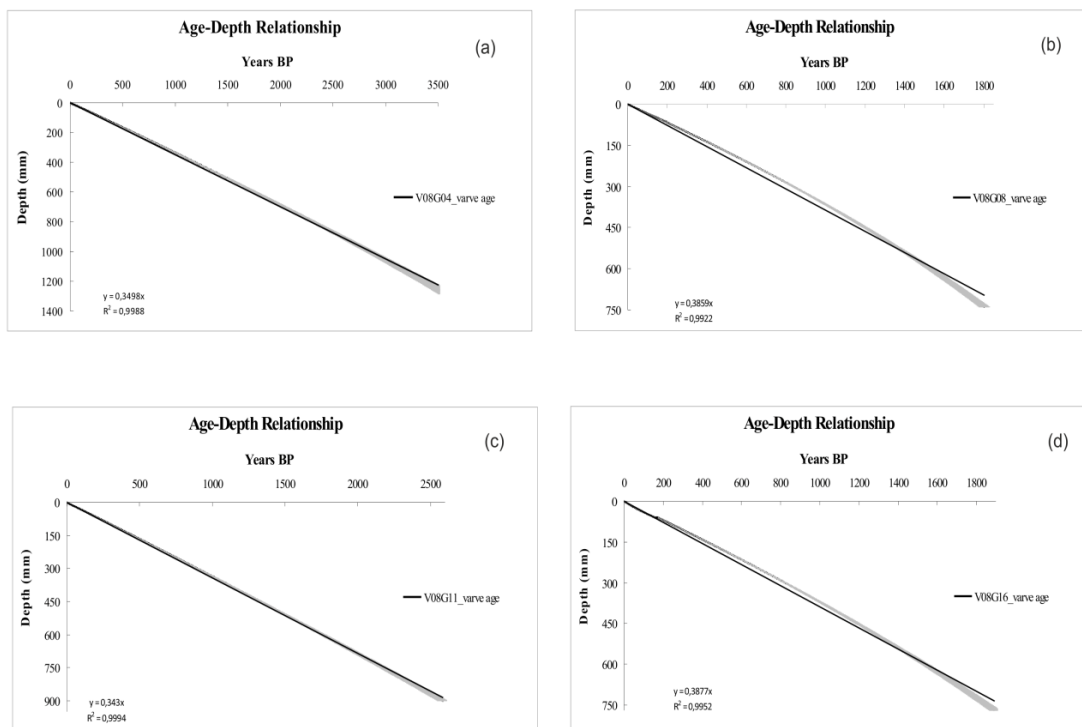
Figure 4.16 : Age (varve years)-depth model for cores (a)V08G04, (b) V08G08, (c) V08G11, (d) V08G16. Gray bands indicate 1σ error range.

4.3.3 Geochronology of Lake Van sediments with ^{14}C and reservoir age of Lake Van

Four ^{14}C ages obtained from the analysis of bulk organic carbon of sediment samples core V08G04 are listed in Table 4.9. These ages differ widely from the varve ages at the same core depth. The varve ages were used to calculate the corresponding

radiocarbon ages using Calib Radiocarbon Calibration Execute Version 6.0 html (Reimer et al., 2009) using an iterative procedure (Makaroğlu et al., 2015). The uncalibrated ages obtained from varve ages are compatible with each other, showing younging towards the core top, except for the third sample located at 60-61 cm core depth (Table 4.9). However, there the AMS radiocarbon ages are considerably older than the varve ages of the radiocarbon dated horizons, indicating to the presence of reservoir age of the dated bulk organic carbon in the lake van samples.

Table 4.9 : [14]C AMS results, calibrated ^{14}C ages and calculated reservoir ages.

Sample	Depth	AMS Measured [14]C Age	Uncalibrated [14]C Age from Varve Age	Varve Age	Calculated Reservoir Age
	(cm)	(years BP)	(years BP)	(years BP)	(years BP)
V08G04	18-19	2800± 110	2958 ±137	557±21	2401 ±139
V08G04	33-34	3150±90	3364 ±102	999±21	2364 ±104
V08G04	60-61	2790±140	2963 ±173	1772±20	1190 ±174
V08G04	80-81	5350±170	6122+172	2325±19	3796 ±173

The ^{14}C reservoir age in lakes is common because of the dilution of the atmospheric $\Sigma^{14}CO_2$ with "dead" ΣCO_2 from the carbonate dissolution in their catchment areas (Broecker and Olson 1961; Stein et al. 2004; Zhou et al. 2009; Soulet et al. 2011). As a result, the radiocarbon content of lake waters are always depleted compared to that of the contemporary atmosphere. Using our AMS radiocarbon ages, and comparing them with the corresponding varve ages, we obtain reservoir ages ranging from ~1200 to 3800 years (Table 4.9).

4.3.4 Stratigraphic correlation of cores using MS values

The magnetic susceptibility is widely used a parameter for stratigraphic correlation of cores recovered from different sites in a given marine or lake environment, because it is primarily indicative of the content of magnetic minerals, but also of the grain size and composition of the magnetic material (Thompson and Oldfield, 1986; Hilton, 1987; King et al., 1982). Therefore, we used this parameter for stratigraphic correlation of our lake Van cores. Core V08G08 recoverd offshore from the Van City is different from the other three cores in having about ten-fold lower MS values. Considering the geology of the catchment area it is difficult to explain these low MS

values. Karasu River discharging into the site of core V08G08 drains mostly the old lake terrace deposits which are derived mainly from the ophiolitic rocks that contains ferro-magnetic minerals. The only probable reason for the low MS values could be the diagenetic reduction of ferro-magnetic minerals at this site. Such a reduction process would be favoured by the relatively high TOC contents in this core, which range from 4 to 8 % and increase downwards (Fig 4.17).

We can wiggle-match some parts of the MS profiles as shown in Figure 4.17. The correlations between the cores are more reasonable for the upper parts corresponding to the last 700 years, but difficult for the older, lower parts. The difficulties in the correlations are probably because of diagenesis and in part to local effects mainly due to the differences in the lithology of the catchment areas close to the core sites.
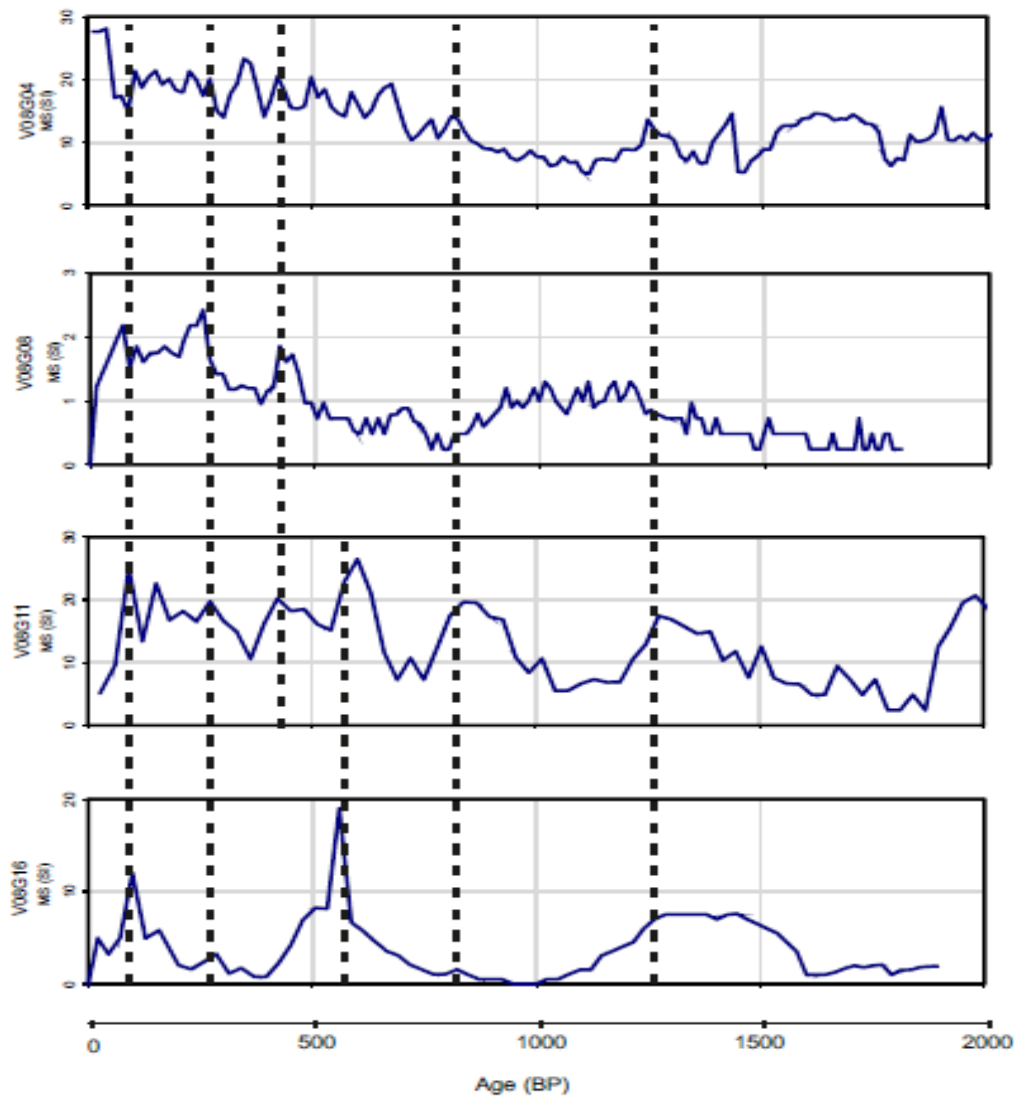
Figure 4.17 : Stratigraphic correlation of cores according to MS values.

4.4 Multi Proxy Analysis

4.4.1 Introduction

Multi-proxy studies are making major contributions to palaeoecology and palaeolimnology. Each proxy reflects the environment at its own spatial scale, taking its place in the network of interactions that comprise an ecosystem, thus providing insights into different facets of an ecosystem. Although some proxies can be used to reconstruct climatic variables directly, most approaches are indirect, and their use requires an understanding of the relationship between the sediment record and water-column processes and between water-column processes and climate.

For the investigation of climate records in sediment cores, different geochemical and physical proxies are used. Geochemical element analysis provide high resolution records of trace elemental concentrations within the sediment and give information about the deposition processes due to evaporation, input of climate-related detrital material, as well as bottom water oxygen conditions in lakes. For instance, Mg/Ca and Sr/Ca ratio gives information about changes in temperature and evaporation/precipitation ratio (Beck et al., 1992; Rosenthal and Boyle, 1993; Wefer et al., 1999); K/Ca, Ca/Ti ratio indicates changes in input of detrital mineral. Especially titanium, little affected by diagenetic processes, is likely related with clay minerals and is a consistent indicator of variable input of terrestrial detrital sediment (Jansen et al., 1992; Yarincik et al., 2000); redox sensitive elements such as Mn, Mo, U, S give important information about changes in the amount of oxygen in the bottom water (Calvert and Pedersen, 1993; Dean et al., 1994, 1997, 1999; Rosenthal et al., 1995; Crusius et al., 1996; Crusius and Thompson, 2000; Anderson et al., 1998; Adelson et al., 2001; Ca record provides a hydrological record of the basin (Boyle, 2001). Sedimentary Ca in many lake systems reflects changes from an open to closed basin during wet to dry periods with calcite reaching saturation during dry periods. In permanently closed basins calcite is always at saturation. This implies that increases in the Ca content of the sediment may be associated with heavy rainfall, increased weathering, and greater fluvial deposition. Fe, Ti, and increased rates of sedimention also reflect greater erosion of the watershed and deposition into the basin. Regional volcanic tephras and other volcaniclastics are in general enriched

in all lithophile elemental concentrations (Fisher and Wefer, 1999; Wefer et al., 1999; Cohen, 2003; Thomson et al., 2006).

Total organic carbon (TOC) is an important proxy for paleo-lake productivity. The amount and type of sedimentary organic matter reflects a dynamic between organic matter sources, production, transport, deposition, and preservation (Meyers and Teranes, 2001). Nitrogen compounds (particularly ammonia and nitrate) are essential bionutrients that can limit productivity in both marine and lacustrine environments. Their prevalence and forms in the sedimentary record provide information on paleoecology. The production and consumption of these essential nutrients depends not only on the source of materials from the watershed, but also the ecological dynamics of the lake water.

Total organic nitrogen (TON) is subject to some of the same influences as organic carbon and is the second largest constituent of total organic matter. This implies a similarity in the responses of OC and ON to changes in productivity and overall biomass. Yet differences in organic matter source commonly result in fluctuations of C/N ratios. This is due to distinct bulk organic matter composition of algae and vascular plants. Algae do not form cell walls made of cellulose and also produce a higher degree of proteins (rich in nitrogen). This causes algae to have C/N ratios ranging from 4-10 while vascular plants rich in cellulose will have C/N ratios of 20+ (Meyers and Teranes, 2001). This compositional difference allows the C/N ratios of sediment organic matter to reflect varying concentrations of algal versus plant material.

Physical measurements such as P-Wave velocity, magnetic susceptibility, density, resistivity, impedance, and fractional porosity of sedimentary records can be assessed by Multi Sensor Core Logger (MSCL) analysis. Physical changes such as detrital input depending on climate, water salinity depending on environment, and grain size changes can be inferred from the MSCL analysis. For instance, increasing MS values commonly indicate an increase in the detrital input (Dahl and Nesje, 1994; Sandgren and Snowball, 1996; Nesje et al., 2000; Wagner and Melles, 2002).

The distribution of ostracoda (in lacustrine and marine basins) and benthic foraminifera (in marine basins) are closely related with physical and chemical properties (temperature, salinity, pH, depth, amount of oxygen and nutrient, and

bottom water oxygen conditions) of the environment in which they live. Therefore they provide important information about the history of salinity, water level changes, and fresh-salty water transitions (Frenzel and Boomer, 2005).

Stable oxygen ($\delta^{18}O$) and carbon ($\delta^{13}C$) isotope ratios are among the most frequently used proxies in palaeoclimate studies, allowing for instance the reconstruction of past changes in temperature, hydrology (precipitation/ evaporation) or vegetation cover (McKenzie 1985; Schwalb 2003; Leng and Marshall 2004).

Stable oxygen isotope analysis of carbonate material provides important information on water temperature, precipitation/evaporation ratio and hence on chemical composition of the host water from which the carbonates deposited. Oxygen isotope values are influenced by temperature, salinity, $\delta^{18}O$ of the host water and disequilibrium effects (so-called vital effects) (e.g., Wefer and Berger, 1991) . The $CaCO_3$ shells of the organisms, usually the ostracod and bivalve shells, in lakes are used for stable isotope analysis. Isotopic fractionation develops as a result of some physical and biogeochemical processes. The degree of fractionation of different isotopes of the same element is controlled by the relative differences in the atomic weight of the isotopes. Phase changes, evaporation/precipitation photosynthesis and biogeochemical reduction reactions all affect the stable isotopic composition of water in different ways (Wetzel, 2001). As a result of the evaporation, lakes are enriched in dissolved ions and salinity increases, in contrast effective rainfall causes dilution of the compound. Oxygen isotope ratio ($\delta^{18}O$) of lake water changes with the same processes. These changes in rate of precipitation/evaporation (P/E) are recorded in the oxygen isotope ratio ($\delta^{18}O$) of the ostracods shells. Therefore, the oxygen isotope values of the shells contain important information about the paleohydrology of the lake (Hodell et al., 1995).

Carbon isotope values can be influenced by several factors, such as temperature, salinity, composition of inflowing waters, photosynthesis of aquatic organisms, upwelling and exchange between atmosphere and water. The factors that may influence carbon stable isotope ratios are more variable than that of oxygen stable isotopes. Therefore these data can be more difficult to interpret (Geary et al., 1992). However, $\delta^{13}C$ were successfully applied for studies regarding nutrient concentrations in shallow waters and consequently about paleoproductivity (Meyer et al., 2011). During photosynthesis, autotrophic organisms use mainly ^{12}C to build the

organic matter. This leads to a natural enrichment in ^{13}C of superficial waters (Bowen, 1998) high values of ^{13}C in penecontemporaneous carbonates indicate a tendency to eutrophic and higher water turbidity conditions, whereas low values of ^{13}C indicate oligotrophic and low water turbidity conditions. Respiration of plants and organic production can be affected by seasonality (Colleta et al.,2001), which can cause water stratification, especially during summer (the period that represents the highest shallow water productivity throughout the year). The stratification can result in large differences in $\delta^{13}C_{TDIC}$ (Total Dissolved Inorganic Carbon) values, reflected in the composition of carbonates precipitated at different depths in the water column. In fact, stratification leads to depletion in organic material through oxidation, which is followed by an increase of $\delta^{13}C_{TDIC}$ (Leng and Marshall, 2004). Upwelling effects are directly controlled by the photosynthetic activity in surface waters: phytoplankton removes ^{12}C from the ambient dissolved inorganic carbon and produce organic matter. That organic matter releases "light" carbon isotopes during its decomposition in depth, causing a depletion of ^{13}C in bottom waters. Consequently, deep waters are enriched in "light" isotopes which might be brought to the surface by upwelling or complete mixing (overturn) of the water column (Krantz et al., 1988).

There are many other chemical and biological paleo-environmental proxies in that have the potential to be measured in lake sedimentary sequence. The ones chosen for this study are the most common, reliable and informative proxies of long-term lake conditions.

In this study, physical (MSCL), geochemical (μ-XRF, TOC-TIC), micropaleontological (octracoda) and isotopic (δ^{18}O and δ^{13}C) properties of Lake Van sediments were analyzed and interpreted, with special emphasis on particular paleoclimate proxies. These include MS (SI), Ti (cps), Ti/Ca, δ^{18}O- δ^{13}C (of bulk carbonate and ostracod), TOC-TIC (% by weight) and C/N ratio of the bulk organic matter.

4.4.2 MSCL analysis

Physical properties measured by MSCL include magnetic susceptibility, gamma density and fractional porosity. Details of the MSCL measurement techniques are given in Section 2.2. Magnetic susceptibility quantifies the magnetic behaviour of a

material in an external magnetic field. It is often used to log and correlate major stratigraphic changes in sediment cores. Magnetic susceptibility provides useful information about changes in the sediment compositon. For instance, magnetite, opal and carbonate have distinct magnetic susceptibility signals. Lithogenic material that contains abundant ferro- or para-magnetic minerals have high magnetic susceptibility. However, diamagnetic, biogenic materials, such as carbonate and silica, exhibit low or even negative magnetic susceptbility values due to the suppression of the magnetic field (Robinson, 1993). Gamma density data provide a precise and high resolution record of bulk density, which is also an indicator of lithology and porosity changes.

Core V08G04

Physical properties of core V08G04 are shown in Figure 4.18. Magnetic susceptibility (MS) values change through the core between 5 SI and 28 SI with the highest MS value occurring at 40 years BP and the lowest MS value at 1100 years BP. Magnetic susceptibility values show distinct increase in between 2300-3300 years BP and 720-0 years BP, indicating the accumulation of relatively iron-oxide rich detrital material during these time intervals.

Gamma density values vary between 1,24 g/cm^3 and 1,61 g/cm^3 with the lowest value at 390 years BP and the highest value at 1850 years BP. Porosity values vary between 0,66 and 0,93 with the highest value at 390 years BP and lowest value at 1850 years BP. Although gamma density and porosity values fluctuates along the core length, there are abrupt changes at 390 years BP for both, indicating a change in the sediment composition.
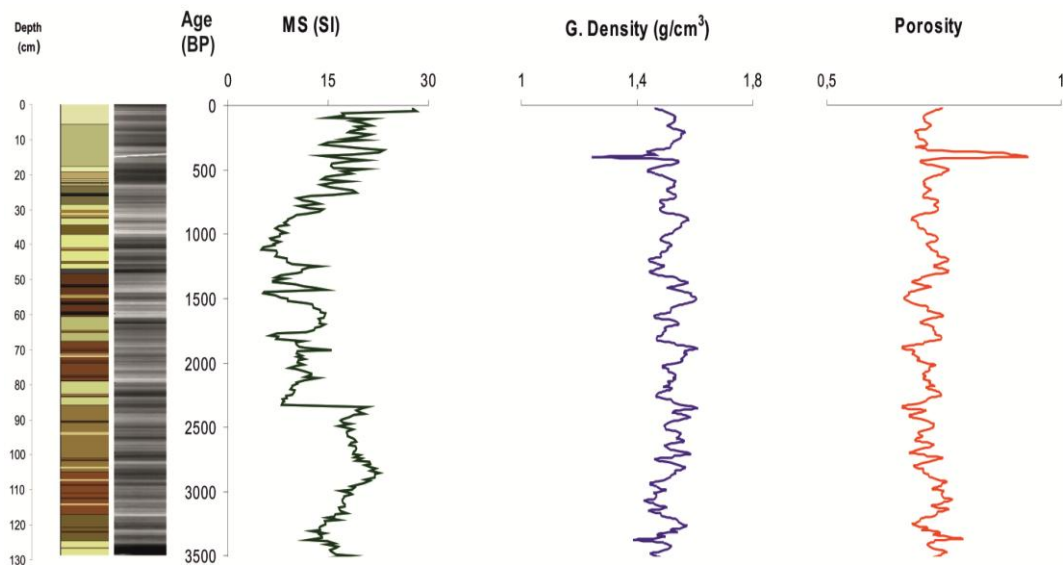
Figure 4.18 : Physical properties (MSCL) of core V08G04.

Core V08G08

Physical properties of core V08G08 are shown in Figure 4.19. Magnetic susceptibility (MS) values change through the core between 0,2 SI and 2,4 SI with the highest MS value at 250 years BP and the lowest MS value at 750 years BP. Magnetic susceptibility values show distinct increase during 1350-950 years BP, 500-420 years BP and 300-0 years BP, indicating accumulation of iron-rich clastic material. Gamma density values change between 1,40 g/cm^3-1,67 g/cm^3 with the lowest value at 320 years BP and the highest value at 1100 years BP. Porosity values vary between 0,63 and 0,78 with the higest value at 320 years BP and lowest value at 1100 years BP. Although gamma density and porosity values fluctuates through the core there are abrupt changes at 320 years BP for both, indicating the change in the sediment composition.
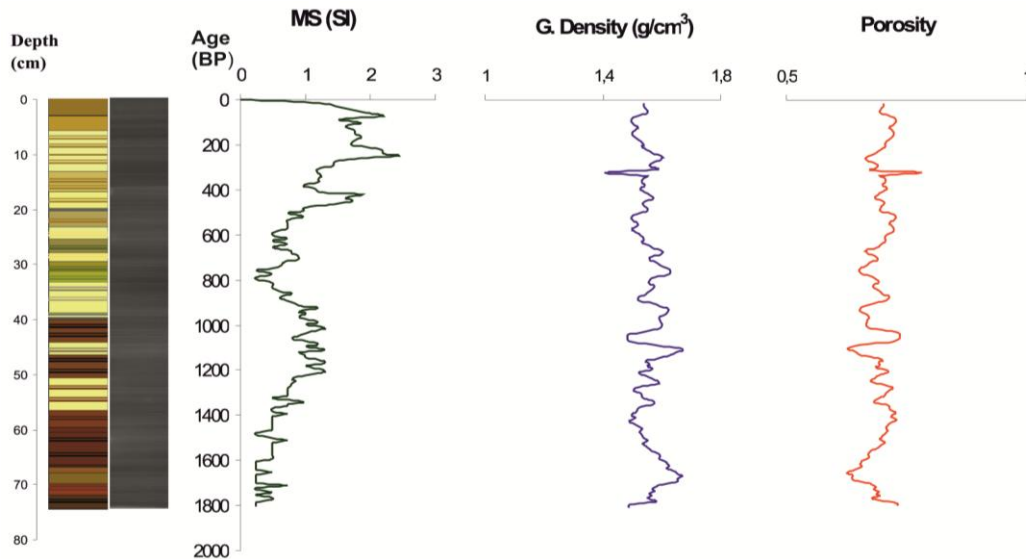
Figure 4.19 : Physical properties (MSCL) of core V08G08.

Core V08G11

Physical properties of core V08G11 are shown in Figure 4.20. Magnetic susceptibility (MS) values change through the core between 2,4 SI and 26 SI with the highest MS value at 600 years BP and the lowest MS value at 1800 years BP. Magnetic susceptibility values show distinct increase in between 2500-2250 years BP, 2100-1900 years BP, 1500-1200 years BP, 700-550 and 350-0 years BP, indicating accumulation of iron-rich material. Gamma density values change between 1,46 g/cm^3-1,67 g/cm^3 with the lowest value at 2280 years BP and the highest value at 1900 years BP. Porosity values change between 0,62 and 0,74 with the higest value at 2280 years BP and lowest value at 1900 years BP. While gamma density and porosity values gradual variations through the core, there are no abrupt changes in the last few centuries, such as the ones observed in cores V08G04 and V08G08.
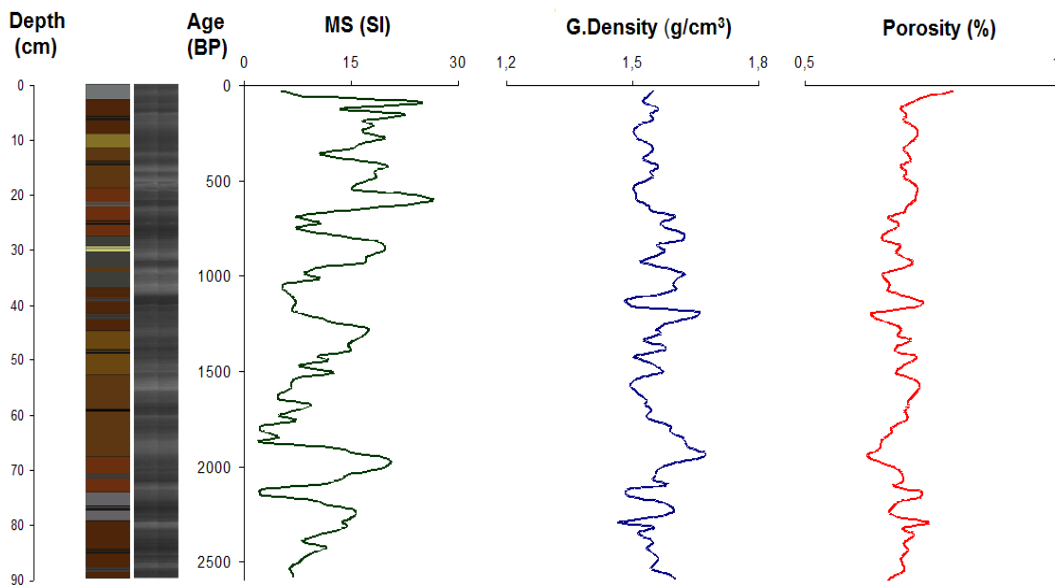
Figure 4.20 : Physical properties (MSCL) of core V08G11.

Core V08G16

Physical properties of core V08G11 are plotted in Figure 4.21. Magnetic susceptibility (MS) values change through the core between 2,4 SI and 26 SI with the highest MS value at 600 years BP and the lowest MS value at 1800 years BP. Magnetic susceptibility values show distinct increase in between 2500-2250 years BP, 2100-1900 years BP, 1500-1200 years BP, 700-550 and 350-0 years BP, indicating accumulation of iron-rich material. Gamma density values change between 1,46 g/cm^3-1,67 g/cm^3 with the lowest value at 2280 years BP and the highest value at 1900 years BP. Porosity values change between 0,62 and 0,74 with the higest value at 2280 years BP and lowest value at 1900 years BP. Gamma density and porosity values show gradual variations through the core with no distinct abrupt changes during the last few centuries.
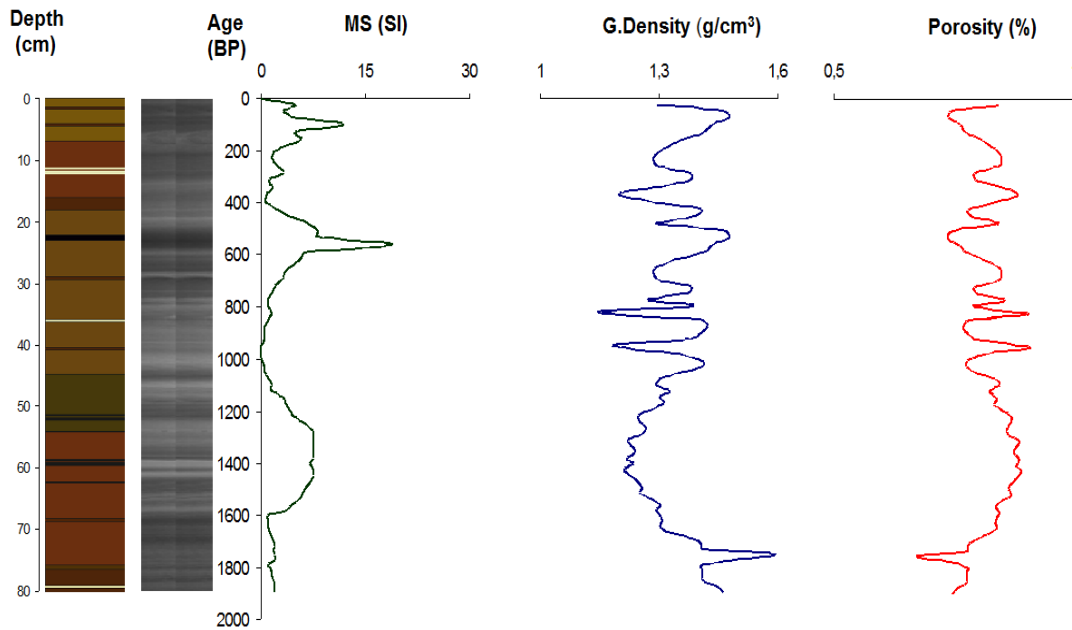
Figure 4.21 : Physical properties (MSCL) of core V08G16.

4.4.3 μ-XRF core scanner analysis

In this section, elemental XRF analyses of K, Ti, Fe, Mn, Ca, Zr and Sr, using the Itrax XRF core scanner are described. These elements are used as proxies for clastic input (K, Ti, Fe, Zr), hydrological record (Ca, Sr), changing redox conditions (Mn, Fe), and volcanic tephras (K, Ti, Zr, Sr). Sedimentary Ca and Sr in many lake systems reflects changes from an open to closed basin during wet to dry periods with calcite reaching saturation during dry periods. In permanently closed basins calcite is always at saturation. This implies that increases in the Ca and Sr content of the sediment are associated with heavy rainfall, increased chemical weathering, greater fluvial deposition, and increased primary production. Sr is also enriched in some volcanic tephra. The Fe, Ti, and content of the sediment also reflect greater erosion of the watershed and deposition into the basin during wetter periods. The amounts of Fe and Mn are sensitive to redox changes in aquatic environments, but they might also relate to clastic input (Calvert and Pedersen, 1993; Davison, 1993; Thomson et al., 1995)). Mn is more soluble under reducing conditions than Fe, making it possible to use the Fe/Mn ratio as a paleo-redox indicator with high values typically implying more reducing conditions (Davison, 1993). Ti and Zr are related with heavy minerals (e.g., zircon, rutile, anatase, ilmenite) and have been used by different authors as sand/silt-size material input proxies in general and aeolian input proxies in particular (Calvert et al., 1996; Haug et al., 2003). High concentrations of incompatible (K,

76

Rb, Sr) and high-field strength (Zr) elements are characteristic of alkaline magma. Ratios of Fe, Ti or K to Ca are used to represent variations in the relative proportion of siliciclastic and biogenic carbonate sedimentation.

Elemental profiles of the collected cores described below. It is important to note that XRF data in this part is presented as XRF counts. This is not an absolute concentration, nor does it represent a percentage of the bulk sediment. Elemental counts provide relative changes over time in each element.

Core V08G04

The elemental profiles of core V08G04 are presented in Figure 4.22. Generally Ti, Fe, and K profiles show contrasting trends to those of Ca and Sr, being depleted in intervals 3200-2900 years BP, 2670-2450 years BP, 2350-2150 years BP, 1850-1600 years BP, 1200-750 years BP. Concentrations of Ti, Fe, and K have local maximums at 2800 years BP and 1470 years BP. Also intervals during 2970-2550 years BP, 2200-1800 years BP, and 1700-1100 years BP, Ti, Fe and K profiles increase whereas Ca and Sr profiles decrease. Zr profile shows uniformly low values along the core.
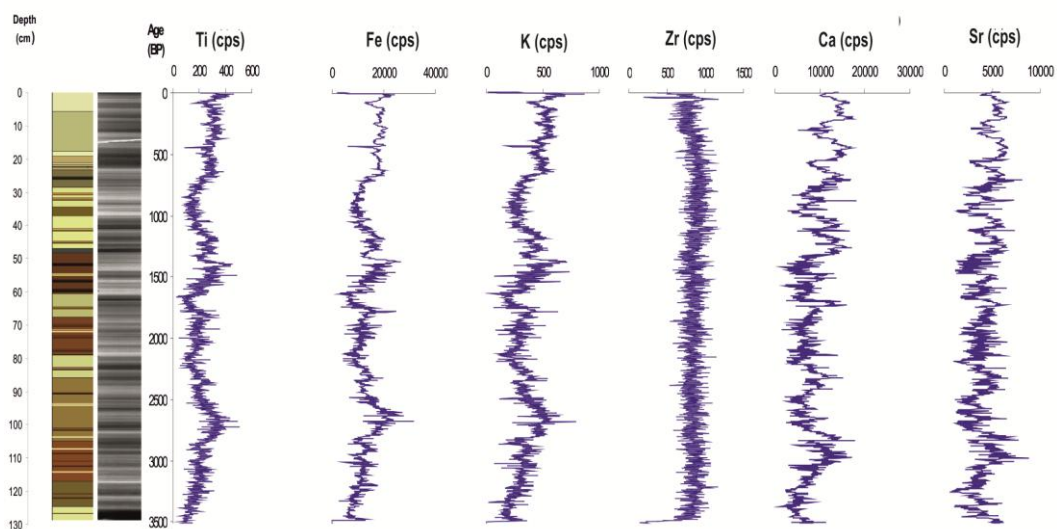
Figure 4.22 : μ-XRF- age profiles of Ti, Fe, K, Zr, Ca, and Sr in core V08G04.

Figure 4.23 presents the ratios of Ti, Fe or K and Zr to Ca. All ratios show very similar downcore distribution with increases during 3600-3300 years BP, 2900-2550 years BP, and 1650-1450 years BP. These periods are interpreted to represent time intervals of higher clastic input from the drainage basin relative to the amount carbonate deposition within the lake.
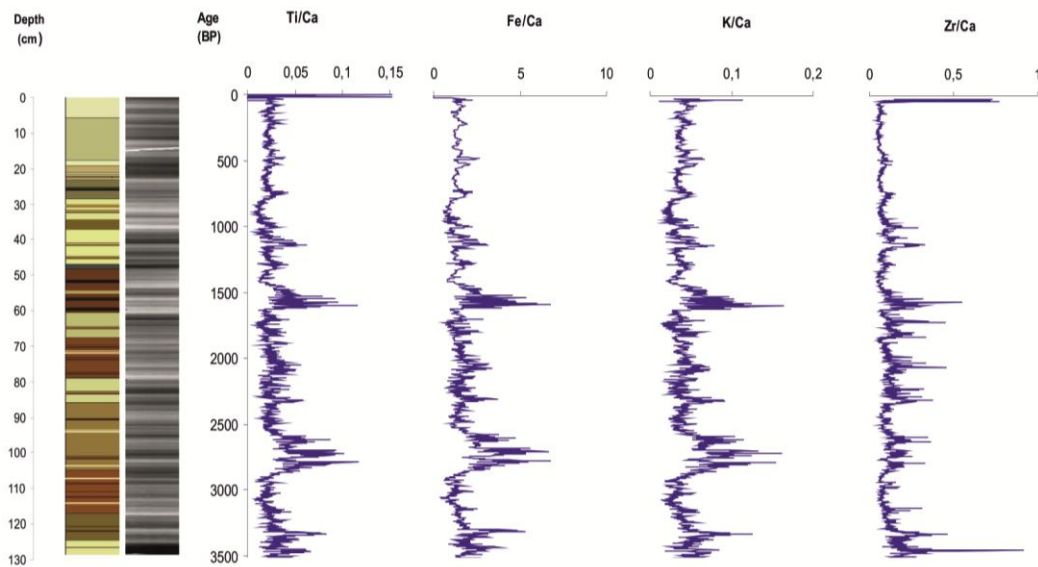
Figure 4.23 : μ-XRF- age profiles of Ti/Ca, Fe/Ca, KCa and, Zr/Ca, in core V08G04.

As mentioned before the amounts of Fe and Mn are related to clastic input, but both elements are also sensitive to redox changes in aquatic environments, with Mn being the more sensitive one (Calvert and Pedersen, 1993; Davison, 1993). Therefore, Fe, Mn profiles and Fe/Mn ratio of the core are presented separately in Figure 4.24. The profiles of both elements show similar distribution along the core, whereas the profile of Fe/Mn ratio have local maxima at 750 years BP, 1950 years BP and 3100 years BP. These Fe/Mn peaks are interpreted to represent relatively high periods of clastic delivery to Lake Van and/or less oxic conditions in the water column.
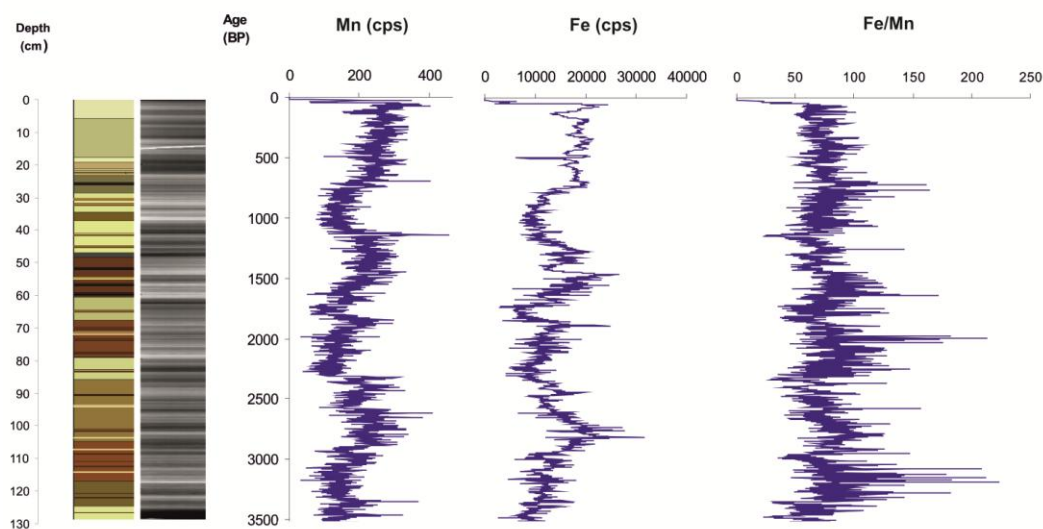
Figure 4.24 : μ-XRF- age profiles of Mn, Fe and, Fe/Mn in core V08G04.

Core V08G08

The XRF results of the selected elements profiles for this core are shown in Figure 4.25. Generally Ti, Fe, and K show very similar distrubitions along the core. In spite of some small fluctuations, these elements show almost uniform distribution during 1800-1350 years BP. During 1350-1000 years BP, these elements show incresing trends. From 1000 years BP to 800 years BP, concentrations of these elements decrease, followed by an increase between 800 and 650 years BP. The concentrations immediately start to decrease from 650 years BP to 600 years BP. From 600 years BP to 450 years BP Ti, Fe and K profiles show increase. After a decreasing trend between 450-300 years BP profiles, the elements show almost a uniform distribution up to the present. Calcium and Sr profiles are similar along the core which are opposite to those Ti, Fe and K. Zirconium profile shows uniformly low values along the core.

Figure 4.26 show the ratio of Ti, Fe, K and Zr to Ca. All ratios show very similar downcore distribution with increasing trends during 1350-1050 years BP and 600-450 years BP, with local maxima during 1700 years BP, 1600 years BP, 900 years BP, and 500 years BP. These periods with high ratios are interpreted to represent high clastic delivery and relatively low carbonate deposition in the lake.
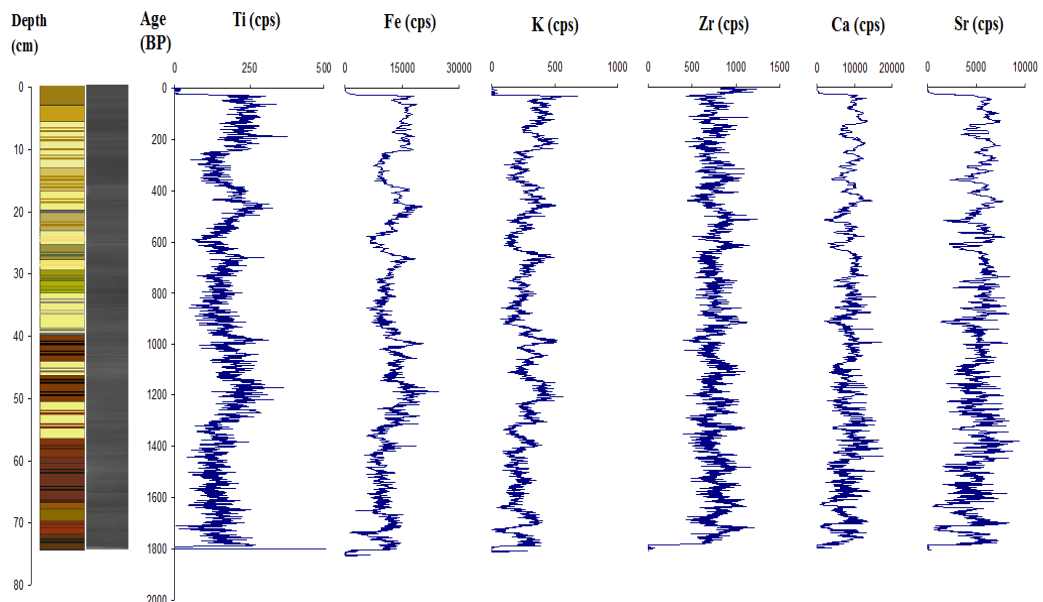
Figure 4.25 : μ-XRF- age profiles of Ti, Fe, K, Zr, Ca, and Sr in core V08G08.

79
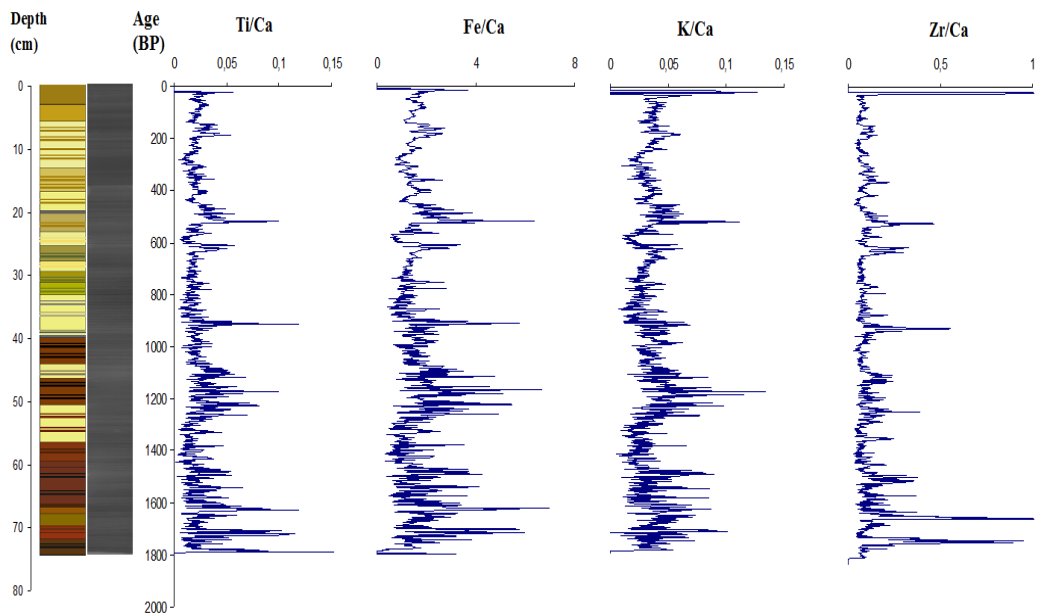
Figure 4.26 : μ-XRF- age profiles of Ti/Ca, Fe/Ca, KCa and, Zr/Ca, in core V08G08.

Fe, Mn and Fe/Mn profiles of this core are presented in Figure 4.27. Iron and Mn have very similar distributions. Beside short-term fluctuations, the long-term trend of Fe/Mn ratio shows slight increases during 1650-1400 years BP, 900-700 years BP and 600-450 years BP. These increases in general correspond in time to the increases in Ti/Ca, Fe/Ca, K/Ca and Zr/Ca ratios and can be interpreted to represent periods of high clastic input in the lake.
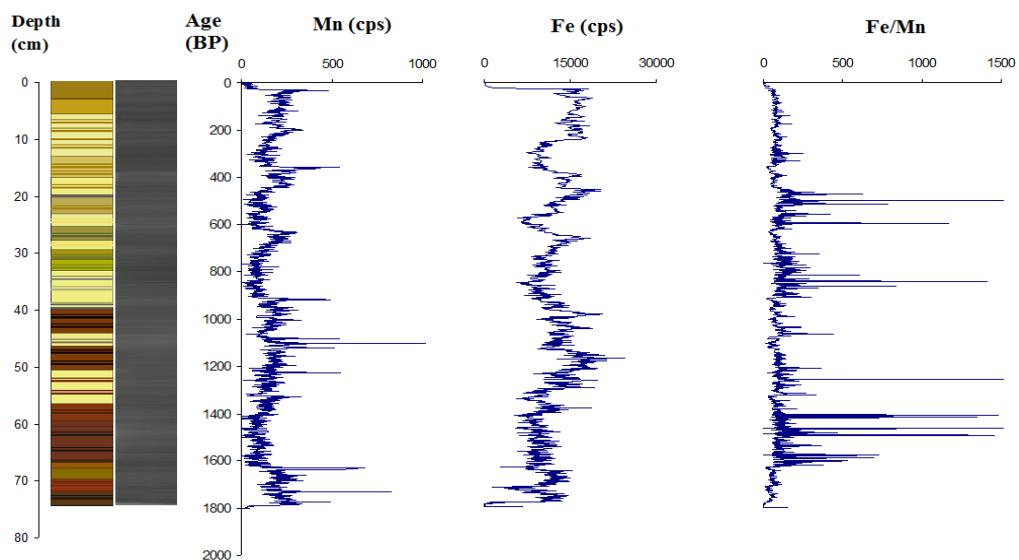
Figure 4.27 : μ-XRF- age profiles of Mn, Fe and, Fe/Mn in core V08G08.

Core V08G11

The XRF results of the selected elements profiles for this core are shown in Figure 4.28. Titanium, Fe, and K show similar downcore distributions with their concentrations increasing during 2300-2200 years BP, 1450-1200 years BP, and 700-550 years BP and showing some local maxima during 1300 years BP. Calcium and Sr profiles are negativly correlated those of Ti, Fe and K profiles. Zr shows almost uniform distribution througout the core.

The ratios of Ti, Fe, K and Zr to Ca ratios also show very similar downcore distributions with each other (Figure 4.29). The ratios, in particular Zr/Ca, increase during 2400-2250 years BP, 1400-1200 years BP, and 650-550 years BP, with sharp peaks during 1980 years BP and 1800 years BP.

However Fe and Mn profiles show very similar trends, there are some differences between them. During the periods between 1050-850 years BP and 750-600 years BP Fe values are increasing while Mn values are decreasing (Figure 4.30). Similarities of Fe profile those of Ti and K suggests that its distribution is mainly controlled by clastic input rather than by redox conditions. Beside short-term fluctuations, the long-term trend of Fe/Mn ratio shows slight increases during1750-1500 years BP, 1050-850 years BP and 750-600 years BP. These periods can be interpreted to represent the time intervals of high clastic material delivery to the lake.
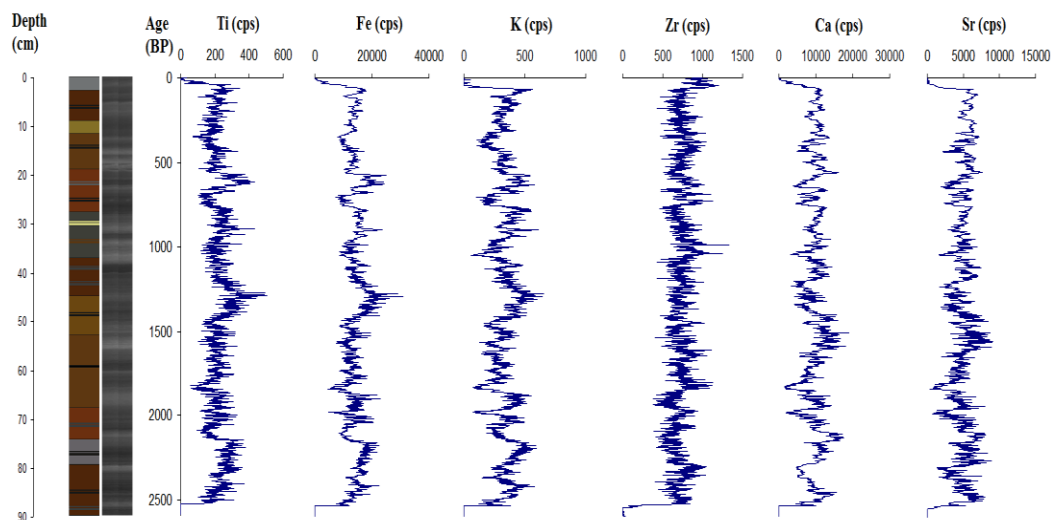
Figure 4.28 : μ-XRF- age profiles of Ti, Fe, K, Zr, Ca, and Sr in core V08G11.

81
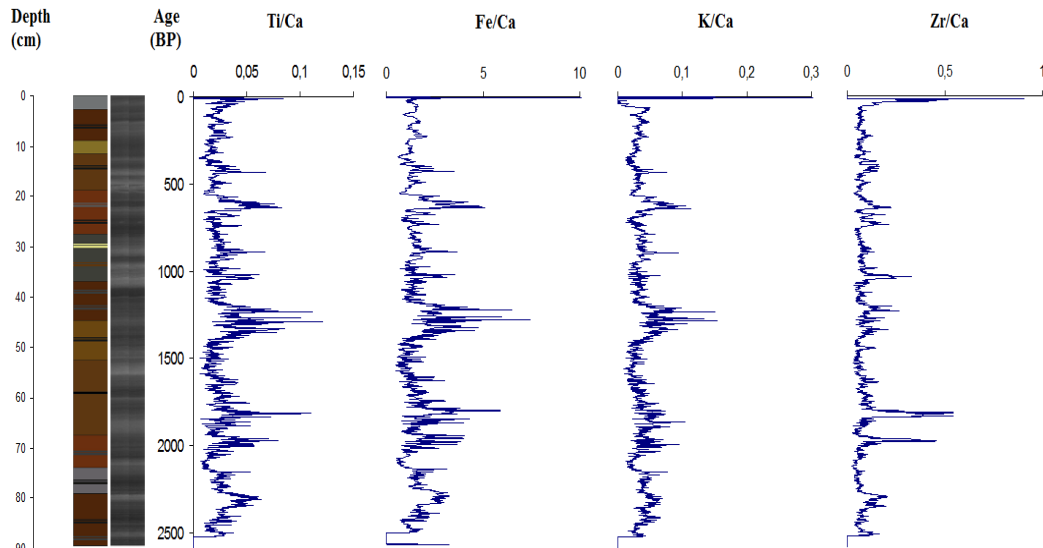
Figure 4.29 : µ-XRF- age profiles of Ti/Ca, Fe/Ca, KCa and, Zr/Ca, in core V08G11.
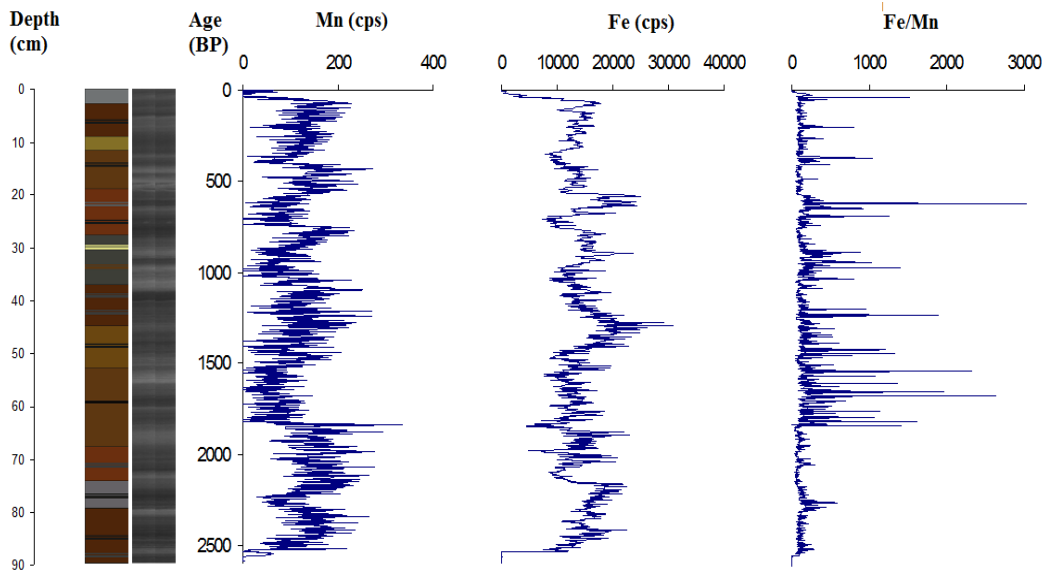
Figure 4.30 : µ-XRF- age profiles of Mn, Fe and, Fe/Mn in core V08G11.

Core V08G16

Commonly Ti, Fe, and K profiles show similar downcore distrubitions that show increases during 2300-2200 years BP and 15000-1200 years BP, and a sharp peak during 550 years BP (Figure 4.31). Trends of Ca and Sr profiles are negatively correlated to those of Ti, Fe and K.
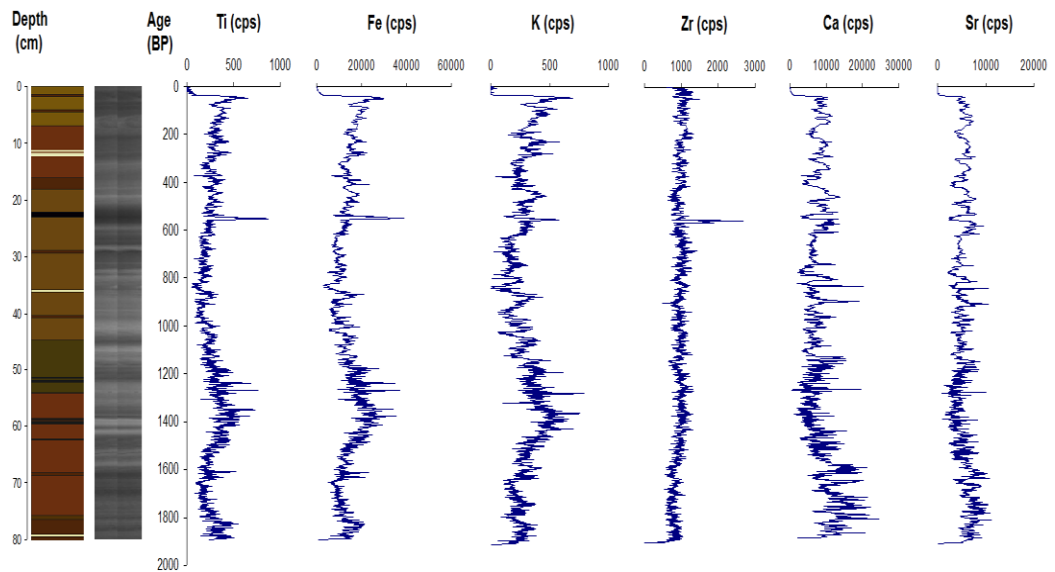
Figure 4.31 : μ-XRF- age profiles of Ti, Fe, K, Zr, Ca, and Sr in core V08G16.

The ratios of Ti, Fe, K and Zr to Ca along the core show similar down core distributions with increases during 1550-1200 years BP and sharp peaks during 550 years BP and 400 years BP (Figure 4.32). Iron and Mn profiles are almost similar to each other except 1900-1200 years BP. (Figure 4.33). However Mn profile shows small fluctuations between 1550-1200 years BP, there is an increasing trend in Fe profile during this interval. Beside short-term fluctuations, the long-term trend of Fe/Mn ratio shows slight increases between 1600-1200 years BP.
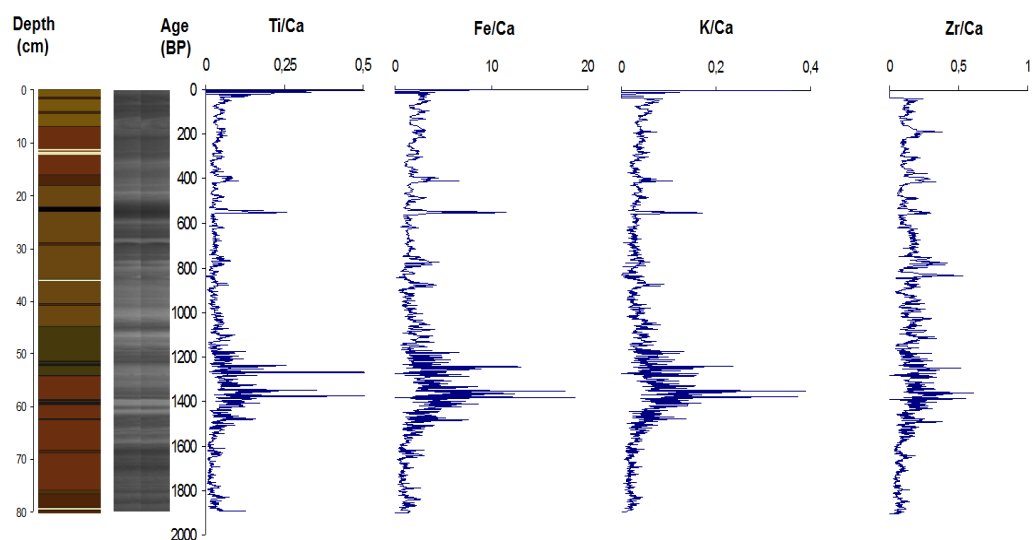
Figure 4.32 : μ-XRF- age profiles of Ti/Ca, Fe/Ca, KCa and, Zr/Ca, in core V08G16.

83
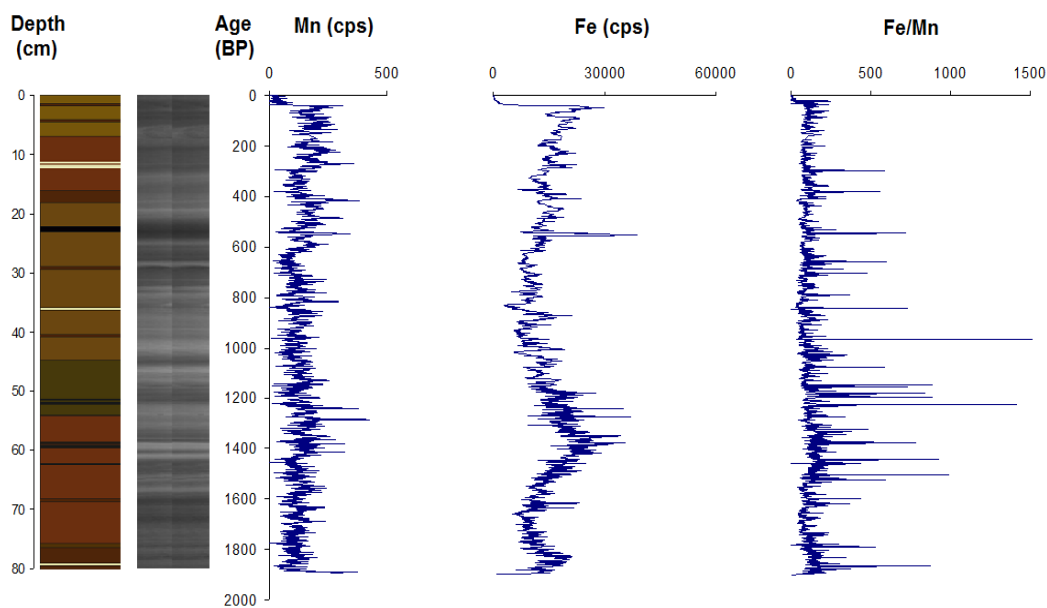
Figure 4.33 : μ-XRF- age profiles of Mn, Fe and, Fe/Mn in core V08G16.

4.4.3.1 μ-XRF heavy metal distributions for last 200 years

Sediments are not only the sinks for trace metals in marine and estuarine ecosystems, but also act as sources of metals for aquatic organisms (Chapman et al., 1998; Dural et al., 2007; Qiu et al., 2011). Copper, Ni, Pb, Zn and Co are some of the most frequent heavy metal pollutants (Hakanson, 1980; Chen et al., 1991; Wong et al., 2001). These metals enter the marine or estuarine ecosystem with the discharge of industrial and municipal wastes, acid mine drainage, storm run-off, dust deposition, and other diffuse sources (Dai et al., 2007; Zhang et al., 2008; Besser et al., 2009; Hosono et al., 2010, 2011).

Also, various diagenetic processes may promote extensive redox-sensitive metal enrichment at oxic/anoxic interface below the water-sediment interface. Depending on the bottom water oxygen conditions and the geochemical behaviour, trace metals can either settle in the sediment column or diffuse to the water column (Calvert et al., 1996). The top layers of sediment column can be mixed by some biological (i.e., bioturbation) and physical processes which homogenise metal concentrations in the mixing zone (Matisoff, 1995).

Heavy metals have an inclination to accumulate on fine grained particles in sediments. (e.g., Zhang et al., 2001; Morillo et al., 2002). The toxicity and mobility of heavy metals vary and depend on some parameters such as the redox conditions within the sediment and water column and their chemical forms. Generally the

mobility of heavy metals in sediment is strictly limited by strong absorption reactions between metal ions and negatively charged particles of sediments, such as the clay minerals and organic matter (Stumm, 1987). Due to their toxic effect, heavy metal accumulation in sediments is an important issue for marine and estuarine environments (Chapman et al., 1998; Singh et al., 2005; Todd et al., 2010). Thus, the simple measurement of heavy metal content cannot provide adequate information about their mobility and bioavailability, and consequently the risk to the marine ecosystem. Instead, heavy metal speciation, together with the physicochemical conditions of the sedimentary environment, makes a more accurate estimation of the real environmental impact (Perin et al., 1985; Cuong and Obbard, 2006).

Heavy metal profiles of the μ-XRF counts of Cu, Zn, Pb, Ni and Co for last 200 years in the collected cores are described below. The main objective of this study is to assess the history of the anthropogenic metal pollution at the four different core sites in Lake Van.

It is important to note that μ-XRF elemental counts provide only the relative changes in the concentrations of each element over time, and that the sensitivity of Cu measurement was not sufficient in core V08G04. To eliminate the porosity effect in the sediment column due to increasing compaction with the core depth, heavy metal μ-XRF counts are multiplied by the Cl counts, with Cl as a conservative element in the pores representing a measure of the porosity.

Core V08G04

Zinc, Pb, Ni, and Co profiles of core V08G04 for last 200 years are shown in Figure 4.34. Although being more pronounced in between 20-30 years BP, all concentrations have an upward increasing trend during the last 60 years. In the case Pb profile, however, there is a decrease from a peak value of 3700 cps at 18 years ago. At their peak values, Zn, Pb, Ni and Co show 4, 18, 3.5 and 4 times enrichment over the background levels, respectively.
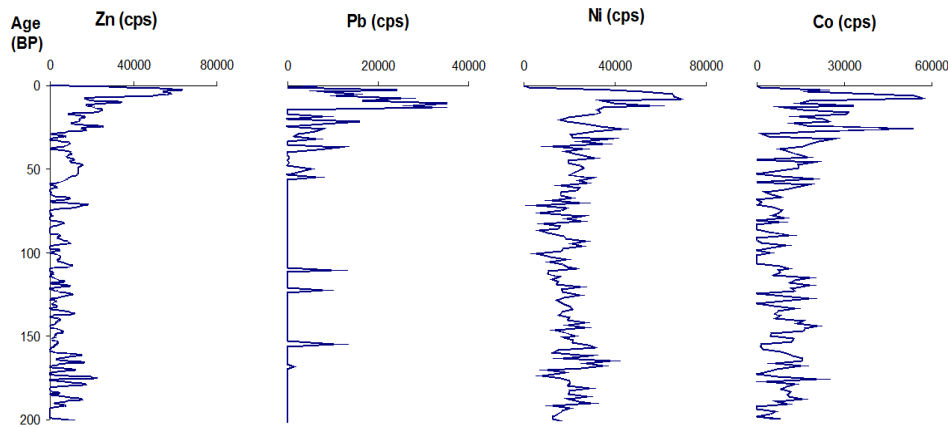
Figure 4.34 : Zn, Pb, Ni and Co profiles of core V08G04 for the last 200 years.

Core V08G08

Copper, Zn, Pb, Ni, and Co profiles of core V08G08 for the last 200 years show a general trend of increasing concentrations over the last 30 years (Figure 4.35). Pb profile has an abrupt peak between at 15 years BP, which decreases upward towards the present. The peak values of Cu, Zn, Pb, Ni, and Co in the upper part of the core are 6, 6, 7, 4.5 and 3.5 times enriched relative to their background values, respectively.
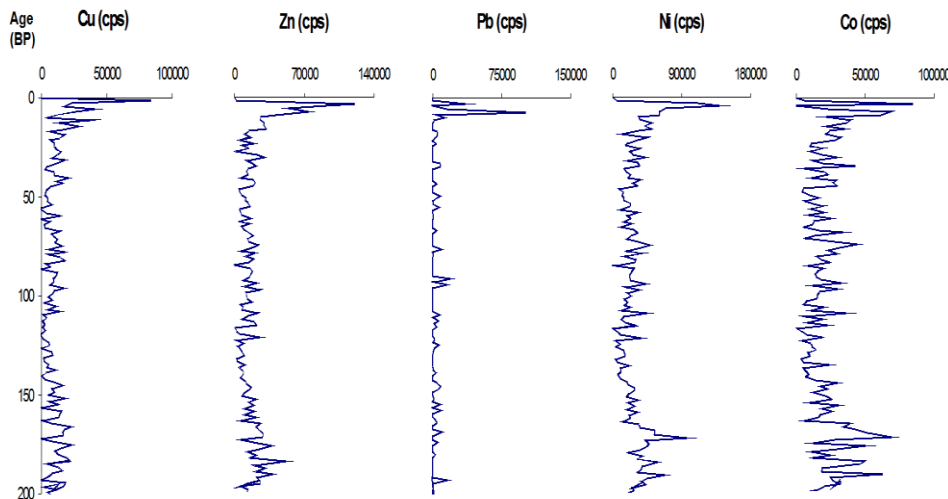
Figure 4.35 : Cu, Zn, Pb, Ni and Co profiles of core V08G08 for the last 200 years.

Core V08G11

Copper, Zn, Pb, Ni, and Co profiles of core V08G11 for the last 200 years show an upward increasing trends over the last 50 years (Figure 4.36). Lead profile includes two sharp peaks at 15 and 5 years BP. Copper, Zn, Pb, Ni, and Co concentrations in

86

the upper part of the core are 2.5, 2, 3.5, 2 and 2 times enriched relative to their background values.
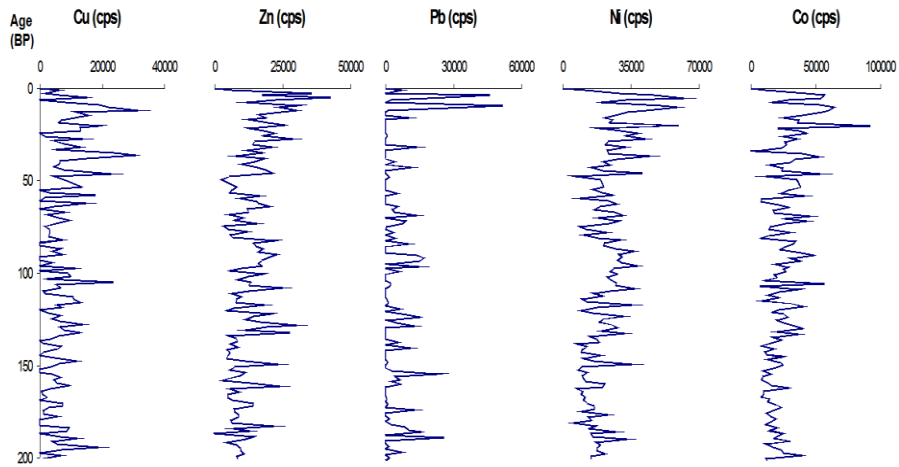
Figure 4.36 : Cu, Zn, Pb, Ni and Co profiles of core V08G11 for the last 200 years.

Core V08G16

Copper, Zn, Pb, Ni, and Co profiles of core V08G16 for the last 200 years are characterised by fluctuating values (Figure 4.37). Only Pb profile has an sharp peak at about 15 years BP. Thes value of Pb peak concentration is 6 times the background value. Copper and Co profiles show no significant enrichment starting about 50 years BP and increasing towards the present, which in contrast with that observed in the other cores. Zinc and Ni profiles, on the other hand show increasing values over the last 30 years, with increases being about 2 and 3 times the fluctuating background values.
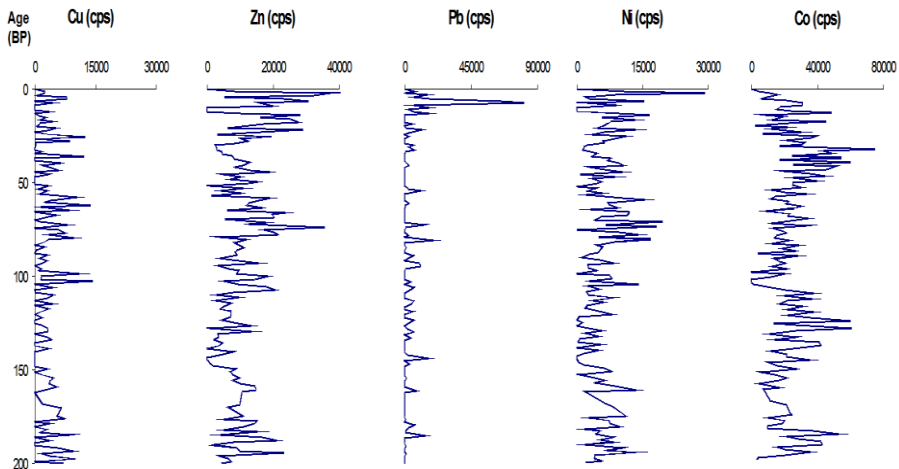
Figure 4.37 : Cu, Zn, Pb, Ni and Co profiles of core V08G16 for the last 200 years.

4.4.4 Total organic carbon (TOC) and total inorganic carbon (TIC) results

Core V08G04

TOC and TIC profiles of core V08G04 show highly variable fluctuations throughout the core (Figure 4.38). TOC and TIC contents in this core range between 3.1-8.1 and 1.8-4.9 dry weight %, respectively with the highest TOC value (8.1 %) at 137 years BP (4,5 cm) and the highest TIC value (4.9 %) at 258 years BP (8.5 cm), according to the varve ages.

In general there is a negative correlation between TOC and TIC contents, these values allow the sediment record to be divided into nine different parts along the core (Figure 4.38). TOC values show a decreasing trend from 5.7 to 3.7 % , during 3650-3240 years BP (130-115 cm), whereas the TIC values show an increasing trend from 3,9 to 4,5 % during the same interval. During 3240-2870 years BP (115-101 cm) TOC values increase from 3.6 to 5.7 % whereas TIC values tends to decrease from 4.1 to 3.3 %). During the next period from 2870 years to 2450 years BP (101-85 cm), TOC values tend to decrease from 5.7 to 4.1 %), whereas TIC values increase from 3.3 to 4.5 %) in this period. During 2450-2180 years BP (85-75 cm), both TOC and TIC values increase from 4.1 to 7.1 % and from 4.5 to 3.5 %, respectively. From 2180 years to 1100 years BP (75-37 cm) TOC values show a decreasing trend (7.1-3.1 %), while TIC values are increasing (3.5-4.8 %). During 1100-1015 years BP (37-34 cm) TOC values increase (3.1-7.2 %) while TIC values decrease (4.8-2.6 %) (Figure 4.38). During 1015-720 years BP (34-24 cm), TOC and TIC values show opposing trends; TOC has a decreasing trend from 7.2 to 3.1 %), whereas TIC values show an increasing trend from 2.6 to 4.3 % (Figure 4.38). During 720-570 years BP (24-19 cm), TOC values tend to increase from 3,9 to 6,0 %, whereas TIC values decrease from 4.0 to 3.1 %. Finally, between 570-0 years BP (19-0 cm), first an increasing trend (4.0-6.3 %) between 423-272 years BP (14-9 cm) is observed, which is followed by decreasing trend from 8.1 at 150 years BP to 5.0 %. at present. TIC values show a decrease from 4.7 to 1.8 % between 423 and 272 years BP, and then sharply increase to 4.9%, before gradually decreasing to 3.8% about 50 years BP and a sharp decrease to 1.8 % at present (Figure 4.38).
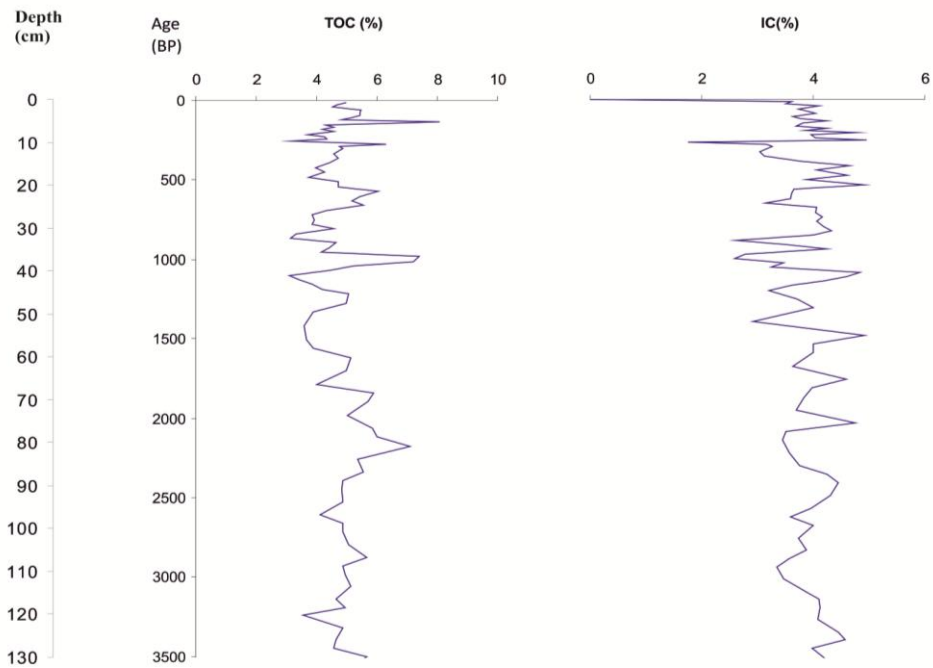
Figure 4.38 : TOC and TIC profiles of core V08G04.

Core V08G08

TOC and TIC values of the core V08G08 show fluctuating downcore distribution. TOC and TIC contents in this core range between 3.3-7.5 and 2.0-4.7 dry weight %, respectively with the highest TOC value (7.5 %) at 1550 years BP (61 cm) and the highest TIC value (4.7 %) at 1380 years BP (53 cm) according to varve ages.

As in core V08G04, TOC and TIC profiles show opposing trends, which can be divided into five different sections. Between 1785-1340 years BP (73-51 cm) TOC values show a decreasing trend (7.5-5.7 %) while TIC values tend to increase (2.9-4.7 %). From 1340 years to 1080 years BP (51-40 cm) TOC values increase (5.7-6.0 %), whereas TIC values tend to decrease (4.7-2.6 %). During 1080-940 years BP (40-34 cm), TOC values show a decreasing trend (6.0-3.6 %), whereas TIC values increase (2.6-4.5 %). During the following period from 940 to 460 years BP (34-16 cm), the fluctuating TOC and TIC values in general show an increasing trend for TOC (3.6-7.3 %) and a decreasing trend for TIC values (4.5-2.0). Finally the last 460 years BP (16-0 cm) the TOC profile includes an increasing trend (3.6-5.8 %) during 350-220 years BP (6-2.5 cm) and a decreasing trend (6.8-4.4 %) during the last 220 years. TIC profile show opposite trends to those of TOC during last 460 years, with an decrease in the values (4.3-3.4 %) during 350-220 years BP and an increase during the last 220 years (Figure 4.39).
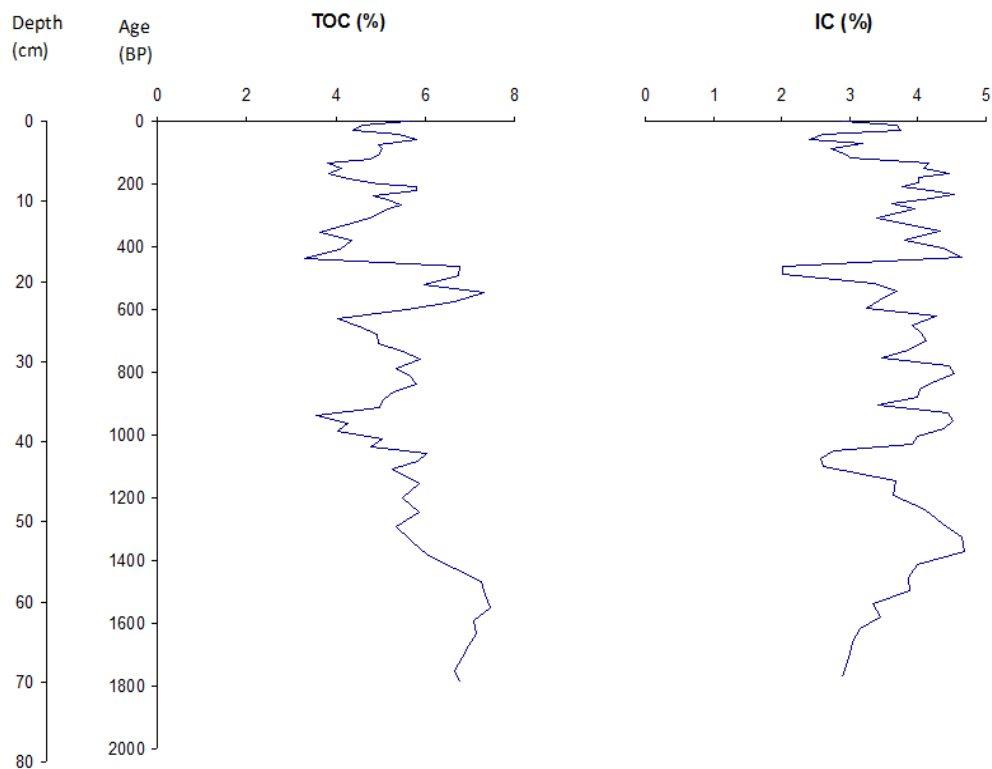
Figure 4.39 : TOC and TIC profiles of core V08G08.

Core V08G11

TOC and TIC values of the core V08G11 show fluctuating downcore distribution (Figure 4.40). TOC and TIC contents in this core range between 2.8-9.2 and 1.7-6.6 dry weight %, respectively with the highest TOC value (9.2 %) at 300 years BP (10 cm) and the highest TIC value (6.6 %) at 1100 years BP (37 cm) according to varve ages Like in the other cores, there is generally a negative correlation between TOC and TIC profiles of this core (Figure 4.40).

The trends of TOC and TIC profiles suggest five different periods. During 2300-2060 years BP (81-71 cm), TOC values show a decrease (6.9-4.4 %), whereas TIC values increase (2.8-5.6 %) (Figure 4.40). During 2060-1730 years BP (71-59 cm), TOC values show an increasing trend (4.4-7.0 %) whereas TIC values tend to decrease (5.6-1.8 %). From 1730 years BP to 1100 years BP (59-37 cm), TOC values decrease (7.0-2.8 %) whereas TIC values increase (1.8-6.6 %). During 1100-650 years BP (37-22 cm), TOC values tend to increase (2.8-7.5 %), while TIC values decrease (6.6-2.8 %). Lastly, during 650-0 years BP (22-0 cm), there are increasing TOC (3.0-9.2 %) between 450 and 270 years BP (15-9 cm), and decreasing values (7.5-3.0 %) during the last 270 years. In contrast, during the same period (650-0

90

years BP), TIC values show opposite trends with decreasing values (5.4-2.8 %) during 450-270 years BP, and increasing values (2.8-5.3 %) during the last 270 years (Figure4.40).
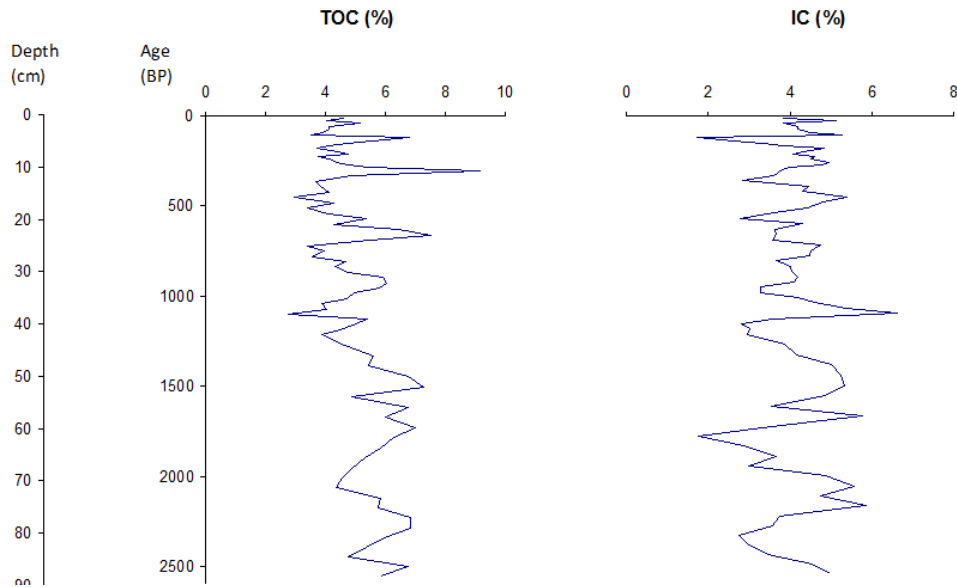
Figure 4.40 : TOC and TIC profiles of core V08G11.

Core V08G16

TOC and TIC profiles of core V08G16 show fluctuations throughout the core (Figure 4.41). TOC and TIC contents in this core range between 2.2-6.5 and 2.4-5.5 dry weight %, respectively with the highest TOC value (6.5 %) at 340 years BP (12 cm) and the highest TIC value (5.5 %) at 1600 years BP (8.5 cm) according to the varve ages. In general there is a negative correlation between TOC and TIC contents.

In the TOC and TIC profiles, five different periods can be distinguished. The period between 770 and 1470 years BP (71-57 cm) are characterized by decreasing TOC values (5.1-2.2 %), and increasing TIC values (4.1-4.8 %) (Figure 4.41). During 1470-970 years BP (57-36 cm), TOC values increase (2.2-5.4 %), whereas TIC values decrease (4.8-2.4 %). During the next period between 970 and 770 years BP (36-28 cm), TOC vealues decrease (5.4-4.2 %) while TIC values increase (2.4-4.2 %). During 770-650 (28-23 cm) years BP, increasing values of TOC (4.8- 5.5 %) and decreasing values of TIC (4.2-2.7 %) are observed. Finally, between 650-0 years BP (23-0 cm) there are (Boyle, 2001) two contrasting trends of TOC and TIC velues (Figure 4.39); during 600-370 years BP (23-13 cm), TOC values decrease (5.5-3.0

91

%) and TIC values are relatively high around 4%, whereas during the last 370 years, TOC values dcrease to around 4% and TIC values decrease only slightly from 4% to about 3.5% (Figure 3.41).
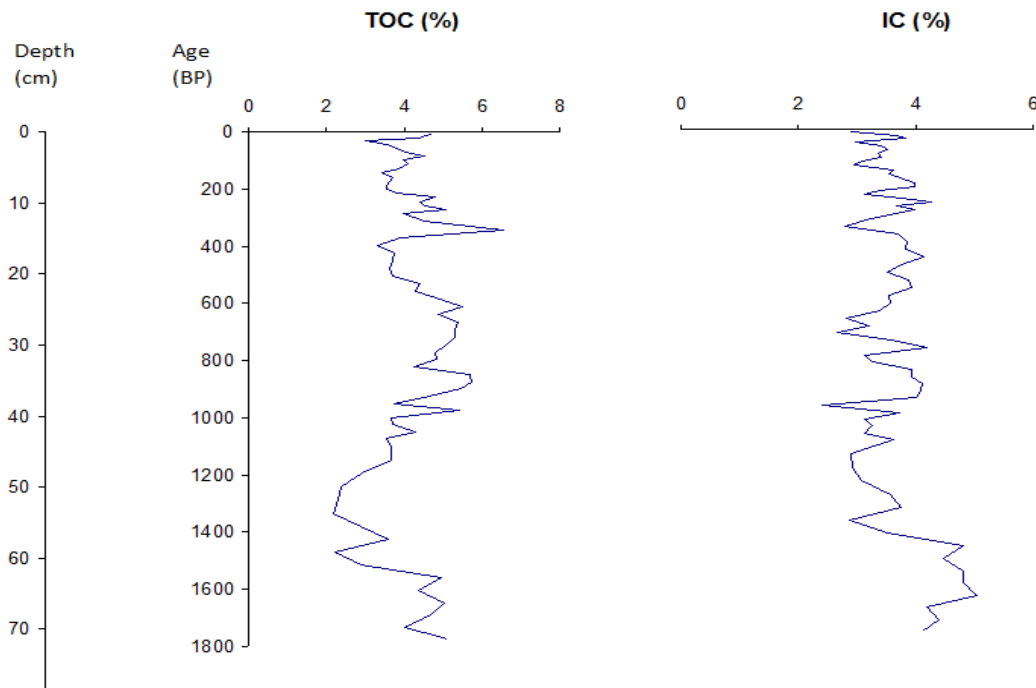
Figure 4.41 : TOC and TIC profiles of core V08G16.

4.4.5 Carbon nitrogen elemental analysis (atomic C-N ratio)

Elemental analyses of total nitrogen and carbon (and sulfur) in the bulk organic matter is performed to investigate the origin of the organic matter (i.e., lacustrine versus terrigenous sources). Atomic C-N ratio of organic matter is used as a proxy to discriminate between the algal and terrestrial organic matter in marine and lake depositional environments (e.g., Prahl et al., 1980; Nakai et al., 1982; Meyers et al., 1984; Prahl et al., 1994; Hedges et al., 1997). Carbon and Nitrogen contents of sediments in aquatic ecosystems are governed by the mixing of terrestrial and autochthonous organic matter (Müller, 1977; Rashid and Reinson, 1979; Nakai et al., 1982; Thornton et al., 1994). C/N ratios of 5 to 6 are reported in phytoplankton and zooplankton, which have proteins containing are primarily nitrogen compounds (Bordowskiy, 1965a; b).

Freshly-deposited organic matter, derived mainly from planktonic organisms, has a C/N ratio of 6 to 9 (Bordowskiy, 1965a; Prahl et al., 1980; Hedges et al., 1997). Phycogenic C/N ratio was found to be between 4 and 10 (Meyers, 1994). This is

contrary to C/N ratios of 15 or higher in terrestrial vascular plants and their derivates and about 39.4 in macrophyte materials (Bordowskiy, 1965b; Ertel and Heges, 1994; Hedges et al., 1986; Orem et al., 1991; Meyers, 1994).

Variations in C-N ratio of the sedimentary organic matter have also been used to understand lake's temporal depth profile apart from analyzing the period of high proportion of terrestrial organic matter input (Guilizzoni et al., 1996). Lower C-N ratios help to identify periods when lake sediments have received a high proportion of algal OM (Kanasassanen and Jaakkola, 1985). However, use of C-N ratio to discern changes in organic matter sources has been the subject of discussion (Goosens, 1989; Thornton and McManus, 1994) in view of the effects of diagenesis; the C-N ratio of terrestrial organic matter decreases during diagenesis, while that of algal organic matter increases (Meyers et al., 1984).

The measured C-N ratios of 23 sediment samples from core V08G04 are plotted in Figure 4.42. The C/N values of the samples for the core range between 1.0 and 32.5 with the average of 11.0.
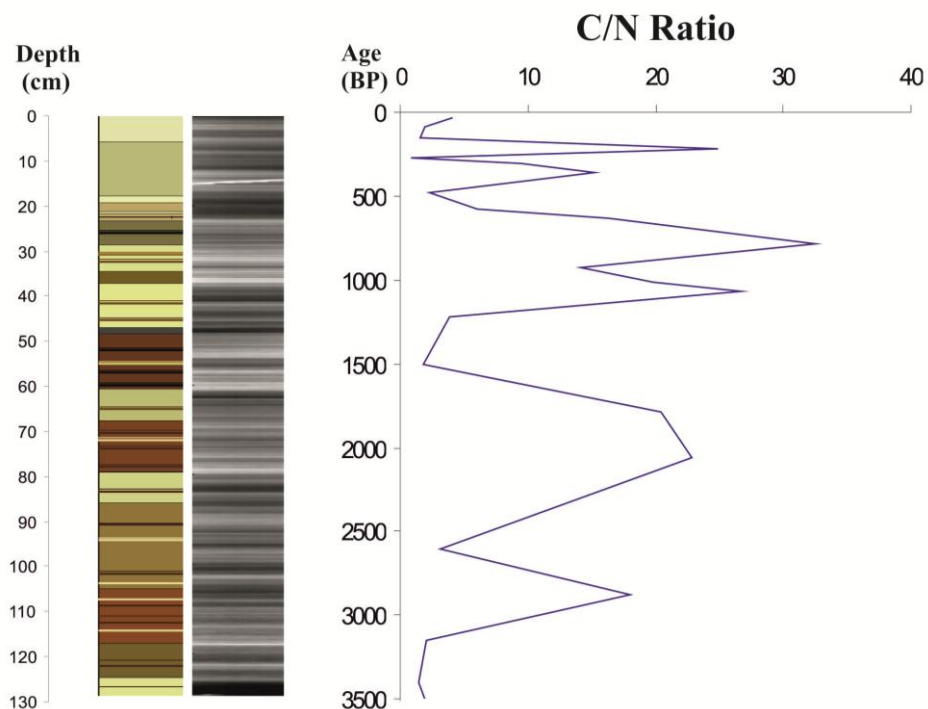
Figure 4.42 : C-N ratio of core V08G04.

4.4.6 Stable isotope profiles

4.4.6.1 Stable oxygen and carbon isotope composition of bulk carbonate and ostracod in core V08G04

In closed lakes such as Lake Van, the major factors controlling the oxygen and carbon isotope composition of waters and precipitating authigenic carbonates are influenced by a wide range of interlinked environmental processes. For instance, a change in temperature will cause a shift in the equilibrium oxygen isotope composition of carbonate forming in lake waters. However, the same temperature change will also affect the isotope composition of the vapour source and precipitation (P), and rate of evaporation, both in the lake and in the catchment. Moreover, factors such as water balance (E-P), temperature, seasonality of precipitation, vapour source and mineral composition of the bulk carbonate will influence the oxygen isotope composition of the lacustrine carbonates (Tarutani et al., 1968; Talbot, 1990; Li ve Ku, 1997; Cole et al., 1999; Gat et al., 2001; Stevens et al., 2001).

Mechanisms responsible for producing different $\delta^{13}C$ signals of any lake system are complex and also controlled by a multiple variables (Myrbo and Shapley, 2006). The $\delta^{13}C$ value varies with water balance, organic productivity and $\delta^{13}C$ value of the carbonate rocks and vegetation cover in the watershed.

The $\delta^{18}O$ and $\delta^{13}C$ values of bulk carbonate of 24 sediment samples from core V08G04 are plotted in Figure 4.43. The $\delta^{18}O$ values of the samples for the core range between -1.2 and +0.6 ‰, with the average of -0.4 ‰ and standard deviation (σ) of 0.5 ‰. The $\delta^{13}C$ values change between +2.5 and -4.2 ‰, with the average of +3.6 ‰ and standard deviation (σ) of 0.4 ‰. There is a positive correlation between the $\delta^{18}O$ and $\delta^{13}C$ values with a correlation coefficient (r) of 0.70.
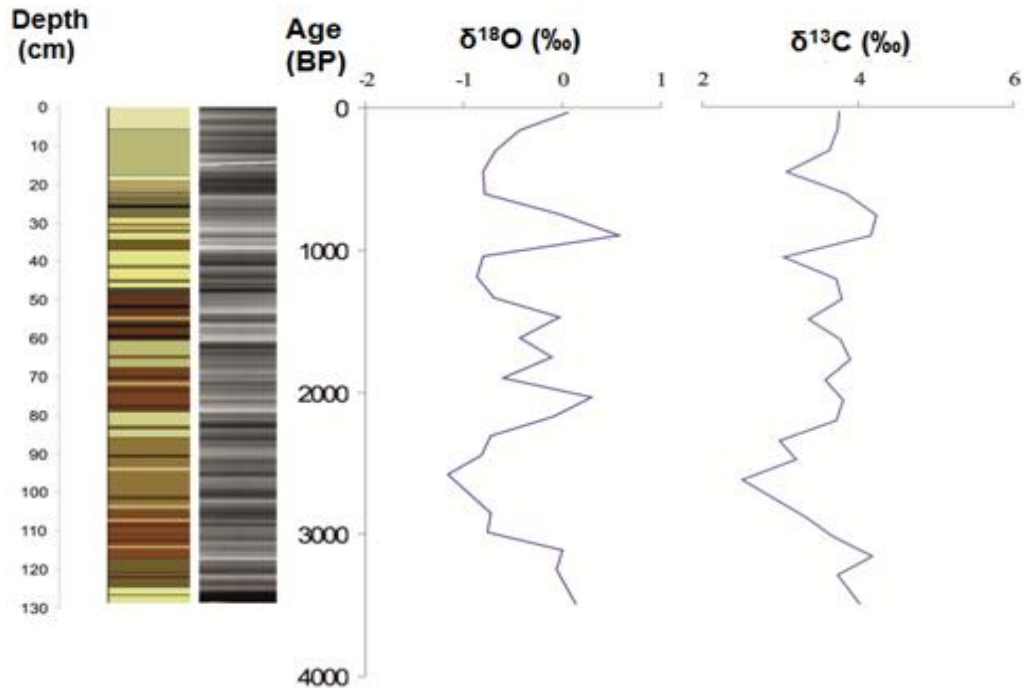
Figure 4.43 : Bulk carbonate δ^{18}O and δ^{13}C profiles of core V08G04.

The δ^{18}O values of the ostracod valves vary between -19.2 and +4.5 ‰ with the average of -0.2 ‰ and standard deviation (σ) of 5.5 ‰, whereas δ^{13}C values range from -17.4 to +2.8 ‰ with the average of -0.1 ‰ (σ=‰ 4.2) Figure 4.44. Downcore trend of the δ^{18}O$_{ostracoda}$ values is commonly similar to that of δ^{13}C$_{ostracoda}$. In other words, there is a strong positive correlation between the δ^{18}O$_{ostracoda}$ and δ^{13}C$_{ostracoda}$ values with a correlation coefficient (r) of 0.96.

The δ^{18}O and δ^{13}C values of the ostracoda and those of the bulk carbonate in the same samples are very different. The ostracoda values show much higher variation (large standard deviations) than the bulk carbonate values and show a general downward decreasing trend. The large deviation in the ostracoda stable isotope values are most likely to be due to "live effects", as dicussed in Chapter 5.
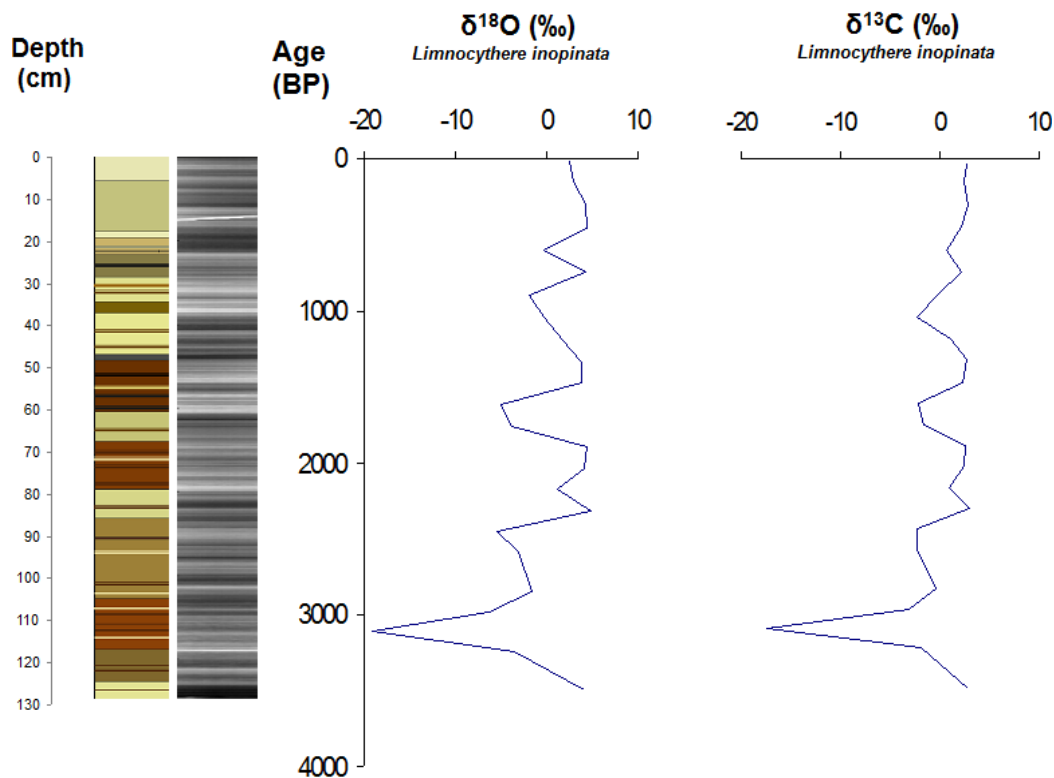
Figure 4.44 : Ostracod δ^{18}O and δ^{13}C profiles of core V08G04.

4.4.6.2 Stable carbon and nitrogen isotope composition of organic matter

A number of factors contribute to the stable C and N isotopic composition of organic matter in lake sediments. The main controlling factor on δ^{13}C and δ^{15}N of lake's sedimentary organic matter is its origin, as to whether it is derived primarily from the lake's drainage basin (allochthonous) or from productivity within the lake (autochthonous). For example, whereas δ^{13}C values of C3 type plants of temprerate climates have -28 ‰ to -25‰, those of marine and lacustrine algae (phytoplankton) -22‰ to -19‰ and soil organic matter -29‰ to -27‰ (Hedges ve diğ., 1997; Goñi ve diğ., 2003). Nitrogen isotopes provide useful information on the conditions of orgnic productivity in the photic zone and early diagenetic processes in the deep water and sediments (Holmes ve diğ., 1999). Nitrogen and carbon isotopic composition of organic matter be used also to identify impacts of anthropogenic activities in the studied area including wastewater and agricultural runoff that yield autochthonous OM with low δ^{13}C and high δ^{15}N (Burnett and Schaffer 1980; Savage et al. 2004).

δ^{13}C and δ^{15}N results of six selected samples from core V08G04 are shown in Table 4.10. The δ^{13}C vary from -23.3 ‰ to -24.7 ‰ with the average of -23.9 ‰ and

standard deviation (σ) of 0.6 ‰. The δ^{15}N values range from 2.0 ‰ to 5.0 ‰ with the average of 3.8 ‰ (σ=‰ 1.2).

Table 4.10 : δ^{13}C and δ^{15}N of selected samples in core V08G04.

Sample (Core)	Depth (cm)	Age (years BP)	δ^{13}C (‰)	Δ^{15}N (‰)
V08G04	11-12	357	-24.7	5.0
V08G04	18-19	565	-24.4	4.4
V08G04	33-34	999	-23.9	3.3
V08G04	38-39	1150	-23.6	5.0
V08G04	70-71	2050	-23.3	3.3
V08G04	90-91	2609	-23.4	2.0

5. DISCUSSION

5.1 The Age Model and Reservoir Age of Lake Van

5.1.1 The age models and sedimentation rates

As presented in Section 4.3, different chronostratigraphic methods such as ^{210}Pb and varve counting were used in this study (Figures 4.11 and 4.13). In addition, ^{137}Cs dating and tephrochronology were used to test the ^{210}Pb and varve counting results (Figure 4.12).

The activity profile of ^{137}Cs in the different cores located in various parts of Lake Van show a good correlation with the ^{210}Pb ages, according to the history of atmospheric deposition of radionuclides derived from nuclear weapons testing and the Chernobyl accident (Figure 4.12). The first detectable ^{137}Cs concentrations are observed at depths of 2.5 cm, 3.5 cm, 2 cm, and 2 cm in cores V08G04, V08G08, V08G11, and V08G16, respectively. These first detection of ^{137}Cs in the cores corresponds to around 1953, which closely matches the early 1950s increase in total fission yields from the explosions (Carter and Moghissi, 1977). The first peak values and increases in ^{137}Cs in the Lake van cores occur at depths of, 2 cm, 2.5 cm, 1.5 cm, and 1.5 cm incores V08G04, V08G08, V08G11, and V08G16, respectively (Figure 4.12). These values correspond to the period of maximum atmospheric nuclear testing in 1963, the year the nuclear weapons Limited Test Ban Treaty was signed (Carter and Moghissi, 1977; Appleby, 2001). The elevated amounts of radioactivity released in the 1960s were therefore recorded in the Lake Van sedimentary record.

Higher up in the profiles of ^{137}Cs, we also see another peak in activity corresponding in age to ~1986 according to the ^{210}Pb age (Figure 4.12). The timing of this peak is consistent with fallout resulting from the release of radioactivity that followed the Chernobyl nuclear power reactor accident in Ukraine. As in some European sites, the deposition of Chernobyl ^{137}Cs provides another datable horizon in the Lake Van sediments, characterized in some cases by an even greater inventory than that

resulting from the bomb tests (Dominik and Span, 1992; Ehlers et al., 1993; Callway et al., 1996; Gevao et al., 1997).

^{137}Cs and ^{210}Pb profiles indicate that the coring technique recovered the uppermost levels of the deposit and that the mobility of both radionuclides within the sediments is small. The correlation between ^{137}Cs and ^{210}Pb specific activities of different sites suggests that the mode of transport of both of these radionuclides is comparable involving attachment to settling particles of different composition. The radionuclide profiles also indicate that there is no or very limited post-depositional redistribution by physical mixing or bioturbation. Thus, the measurement of both ^{210}Pb and ^{137}Cs in sediment cores provide much more information than can be gained from either radionuclide alone with regard to understanding the physical and chemical nature of the sedimentation process.

Figure 4.13 shows the age-depth models obtained for the upper part of all cores using both the ^{210}Pb and the varve dating. Note that the use of varve counts instead of the ^{210}Pb CRS model in the top 7-8 cm of the core would not have changed the age estimates significantly.

Results of the ^{210}Pb dating method show different sedimentation rates in different core locations (Figure 4.13). The highest sedimentation and mass accumulation rates are observed in core V08G08 located offshore the city of Van, followed by cores V08G04, V08G16 and V08G11. According to ^{210}Pb dating with CRS model, the highest sedimentation and mass accumulation rate in core V08G08 are 0.58-0.71 mm.year^{-1} and 0.49-0.60 kg.m^{-2} .year^{-1} respectively. The highest sedimentation and accumulation rates at this site is probably due to the anthropogenic activities in the provincial city of Van as well as the Karasu river input with a relatively large drainage area (Figure 4.1). The other three cores show almost similar sedimentation rates (0.42-0.54 mm.year^{-1} for core V08G04, 0.31-0.44 mm.year^{-1} for core V08G11 and 0.34-0.46 mm.year^{-1} for core V08G16).

The comparison of the SRs and MARs in Lake Van cores in different studies show that SR and MAR values varies considerably in different parts of the Lake (Landmann et al., 1996a; Yıldız and Yener, 2010; Meydan, 2013). One of the studies by using ^{210}Pb dating model with CS:CF age model showed that sedimentation rates varies between 0.6-3.6 mm.y^{-1} near river mouths in different parts of Lake Van

(Figure 5.1, Meydan, 2013). According to this study core Van09-04, very far from the river mouths, has the lowest SR (0.6 mmy^{-1}), while core Van09-09, very close to the mouths of Benmahdi, Deliçay and Zilan Streams, has the highest SR (3.6 mmy^{-1}). Another study determining MAR values in Lake Van sediments using ^{210}Pb dating method with CRS age model showed the MAR values varies between 0.31-0.77 kg.m^{-2}.y^{-1} (Yıldız and Yener, 2010) which are very close to MAR values calculated in our study. In this study (Yıldız and Yener, 2010) the highest MAR value belongs to core B (0.77 kg.m^{-2}.y^{-1}), which is closer to the river mouth than Core A and Core C (Figure 5.1).
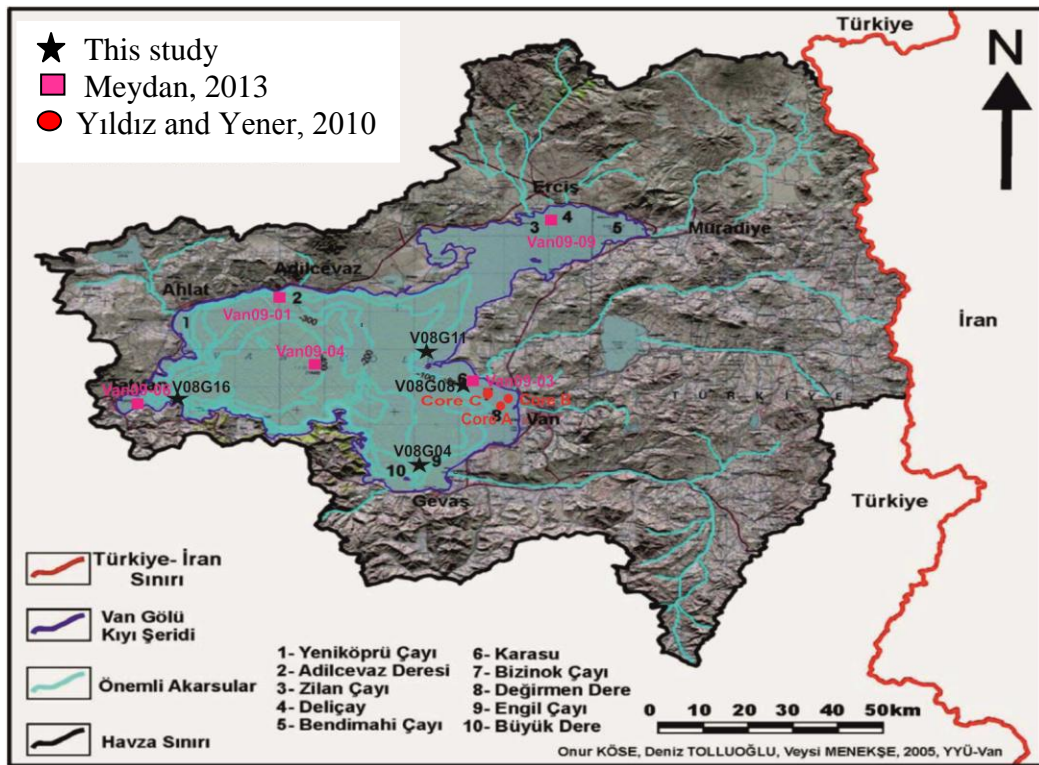
Figure 5.1 : Drainage area of Lake Van showing core locations from different studies.

Considering all these studies, it can be concluded that SR and MAR values are affected by the distance of core location to river mouths.

Varve counting of annually laminated sediments of Lake Van using digital X-ray radiographic images provided another means of dating the cores (Damcı and Çağatay, 2015). This method allowed us to extend the age dating beyond the limits of the radionuclide techniques (up to 150 years). Our study shows that varve counting method detects and counts fine-scale laminae, and produces robust varve ages that

are comparable with independently determined ^{210}Pb and ^{137}Cs ages (Table 4.6, Table 4.7, Table 4.8, Table 4.9 and Figures 4.11-4.14).

Another independent evidence for the robustness of our varve age model is the varve age of 590 year BP obtained for the a tephra layer detected in core V08G16 (Figure 4.9). This tephra originated from the Nemrut Volcano was previously dated at 600 years BP in Lake Van cores by Litt et al. (2009). It corresponds to the historical erruption of AD 1441 (Aydar et al., 2003; Haroutiunian, 2006). This tephra is only observed in core V08G16 which is the closest to the Nemrut Volcano. The other older eruptions (i.e , 2000, 2600, 2700 years BP) found by Litt et al. (2009), Landmann (2011) were not detected in any of our cores.

5.1.2 Radiocarbon ages and reservoir age

The radiocarbon ages of the four samples measured on bulk organic carbon are much older than the varve-model ages, corresponding to their respective levels in the cores (Table 4.10). The difference between the radiocarbon ages and the varve ages is variable along the cores, indicating the variable reservoir effect with time, as discussed below.

The reservoir ages of the samples, calculated as the difference between its determined radiocarbon age and the uncalibrated radiocarbon age of the same level derived iteratively from the age model, range from 1190 years BP to 3800 years BP (Table 4.9). A similar study by Lemcke (1996) using the AMS dating of the bulk carbonates in Lake Van indicated a reservoir age of 2.6 ka for the surface sediments increasing to about 4.7 ka for sediments of 14 ka varve a BP. In our study also there is a general increasing trend with increasing varve age. The only exception is the sample with the varve age of 1770 years BP, having the lowest reservoir age of 1200 years. The age of this sample corresponds in time to a low detrital input (low Ti, Fe and K contents) and δ^{18}O values (Figure 4.20 and Figure 4.40). These low elemental and isotopic values suggest a relatively wet climate with dense vegetation cover for this time interval. The C/N ratio of the sample is one of the highest (20) which indicates high proportion of land plant material (Meyers, 1994). This composition of organic matter with high proportion of contemporaneous land plant material with no reservoir effect explains the low reservoir age for this sample. The lower proportion

102

of algal organic matter during this humid period is probably due to higher contribution of winter-snow precipitation relative to spring season precipitation.

The sample with the highest reservoir age (~3800 years, located at 80-81 cm core depth) also has relatively low detrital input and $\delta^{18}O$ values, suggesting similar wet climatic conditions, with high vegetation density in the Lake Van drainage basin. However, this sample has a very low C/N ratio (~5) indicating organic matter of predominantly lacustrine algal origin (e.g., Meyers et al., 1984; Prahl et al., 1994; Hedges et al., 1997). The high reservoir age of this sample is caused by the lacustrine algal origin of its organic matter because lacustrine algea utilizes desolved carbon dioxide from the lake waters with "hard water effect" (Broecker and Olson 1961; Zhou et al. 2009; Ascough et al. 2011; Soulet et al. 2011). The high proportion of lacustrine organic matter suggests high contribution of spring precipitation during the deposition of the sample resulting in the highest reservoir age.

5.2 Factors Affecting the Stable Isotope Composition of Bulk Carbonate in Lake Van Sediments

We analyzed the stable carbon and oxygen isotopes' compositions of bulk carbonate and ostracod *Limnosthere inopinata* shells from core V08G04 for interpretation of environmental conditions including water balance, organic productivity and seasonality of precipitation. There is a high positive correlation between $\delta^{18}O$ and $\delta^{13}C$ values of both bulk carbonates and ostracod shells in core V08G04, with a correlation coefficient (r) of 0.70 and 0.96. These high corrrelations suggest that these variables are controlled mainly by the precipitation (P) and evaporation (E) (P-E) balance in a closed lake (e.g., Talbot, 1990; Li and Ku, 1997; Roberts et al., 2008). However, there are also other parameters that may affect the $\delta^{18}O$ content of lake water, such as temperature, seasonality and source of moisture (Rozanski et al., 1992; Bar-Matthews et al., 1999; Cole et al., 1999; Gat et al., 2001; Çağatay et al., 2014; Kwiecien et al., 2014).

The main source of moisture in Lake Van region is the storm track originating in the North Atlantic, which is strongly modified in the Mediterranean (Karaca et al.,

2000). Temperature controls the isotopic composition of precipitation by condensation and isotope partitioning during phase transitions (i.e., evaporation and condensation) (Cole et al., 1999). Moreover, interpreting the influence of temperature on stable isotope values, attention should be paid to two processes with opposite effects. An increase in temperature leads to an increase in the evaporation/precipitation ratio and enrichment in "heavy" stable isotopes in the ambient water with a gradient of approximately +0.6 ‰/°C (Dansgaard, 1964). At the same time the equilibrium isotope fractionation between carbonate and ambient water has a gradient of -0.23‰/°C (O'Neil et al., 1969). A non linear relationship can occur between these two processes, consequently the resultant gradient of ~0.36 ‰/°C may be unreliable (Leng and Marshall, 2004). However, the overall effect of temperature is to enrich the precipitation in the heavy isotope. The rate of enrichment for the Anatolian stations is between 0.6 and 0.7 ‰ °C^{-1} (IAEA/WMO, 2014). Thus, an increase in average temperatures during the warm and wet periods would be an important factor raising the precipitation $\delta^{18}O$ values.

Seasonal variations in the amount and isotopic composition of precipitation are large in continental regions (e.g., Jouzel et al., 1997), which can cause considerable changes in the weighted mean of precipitation $\delta^{18}O$ value (Stevens et al., 2001). Seasonality of precipitation is therefore an important factor to consider, as has already been proposed for Lake Van (Çağatay et al., 2014; Kwiecien et al., 2014).

The $\delta^{13}C$ value depends mainly on water balance, organic productivity and $\delta^{13}C$ value of the carbonate rocks in the watershed. Water balance has similar effect on $\delta^{13}C$ values as on the $\delta^{18}O$ values, with the $\delta^{13}C$ values becoming more negative with increase in the P-E balance. Increase in organic productivity (eutrophication) in a lake results in more positive $\delta^{13}C$ values of lake waters, and lowers the corelation between the $\delta^{13}C$ and $\delta^{18}O$ values.

For core V08G04, significant differences between the stable isotope values of bulk carbonate and ostracoda shells exist. The $\delta^{18}O$ and $\delta^{13}C$ values of ostracod shells range between -19.2 ‰ and +4.5 ‰ and -17.4 ‰ and +2.8 ‰, respectively, whereas the same values of the bulk carbonates vary between -1.2 ‰ and +0.6 ‰ and +2.5 ‰ and +4.2 ‰. The wide range of $\delta^{18}O$ and $\delta^{13}C$ values of the ostracoda compared to

those of bulk carbonates imply that one must consider the influence of vital effects on stable isotope values. The lower correlation between the $\delta^{18}O$ and $\delta^{13}C$ of bulk carbonate compared to the correlation for the ostracod shells may suggest that the the bulk carbonate $\delta^{13}C$ values are more effected by organic productivity in lake waters.

Like most ostracods the shells of the only ostracod species *Limnosthere inopinata* in Lake Van consist mainly of Low-Mg calcite with the presence of amorphous calcium carbonate in some cases (Xia et al., 1997a). It is widely accepted that the carapace mineral composition reflects the host water chemistry, because ions that form the shells (Ca^{2+} and HCO_3^-) are directly taken from the host water. The ostracod vital cycle requires 8 to 9 moults before reaching the adult stage with a very short duration for calcification after each moult (Holmes, 1996). Neverthless, it is necessary to take into account that the calcification moment is depending on species-specific characteristics such as the number of generations per year, the season in which a generation originates, the time passed between the first instar and adult specimen. In order to improve the stable isotope analysis interpretation, all these variables have to be considered. Hence, it is essential to gain information about ostracods' ecology. Unfortunately, the large part of ostracod's life cycle including that of *Limnosthere inopinata* is still unknown. As a result, the vital offset influence on $\delta^{13}C$ of ostracod valves is still not completely understood, which appears to create systematic variations (Xia et al., 1997b). Moreover, it is hard to define the variations caused by the vital effects on $\delta^{13}C$ with the same resolution obtainable for the $\delta^{18}O$ values, because it is difficult to separate vital effect influence from variations due to seasonality. Consequently, stable isotope data measured on ostracods have some difficulties in interpratation of environmental parameters.

5.3 Climate Records and Global and Regional Comparisons

5.3.1 Climate records

Our multi-proxy data sets from Lake Van have different resolutions ranging from 0.5 mm for the XRF elemental data to 5 cm for the ostracod data. Therefore it is not possible to make detailed (high-resolution) comparisons between the different data sets. However, it is possible to interpret the data sets in terms of centennial time scale

environmental reconstructions, based on the following relationships between the multi-proxy records:

1) There is a weak negative correlation between TOC and IC (for core V08G04 r=-0.40) which suggests that carbonate precipitation in the lake is controlled by other factors such as seasonality of precipitation, in addition to the primary productivity (photosynthesis).

2) Lithogenic element concentrations (XRF counts), such as those of Ti, Fe, and K, appear to be inversely correlated with Ca (IC, carbonate) content. The high detrital input occurs during the dry periods because of low vegetation density, whereas the Ca enrichment is observed during the wet periods when Ca-rich river water input increases, promoting the carbonate precipitation in the bicarbonate-rich Lake Van waters. This is supported by the negative correlation between $\delta^{18}O$ and IC values (r=-0.61), which indicates that the carbonate precipitation occurs during periods of isotopicaly light fresh water input.

3) In general, decreases in the ostracod (*Limnosthere inopinata)* numbers correspond to increases in the Ca (IC) contents, suggesting decrease in the salinity and unstable environmental conditions for the ostracods by seasonal input of river waters (F.Ruiz et al., 2012). The only ostracod species present in Lake Van, *L.inopinata,* is known from both fresh and saline water: It lives in lakes with salinities up to 46 g L^{-1}, with low calcium concentrations, but rich in sodium and bicarbonates (Forester, 1983; Neale, 1988). The river input, mainly driven by climate, often leads not only to a simple dillution of the lake water but also a change of water chemistry, depending on the hydrogeological regime of the basin (Mackenzie et al., 1995). Hence, the changes in river input would result instability in the living conditions of the ostracod.

4) The positive correlation between $\delta^{18}O$ and $\delta^{13}C$ of the bulk carbonate fractions of Lake Van sediments (r=0.70) suggests that these parameters are controlled by the water balance (E/P) (Tarutani et al., 1969; Talbot, 1990; Cole et al., 1999; Stevens et al., 2001). In addition, the Lake Van $\delta^{18}O$ values are affected by the type of precipitation, with winter precipitation promoting relatively low, negative values (Çağatay et al., 2014; Kwiecien et al., 2014). The effect of organic productivity on

$\delta^{13}C$ values appears to be insignificant considering the very low negative correlation (r=-0.10) between the TOC and $\delta^{13}C$ values.

5) The C/N ratio of organic matter in Lake Van sediments range between 1.0 and 32.5 and its downcore distribution suggests a relatively high fraction of lacustrine algal matter during the wet periods, as discussed below. The carbon isotope composition of organic matter in Lake Van sediments changes in a very narrow range (-24.7 to -23.3) and suggests the predominance of organic matter of lacustrine algal origin (Figure 5.2).
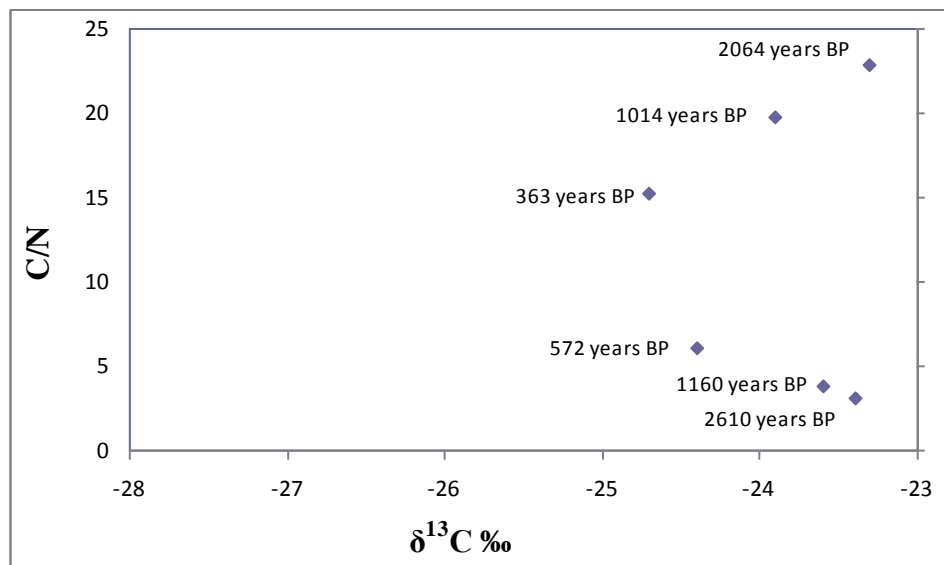
Figure 5.2 : $\delta^{13}C$ – C/N cross plot of organic matter in core V08G04. The numbers indicate the varve ages of samples.

According to the above multi-proxy relationships, the core V08G04 records show significant centennial scale variations in climatic conditions for the last 3500 years. The period 3500-3300 years BP is characterized by high Ti/Ca ratio (low Ca, intermadiate Ti values), intermediate TOC (4.9-5.7 %) and TIC (4.0-4.6 %) values, relatively high +0.2 to -0.1 ‰ $\delta^{18}O$ values, low C/N (1.5-3) and low ostracod numbers (71-264) (Fig 5.3). Considering all these multi-proxy parameters together, this period is considered a cold and dry time interval with intermediate detrital input and relatively high evaporation-precipitation ratio. Organic productivity is intermediate with relatively stable values averaging around 5 %.

The period between 3300 and 2900 years BP shows low Ti, low to intermediate Ca and intermediate to low Ti/Ca values (Figure 5.3). These proxies suggest that the period was relatively warm and humid with low detrital input because of low erosion rate due to high vegetation cover. Intermediate TOC values (3.6-5.1 %) with low C/N ratio (~ 2) suggest intermediate organic productivity mainly of algal origin. Relatively low $\delta^{18}O$ values and low ostracod numbers (~70) suggest unstable environmental conditions with low evaporation-precipitation ratio.

The following period during 2900-2600 years BP is charectrized by very high Ti values and Ti/Ca ratio, suggesting cold and dry climatic conditions with high detrital input. The relatively low $\delta^{18}O$ values (-0.7 to -1.2) is probably due to high winter precipitation during this period. The C/N ratio is higher (3-18) than in the previous period, showing relatively high input of terrestirial organic matter. Relatively high and increasing ostracod numbers (20-1330) suggest stable conditions despite the cold and dry climate.

The next period between 2600 and 2400 years BP shows intermediate Ti, low to intermediate Ca and intermediate Ti/Ca values. These proxies suggest that the period was relatively warm and humid. Intermediate TOC values (4.9-4.8 %) with low C/N ratio (~ 10) suggest intermediate organic productivity mainly of lacustrine algal origin. Relatively low $\delta^{18}O$ values (-0.7 to -0.8) and high ostracod numbers (4400-5200) suggest stable and humid environmental conditions with relatively low evaporation-precipitation ratio.

The period 2400-1800 years BP is characterized by relatively high Ti/Ca ratio (low Ca, intermadiate Ti values), intermediate TOC (5.9-7.1 %) and TIC (3.7-4.6 %) values, relatively high (0 to -0.4 ‰) $\delta^{18}O$, and C/N (20.4-23) values and very high ostracod numbers (1400-6000) (Fig 5.3) . This period includes a time interval between 2300 and 2100 years BP with relatively low Ti and Ti/Ca values, and intermediate ostracod numbers (~2500) . Considering all these multi-proxy parameters together, the period during 2400-1800 years BP is considered to be a commonly cold and dry time interval with intermadiate detrital input, intermediate.
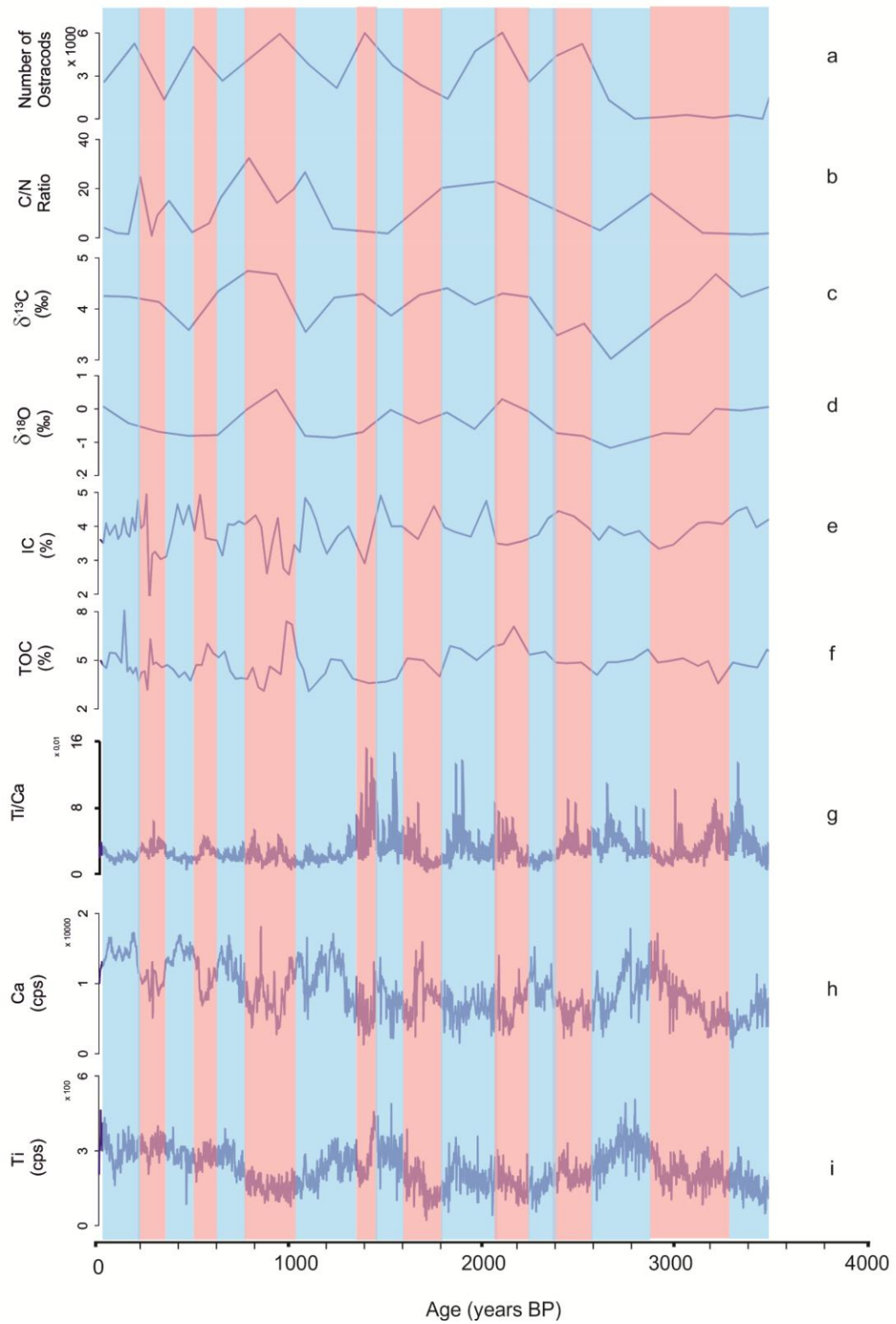
Figure 5.3 : Multi-proxy data for core V08G04 representing the last 3500 years: number of ostracods (a), C/N (b), $\delta^{13}C$ (c), $\delta^{18}O$ (d), IC (e), TOC(f), Ti/Ca (g), Ca (h), and Ti (i) profilesG in core. Blue and pink stripes show the cold/dry and warm/humid intervals, respectively.

organic productivity and relatively high evaporation-precipitation ratio. It is interrupted by a two hundred-year warm and wet interval during 2300-2100 years

BP, charecterized by relatively high organic productivity and unstable conditions as shown by high TOC and low ostracod numbers.

The period between 1800 and 1600 years BP shows low Ti, intermediate to high Ca and low Ti/Ca values (Figure 5.3). These proxies indicate that the period was relatively warm and humid. Intermediate TOC (~ 5.0 %) and TIC (3.6-4.0 %) values with high C/N ratio (~20), which suggest intermediate organic productivity mainly of terrestirial origin. Relatively low $\delta^{18}O$ values (-0.4 ‰) and intermediate ostracod number (~1900) suggest almost stable environmental conditions with relatively low evaporation-precipitation ratio.

The following period during 1600-1450 years BP is charectrized by very high Ti values and Ti/Ca ratio, suggesting cold and dry climatic conditions with high detrital input (Figure 5.3). The intermediate to low TOC (3.7-3.9 %) and intermediate to high TIC (4.0-4.9 %) values are probably due to intermediate organic productivity during this period. The low C/N ratio (~2) suggests organic productivity of algal origin. The intermediate $\delta^{18}O$ values (~0.0 ‰) indcate intermediate evaporation-precipitation ratio. Relatively high and increasing ostracod numbers (~3700) suggest that stable environmental conditions prevail during this period.

During the hundred year interval between 1450 and 1350 years BP, relatively low Ti, Ca values and relatively high Ti/Ca ratio point to a wet and humid climate with relatively low detrital input (Figure 5.3). Commonly low TOC (~ 3.6 %) and TIC (~ 2.9%) values with low C/N ratio (~2) suggest low organic productivity of algal origin. Low $\delta^{18}O$ values (~ -0.7 ‰) and very high ostracod numbers (~6000) suggest low evaporation-precipitation ratio with high lake levels and stable environmental conditions.

The next period between 1350 and 1050 years BP is characterized by intermediate Ti/Ca ratio (intermediate to high Ca and Ti values), low to intermediate TOC (3.1-5.1 %) and intermediate to high TIC (3.2-4.8 %) values, relatively low 9 ‰ $\delta^{18}O$ values (-0.8 to -0), highly variable C/N (4-27) and intermediate ostracod numbers (~2200) (Figure 5.3). Considering all these multi-proxy parameters together, this period is considered to be a generally cold and dry time interval with high detrital

input and relatively high winter precipitation. Organic productivity is intermediate with variable contribution of algal and terrestrial organic matter.

The period 1050-770 years is charectrized by low Ti values and intermediate Ti/Ca ratio, suggesting warm and humid climatic conditions with low detrital input (Figure 5.3). The variable TOC (3.1-7.2 %), low to intermediate TIC (2.5-4.2 %) values and are probably due to variable organic productivity. The intermediate C/N ratio (~14) suggests organic productivity of mixed algal and terrestrial origin. The relatively high $\delta^{18}O$ values (~ +0.6 ‰) point to relatively low winter precipitation rather than high evaporation-precipitation ratio. There is only one high ostracode number (~5900) which suggests favourable environmental conditions at the sampling level. However, a single ostracod value does not allow any correlation with the other multi-proxy parameters which show variable environmental conditions.

The following period during 770-600 years BP, intermediate Ti, low Ca values and relatively intermediate Ti/Ca ratio suggest that this time interval has cold and dry climatic conditions (Figure 5.2). The low to intermediate TOC (3.9-5.6 %) and TIC (3.1- 4%) values, relatively low $\delta^{18}O$ (~ -0.8 ‰) values) is probably due to intermediate organic productivity and low evaporation-precipitation ratio during this period. The intermediate C/N values (~16) and ostracod number (~2600) suggest organic productivity of mixed algal and terrestrial origins and favourable environmental conditions for the ostracoda.

The next period between 600 and 500 years BP is characterized by relatively high Ti/Ca ratio (intermediate Ti, low Ca values), intermediate to high TOC (4.7-6 %) and TIC (3.7-4.9 %) values, low C/N values (6), relatively low (~ -0.8 ‰) $\delta^{18}O$, and intermediate ostracod number (~3000) (Figure 5.3). Considering all these multi-proxy parameters together, this period is considered to be a warm and humid time interval with low detrital input and low evaporation-precipitation ratio. Organic productivity is intermediate of algal origin. The intermediate ostracod number indicates relatively stable environmental conditions.

The period during 500-350 years BP is charactrized by intermediate Ti values and intermediate to low Ti/Ca with relatively high Ca values, suggesting mildly cold and

dry climatic conditions with intermediate detrital input (Figure 5.3). The cold and dry conditions were not as severe as during the previous periods such as those during 2900-2600 and 1600-1450 years BP. The low TOC (3.7-4.7%) and variable C/N values (2.3-15) show low organic productivity with variable proportions of algal and terrestrial organic matter input. The high TIC (3.1-4.7) and Ca values are either related to high evaporation-precipitation balance or high Ca-rich river water input rather than organic productivity. The relatively low $\delta^{18}O$ values (~ -0.8) is probably due to high winter precipitation during this period. Intermediate ostracod number (~3000) suggests stable environmental conditions during this cold and dry time interval.

The period between 350 and 200 years BP is represented by low Ca and TIC (1.8-4.9 %), intermediate Ti values and relatively high Ti/Ca ratio, variable TOC (3.2-6.3 %), low C/N ratio (1-9) and $\delta^{18}O$ value (-0.7 ‰) (Figure 5.3). These multi-proxy values suggest relatively warm and wet conditions with variable organic productivity of algal origin. The low $\delta^{18}O$ value may suggest low evaporation-precipitation ratio with low Ca input.

The last 200 years BP show low to intermediate Ti values, high Ca and TIC (3.5-4.3 %) contents, intermediate to high TOC (4.6-8.1 %) values, intermediate $\delta^{18}O$ (-0.4 to 0.1 ‰) and very low C/N values (1.5-4) (Figure 5.3). According to these multi-proxy parameters mildly cold conditions prevailed in Lake Van compared to the previous period. The organic productivity is intermediate to high and mainly represented by organic material of algal origin. Ostracod values decrease from 5300 to 2600 from the beginning to the end of this period.

From the above description of changes in the multi-proxy parameters, in particular the high resolution core scanner µ-XRF Ca and Ti/Ca profiles, we conclude that there are centennial scale climatic variations in Lake Van over the last 3500 years. These variations correspond to alternation of cold/dry and warm/wet periods with durations rangeing from 100 to 350 years (Figure 5.3). Especially high Ca contents during cold and dry periods and low contents during warm and wet periods are clearly observable from the profiles. The high Ca contents during cold and dry periods can be explained by the increased winter precipitation in the form of snow in the

mountainous drainage basin of Lake Van. Even though the cold periods were dry during spring and summer they were most probably characterized by increased winter snow precipitation (i.e., increased seasonality of precipitation) (Tarutani et al., 1968; Talbot, 1990; Cole et al., 1999; Stevens et al., 2001). During such cold periods, snow melting in late spring and summer would supply large amount of Ca-bearing water drived from volcanic rock weathering. The Ca-rich waters would promote precipitation of $CaCO_3$ in the lake waters with high HCO_3 content (Reimer et al., 1996). On the contrary, during the warm and wet periods with low winter precipitation and relatively high spring and summer precipitation there would be less Ca-rich fresh waters delivered to the lake from the drainage basin, probably because of increased evaporation from the spring and summer precipitation. Hence, it is expected that less $CaCO_3$ would precipitate during the warm and wet periods compared to the cold and dry periods.

5.3.2 Global and regional comparisons

On a regional scale, Lake Van records in core V08G04 can be confidently correlated with various climate records from Lake Nar (Central Anatolia), Sofular Cave speleothem (North-West Turkey), Lakes Zeribar and Mirabad (Iran) and Soreq Cave (Israel) (Figure 5.4). These records from west and south of the Lake Van region in Anatolia and the Near East have yielded important paleoclimatic archives for the region that is on the direct path of westerly sourced moisture from the Atlantic Ocean and Mediterranean Sea.

First, we compare the Lake Van records with the Anatolian records (Lake Nar and Sofular Cave) and historical European records over the last 1800 years, and then with the Near East continental records for Lakes Zeribar and Mirabad, and Soreq Cave) over the last 3500 years. In this comparison we have adjusted the time scale so that the present day represents the year 1950 for all records in Figure 5.5. Our time scale is in good conformity with the age scale of the Sofular record (Fleitmann et al., 2009) based on U/Th series dating of speleothems, but shows about 50 year difference from the Lake Nar age scale. Therefore, the Lake Nar oxygen isotope record was tuned to conform with age scale of our study.

Figure 5.4 : Locations of Lake Nar (Central Anatolia), Sofular Cave (North-West Turkey), Lakes Zeribar and Mirabad (Iran) and Soreq Cave (Israel).

Comparison with the Anatolian records and historical European records

The period 1750-1550 years BP (P, present being 1950), with relatively low Ti and high Ca values, indicate warm and wet conditions in Lake Van region. This is also the case in Lake Nar with relatively high $\delta^{18}O$ values, showing evaporative conditions (Eastwood et al., 2008), in Sofular Cave with low $\delta^{13}C$ values (Fleitmann et al., 2009) and in the Alps with glacier retreat (Holzhauser et al., 2005) for the same time interval (Fig 5.5). This period corresponds to the main part of the Roman Warm Period (RWP) which is considered to be between 2000 and 1500 years BP (Bianchi and McCave, 1999).

1550-1400 years BP is a cold and dry period both in Lake Van and Lake Nar (Fig 5.5a, b, c ,f). The Sofular Cave $\delta^{13}C$ record also show low vegetation density implying cold and dry conditions that are further supported by the glacier advance in the Alps (Figure 5.5e).

The period between 1400 and 1300 years BP is a warm and wet time interval in Lake Van, Lake Nar and Sofular Cave as suggested by low Ti and Ca counts, low bulk carbonate $\delta^{18}O$ values in Lake Van and low speleothem $\delta^{13}C$ values, respectively (Fig 5.5). The period also corresponds to the glacial retreat in the Alps (Figure 5.4e).
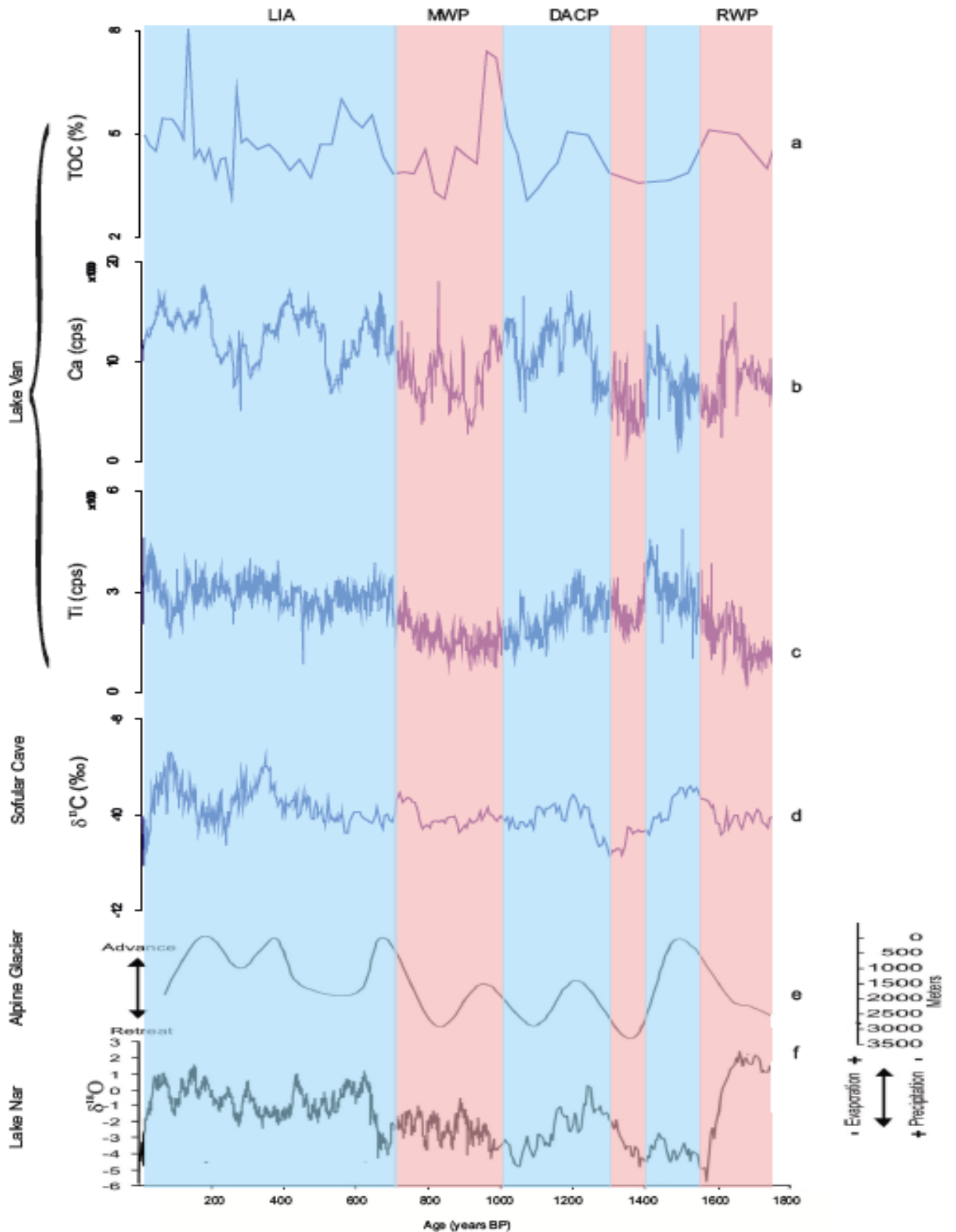
Figure 5.5 : Ti and Ca μ-XRF counts and TOC(%) of Lake Van sediments (a, b,c) compared with Lake Nar (e), Sofular Cave stable isotope records (f) (Jones et al., 2006; Fleitmann et al., 2009) and Alpine Glacier advances and retreats (e) (Hoizhauser et al., 2005).

This short warm and wet period is followed by a cold and dry time interval during 1300-1000 years BP (AD 650-950) which is marked by high Ti and Ca counts in Lake Van, high $\delta^{13}C$ values in Sofular Cave and high $\delta^{18}O$ values in Lake Nar (Figure 5.5 b-d, f). This conclusion is supported by the glacier advance in the Alps (Figure 5.5 e). This period partly corresponds to Dark Ages Cool Period (AD 440 to AD 900) characterized by a marked cooling. A particularly puzzling event apparently occurred in AD 540 when tree rings suggest greatly retarded growth, the sun appeared dimmed for more than a year, temperatures dropped in Ireland, Great Britain, Siberia, North and South America, fruit did not ripen, and snow fell in the summer in southern Europe (Singer and Avery, 2007). In AD 800, the Black Sea froze and in AD 829 the Nile River froze (Oliver, 1973).

The three-hundred long period between 1000 and ~700 years BP (AD 950-1250) is characterized by low Ti and variable Ca counts and TOC values in Lake Van, low $\delta^{18}O$ values in Lake Nar, low and uniform $\delta^{13}C$ values of cave carbonates in Sofular suggesting warm and wet conditions (Figure 5.5). This period includes one relatively small advance and one retreat of Alpine Glaciers impling variable climatic conditions (Figure 5.5e). This is supported by variable Ca counts and TOC contents in Lake Van region. This period corresponds to the major part of the Medieval Warm Period (MWP) which is considered to be between AD 900 and AD 1300 when global temperatures were apparently somewhat warmer than at present (Oliver, 1973, Tkachuck, 1983). Its effects were evident in Europe where grain crops flourished, alpine tree lines rose, many new cities arose, and the population more than doubled. The Vikings took advantage of the climatic amelioration to colonize Greenland, and wine grapes were grown as far north as England where growing grapes is now not feasible and about 500 km north of present vineyards in France and Germany.

Titanium counts in Lake Van and $\delta^{18}O$ values in Lake Nar show a steep increase starting ~ 700 years BP (AD 1250) and remain relatively high with only small oscillations (Figure 5.5 c, f). These trends in Lake Van and Lake Nar records suggest a change to cold and dry conditions, corresponding to the onset of the Little Ice Age (LIA) which is well recorded in Europian history. While there is evidence that many other regions outside Europe exhibited periods of cooler conditions, expanded glaciation, and significantly altered climate conditions, the timing and nature of these variations are highly variable from region to region, and the notion of the Little Ice

Age as a globally synchronous cold period has all but been dismissed (Bradley and Jones, 1993; Mann et al., 1999). If defined as a large-scale event, the Little Ice Age must instead be considered a time of modest cooling of the Northern Hemisphere, with temperatures dropping by about 0.6 °C during AD 1300-1900 (Bradley and Jones, 1993; Jones et al., 1998; Mann, 2002). The sharp increase in $\delta^{18}O$ observed in Lake Van (Figure 4.41) and Lake Nar records (Figure 5.5f) does not correspond to a decrease in the Sofular Cave $\delta^{13}C$ record (Figure 5.5d). However, the Sofular $\delta^{13}C$ record shows similarities with Ca counts, in Lake Van and the Alpine Glacier advances for the last 550 years. Calcium record in Lake Van shows marked oscillations with three positive excursions during 700-550, 500-350 and 200-0 years BP. As explained in section 5.3, these high Ca counts are related to cold time intervals. One of these cold intervals with high Ca counts and low TOC contents can be correlated with the coldest interval of LIA, the Late Maunder Minimum during AD 1650-1700 (Pfister, 1999; Wanner et al., 2000). This period coincides with an enhanced concentration in atmospheric ^{14}C (Stuiver and Braziunas, 1993), several large volcanic eruptions (Briffa et al., 1998), a reduced solar activity, and a low number of sunspots (Spörer, 1887; Maunder, 1922; Eddy, 1976; Lean et al., 1995). Solar activity during the Late Maunder Minimum was near its lowest levels of the past 8000 years (Lean and Rind, 1999). Jones et al. (1998) and Briffa (2000) found a decrease of the Northern Hemisphere (NH) April–September temperatures on the order of approximately 0.3–0.6ºC compared to the reference period of 1961–1990. The Late Maunder Minimum (LMM, AD 1675–1715) is one of the few cold periods in recent centuries that persisted for decades. A broad spectrum of high resolution multi-proxy and instrumental data are available for this period (Wanner et al., 1995; Luterbacher et al., 1999; Pfister, 1999; Luterbacher, 2000; Luterbacher et al., 2000).

Part of the increse in Ti counts starting at 700 years BP may partly be due to human activities, such as deforestation and cultivation of the land. Such activities would greatly increased erosion rates and supply large amount of terrigenous material to the lake (Judson, 1968; Trimble,1975).

Comparison with the Near-East records

In this section we compare our Lake Van records for the last 3500 years with those from Lake Zeribar, Lake Mirabad and Soreq Cave in the Near East (Bar-Matthews et al., 1999,2003; Stevens et al., 2001, 2006)(Figure 5.6). However the resolution of these Near East records are not sufficiently high enough for comparison, especially with our µ-XRF elemental records from Lake Van. Therefore we can only make some general comparisons with the Near East records (Figure 5.6).
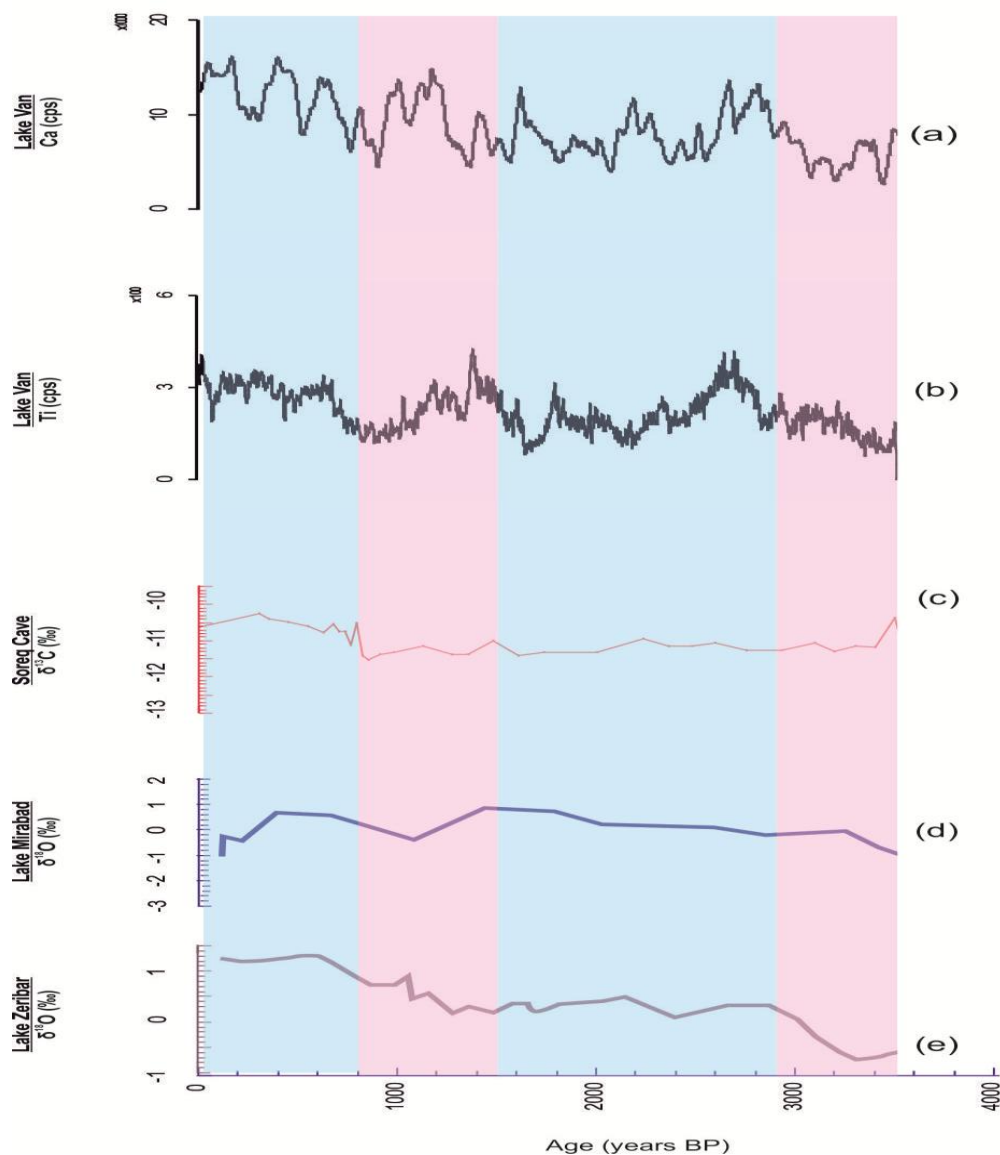
Figure 5.6 : Comparison of Lake Van µ-XRF Ti record (this study) with stable isotope records from Near East (Soreq cave: Bar-Matthews et al., 1999, 2003; Lake Mirabad: Stevens et al., 2001; Lake Zeribar: Stevens et al., 2006).

118

The period from 3500 to 2900 years BP is characterized by relatively low $\delta^{18}O$ values (-0.5 to -1‰) in Lake Zeribar, intermediate $\delta^{18}O$ values (-0.5 to 0 ‰) in Lake Mirabad and generally low $\delta^{13}C$ values in Soreq Cave all suggesting a humid climate (Figure 5.6). These Near East records are comfortable with relatively low Ti and Ca counts in Lake Van (Figures 5.5 and 5.6). Intermediate $\delta^{18}O$ values in Lake Mirabad can be explained by predominance of summer precipitation (Stevens et al., 2001). $\delta^{18}O$ values show an increasing trend from 2900 to 1500 years BP in Lake Zeribar and Lake Mirabad suggesting a change towards drier conditions. The Soreq $\delta^{13}C$ values for the same period, however, show a slight decreasing trend with time implying increasing humidity (Figure 5.6c). The same period in Lake Van is represented by alternating three positive, four negative excursions of Ti and four positive, four negative excursions of Ca counts located on a decreasing trend with decreasing age (Figure 5.6a, b). The general decreasing trend of Ti in Lake Van suggests decreasing erosion rates with time under increasingly humid conditions. Hence, the Lake Van records are conformable with the Soreq Cave records but discomformable with the Lake Zeribar and Lake Mirabad records.

$\delta^{18}O$ values for lakes Zeribar and Mirabad, $\delta^{13}C$ values for Soreq Cave and Ti counts in Lake Van all appear to show a decrease from 1500 to 800 years BP which imply a relatively humid period in the region. On the contrary, the same proxies in all four sites show a distinct increase over the last 800 years, which suggest a change to dry conditions. The Ca counts for this period in Lake Van are represented by three positive excursions that are related seasonality of precipitation, such excursions are not observed in Lake Zeribar, Lake Mirabad and Soreq isotope records because of the low resolution of the records at these sites.

Whereas the Lake Zeribar and Lake Mirabad records in Iran by Stevens et al. (2001, 2006) do not provide a clear evidence of the high-resolution climatic changes during the late Holocene, further to the west at Soreq Cave (Israel), speleothem records show changing moisture and temperature conditions in the eastern Mediterranean (Bar-Matthews et al., 1998, 1999). A comparison between Soreq Cave speleothems and eastern Mediterranean planktonic foraminiferal oxygen-isotope records (Schilman et al., 2002) have shown the presence of a strong link between marine and land hydrology during the late Holocene with three humid events dated to around BC 1250, AD 650 and AD 1250 with three distinct dry events

at BC 150, AD 1050 and AD 1650. The AD 1250 and AD 1650 events represent the Medieval Warm Period and the Little Ice Age, respectively.

In Soreq Cave (Israel), the time span AD 0–400 is characterised by negative precipitation anomalies (Schilman et al., 2002), implying reduced cyclogenesis in the Eastern Mediterranean region. Since the latter is the main source of overall moisture availability to the middle east and west Central Asia (Roberts and Wright, 1993; Aizen et al., 2001; Lioubimtseva, 2002), the cold and arid climate that persisted during ca. AD 0–400 most probably originated from the failure of depressions to penetrate into those continental regions of Central Asia which are reliant upon the westerly transport of cyclones, and/or the shift of storm tracks farther north (as happens during the positive NAO phase).

5.4 Assessment and History of Heavy Metal Pollution for Lake Van Region

The profiles of μ-XRF Zn, Pb, Ni, and Co counts in the four cores show general similar upward increasing trends, reaching maximum values near or at the core tops (Figures 4.34, 4.35, 4.36, and 4.37). A significant increase occurs in metals such as Zn, Pb, Ni, and Co over the last 30-60 years in Lake Van region. Especially significant increases in Zn and Pb occurred starting in 1960s due to the intensification of agricultural and industrial activities. Among the heavy metals studied, Cu in core V08G04 and Cu and Co in core V08G16 do not show any enrichment in the upper part of the cores, which are located south-east of Lake Van and east of Tatvan respectively. This is more likely to be due to the relatively low population density of the coastal areas close to these cores.

Comparison of heavy metal concentrations (μ-XRF counts) of the cores indicate that the maximum concentrations of all metals occur in the upper part of the core V08G08, located west of the Van city (Figures 4.34-4.37). This observation strongly suggests that the main source of heavy metals is the antropogenic pollution. The least heavy metal counts are found in the core V08G16 located east of Tatvan. Although Tatvan is a relatively large town the effects of its pollution sources are not observed in this core because of its relatively isolated location in a small crater (Figure 4.1). Some exceptions related to the occurence of Pb concentrations are observed in core V08G16. Relatively high Pb counts in this core is more likely to be due to its

location close to Van-Tatvan highway and Pb input fom leaded-gasoline use prior to about the year 2000.

The pattern of metal enrichments in the upper part of the cores representing the last 50 years in conformity with the fact that the urbanization and industry have developed more rapidly for Van city after 1960, when the coasts on both sides of the lake were opened to transportation. An overwhelming portion of the workforce in the industry is working in the textile and food industries located in the Lake Van drainage basin. The contamination of heavy metals in the lake was influenced also by agricultural intensification since 1960. As fertilizers contain heavy metals, their continuous application potentially exacerbates the accumulation of heavy metals in agricultural soils (Zeng et al., 2008). Other agricultural sources were related to the application of more and more machines in agricultural operations for cultivation, water pumping, and harvesting, and pesticides containing heavy metals since the 1960s. Furthermore the land use pattern in the whole watershed has changed over the past thirty years with increasing urban expansion, and industrial activities in recent decades. An increasing number of machines employed in agricultural operations introduced another anthropogenic Pb source in the form leaded-gasoline. The result of this activity is observed with a significant Pb anomaly in all near the studied core tops. The anomalous Pb values are followed upward by normal background Pb values which indicate the end of the use of leaded fuel by about the year 2000.

Furthermore, a significant Zn pollution is also related to utilization of Zn in fertilizers. This metal is a micro nutrient and purposefully added to regular blend fertilizers to meet the demand of plant growth. Thus, pollutants originating from the cultivated areas could enter into the lake directly or through river transportation. Moreover, the principal contributors of heavy metals in city runoff are the automobiles and structures that use of various metallic components. The traffic activities which produce heavy pollution include tire wear (Zn), fuel combustion (Pb), engine wearing and fluid leakage (Cu), and the building siding as a source of Pb, Cu, Zn.

6. CONCLUSION

It has been shown that Lake Van sediments, with their potential ability to record various climatic and environmental parameters, are valuable natural archives to study the Holocene climate of the region. However, they have also their own shortcomings. This study highlights the use of a multi-proxy approach to understanding sedimentation processes and paleoenvironmental changes in Lake Van. The study focuses on climate over the period of the last 3500 years at sub-centennial resolution. The results are discussed with other continental records in Anatolia and Near East.

In this study, multiple methods were used as chronostratigraphic markers. ^{210}Pb and varve counting methods were used as the main chronostratigraphic methods. In addition, ^{137}Cs dating and tephrochronology were used to test the age models based on ^{210}Pb and varve counting. Accelerator Mass Spectrometry (AMS) ^{14}C dates from total organic carbon (TOC) in one core diverges widely from the corresponding varve ages at the same level, suggesting significant reservoir ages, which range from 1.2 to 3.8 ka BP.

Double energetic window method by LSC which relies on the direct determination of ^{210}Pb without waiting for the in growth of ^{210}Po from ^{210}Pb was used to construct the chronology for the past environmental changes in Lake Van and surrounding region. The results show that the sedimentation rate varies significantly among the four study sites in the lake, ranging between 0.3 and 0.7 mm/year. This variation in sediment deposition rates can be explained by the amount of sediment input in different parts of Lake Van, which is in turn controlled by the variations in topography, bed rock lithology, drainage conditions and anthropogenic activities. The highest sedimentation rate is observed in core V08G08, followed by cores V08G04, V08G16 and V08G11. According to ^{210}Pb dating with CRS model, the highest sedimentation and mass accumulation rates in core V08G08 are 0.58-0.71 mm.year^{-1} and 0.49-0.60 kg.m^{-2}.year^{-1} respectively. The highest sedimentation and accumulation rates at this site is probably due to the anthropogenic activities in the provincial city of Van as well as the Karasu river input with a relatively large

drainage area(Figure 4.1). The other three cores show almost similar sedimentation rates (0.42-0.54 mm.year^{-1} for core V08G04, 0.31-0.44 mm.year^{-1} for core V08G11 and 0.34-0.46 mm.year^{-1} for core V08G16).

Varve counting of annually laminated sediments of Lake Van using digital X-ray radiographic images provided another means of dating the cores. This method permits the age dating to be extended beyond the limits of the radionuclide techniques (up to 150 years). Our study shows that varve counting method detects and counts fine-scale laminae, and produces robust varve ages that are comparable with independently determined ^{210}Pb and ^{137}Cs ages.

The low oxygen-isotope values in Lake Van during the late Holocene are interpreted to be the result of greater contribution of winter precipitation (snow). We consider that the increasing winter precipitation was caused by the extention of the "classic" Mediterranean climate with the earlier onset of local summer easterlies that block the penetration of spring moisture into the mountains.

All multi-proxy parameters including ostracods population, C/N ratio, stable isotope values, organic matter, Ti/Ca ratio showed alternations of cold/dry and warm/wet periods with 100-350 years duration over the past 3500 years. The cold/dry periods occured 3500-3300, 2900-2600, 2400-1800, 1600-1450, 1350-1050, 770-600, 500-350 and 200-0 years BP, whereas the warm/wet intervals were during 3300-2900, 2600-2400, 2300-2100, 1800-1600, 1400-1350, 1050-770, 600-500, 350-200 years BP (Figure 5.3).

The Lake Van climate records are conformable with the Lake Nar (Central Anatolia) and the Sofular (North-west Anatolia) speleothem records for the last 1800 years. These records include RWP, DACP, MWP and LIA, indicating teleconnections with the North Atlantic system. On a regional scale, the Lake Van records correlate with those from the lakes Zeribar and Mirabad in Iran, and Soreq Cave in Israel despite the poor resolution of the data from Iranian lakes.

μ-XRF heavy metal profiles along the Lake van cores show antropogenic inputs since 1960s.

A significant increase occurred in metals such as Zn, Pb, Ni, and Co in the last 30-60 years in Lake Van region. Especially increases in Zn and Pb in the upper parts of the cores indicate that the effect of important agricultural and industrial pollution began in the 1960's. Comparison of heavy metal concentrations (μ-XRF counts) indicate that the maximum concentrations of all metals occur in the upper part of the core V08G08, located west of the Van city (Figures 4.32-4.35). This observation strongly suggests that the main source of heavy metals is the antropogenic pollution. The pattern of metal enrichments in the upper part of the cores representing the last 50 years in comformity with the fact that the urbanization and industry have developed more rapidly for Van city after 1960, when the coast on both sides of land routes opened to transportation. An increasing number of machines employed in agricultural operations for cultivation, water pumping and harvesting represents another anthropogenic Pb source because Pb was previously added to gasoline. The result of this activity is observed with a significant Pb anomally in all the studied cores. These anomolous values are followed upward by normal background Pb values which corresponds to the end of the use of leaded fuel by the begining of 2000s. Furthermore, a significant Zn pollution is also related to utilization of Zn in fertilizers. Thus, pollutants originating from these cultivated areas could enter into the lake directly or through river transportation. Moreover, the principal contributors of heavy metals in city runoff were automobiles and structures that use of various metallic components. The traffic activities which produce heavy pollution include tire wear (Zn), fuel combustion (Pb), engine wearing and fluid leakage (Cu), and the building siding was a source of Pb, Cu, Zn.

REFERENCES

Adelson J. M., Helz G. R. and Miller C. V. (2001). Reconstructing the rise of recent coastal anoxia; molybdenum in Chesapeake Bay sediments, *Geochim. Cosmochim. Acta, 65 (2)*, 237–252.

Aizen, E.M., Aizen, V.B., Melack, J.M., Nakamura, T., Ohta, T. (2001). Precipitation and atmospheric circulation patterns at mid-latitudes of Asia, *International Journal of Climatology, 21*, 535–556.

Akçar, N. and Schlüchter, C. (2005). Paleoglaciations in Anatolia: A schematic review and first results, *Eiszeitalter und Gegenwart, 55*, 102–121.

Altınlı, E. (1964). Explanatory text of the geological map of Turkey (Van), *M.T.A. PubL*, Ankara.

Altunkaynak, A., Ozger, M., and Sen, Z. (2003). Triple diagram model of level fluctuations in Lake Van, Turkey, *Hydrol. Earth Syst. Sci.*, *7*, 235–244.

Anderson R. F., Kumar N., Mortlock R. A., Froelich P. N., Kubik P., Dittrich-Hannen B., and Suter M. (1998). Late-Quaternary changes in productivity of the Southern Ocean, *J. Mar. Sys., 17*, 497–514.

Appleby, P. G. and Oldfield, F. (1978). The calculation of lead-210 dates assuming a constant rate of supply of unsupported ^{210}Pb to the sediment, *Catena, 5*: 1-8.

Appley, P.G. and Oldfield, F. (1983). The assessment of ^{210}Pb data from sites with varying sediment accumulation rates, *Hydrobiologia, 103*, 29-35.

Appley, P.G, Richardso, N., Nolon, P.J., Oldfield, F. (1990). Radiometric dating of the United Kingdom SWAP sites, *Phil Trans. R. Soc. Lond.B, 327*, 233-238.

Appleby, P. G. (2001). Chronostratigraphic techniques in recent sediments. In tracking environmental change using lake sediments, basin analysis, coring, and chronological techniques, development in paleoenvironmental research, ed. W.L. Last and J.P. Smol. Dordrecht: Kluwer Academic Publishers.

Ascough, P. L., Cook, G. T., Hastie, H., Dunbar, E., Church, M. J., Einarsson, Á., McGovern, T. H. and Dugmore, A. J. (2011). An Icelandic Freshwater Radiocarbon Reservoir Effect: Implications for Lacustrine ^{14}C Chronologies, *The Holocene*, *21*: 1073–1080.

Ashley, G. M. and Driese, S. G. (2000). Paleopedology and paleohydrology of a volcaniclastic paleosol interval; implications for early Pleistocene stratigraphy and paleoclimate record, Olduvai Gorge, Tanzania, *Journal of Sedimentary Research*, *70(5)*, 1065-1080.

Aydar, E., Gourgaud, A., Ulusoy, İ., Digonnet, F., Labazuy, P., Şen, E., Bayhan, H., Kurttaş¸, T., Tolluoğlu, A.Ü. (2003). Morphological analysis of active Mount Nemrut stratovolcano, Eastern Turkey: evidences and possible impact areas of future eruption, *Journal of Volcanology and Geothermal Research*, *123*, 301–312.

Bahr, A., Lamy, F., Arz, H., Holger, K., Gerold, W. (2005). Late glacial to Holocene climate and sedimentation history in the NW Black Sea, *Marine Geology*, *214*, 309–322.

Bar-Matthews, M., Ayalon, A, Kaufman, A., Wasserberg, G.J. (1999). The Eastern Mediterranean plaeoclimate as a reflection of regional events: Soreq cave, Israel. iming and hydrological conditions of Sapropel events in the Eastern Mediterranean, as evident from speleothems, Soreq cave, Israel, *Earth and Planetary Science Letters, 166*, 85–95.

Bar-Matthews, M., Ayalon, A., Gilmour, M., Matthews, A., Hawkesworth, C.J. (2003). Sea-land oxygen isotopic relationships from planktonic foraminifera and speleothems in the Eastern Mediterranean region and their implication for paleorainfall during interglacial intervals, *Geochimica et Cosmochimica Acta*, *67*, 3181–3199.

Barlas Simsek, F., Çağatay, M.N. (2014). Geochronology of Lake Sediments Using ^{210}Pb with Double Energetic Window Method by LSC: An Application to Lake Van, *Applied Radiation and Isotopes*, *93*, 126–133.

Barnston A.G., Livezey, R.E. (1987). Classification, seasonality, and persistence of low-frequency atmospheric circulation patterns. Mon. Weather Rev. **115**, 1083–1126.

Beck, J. W., Edwars, R. L., Ito, E., Taylor, F. W., Recy, J., Rougerie, F., Joannot, P. And Henin. C. (1992). Sea-surface temperature from coral skeletal strontium/calcium ratios, *Science,* **257,** 644–647.

Bertrand, S., Sterken, M., Vargas-Ramirez, L., et al. (2009). Bulk organic geochemistry of sediments from Puyehue Lake and its watershed (Chile, 40°S): Implications for paleoenvironmental reconstructions, *Palaeogeography Palaeoclimatology Palaeoecology*, *294*, 56–71.

Besser, J., Brumbaugh, W., Allert, A., Poulton, B., Schmitt, C., Ingersoll, C. (2009). Ecological impacts of lead mining on Ozark streams: toxicity of sediment and pore water, *Ecotoxicol. Environ. Saf.*, *72*, 516–526.

Bianchi, G.G. and McCave, I.N. (1999). Holocene periodicity in North Atlantic climate and deep-ocean fl ow south of Iceland, *Nature*, *397*, 515–517.

Bjorck, S., and Wohlfarth, B., 2001. 14C chronostratigraphic techniques in paleolimnology: in Last, W.M. et al., eds., Tracking environmental change using lake sediments, volume 1: Basin analysis, coring and chronological techniques: Netherlands, Kluwer Academic Publishers, 205-245.

Blumenthal, M.M., Van der Kaaden, G., and Vlodavetz, V.I. (1964). Catalogue of the active volcanoes of the World including solfatara fields. Part

XVII Turkey and the Caucasus, *International Association of Volcanology*, *17*, 1–23.

Bond, G. C., Showers, W., Cheseby M., Lotti R., Almasi P., de-Menocal P., Priore P., Cullen H., Hadjas I., Bonani G. (1997). A pervasive millennial-scale cycle in north atlantic holocene and glacial climates, *Science*, *278*, 1257–1266.

Bordowskiy, O. K. (1965a). Source of organic matter in marine basins, *Mar. Geol.*, *3*, 5–31.

Bordowskiy, O. K. (1965b). Accumulation of organic matter in bottom sediments, *Mar. Geol., 3*, 33–82.

Bowen, R. (1998). Isotopes in the Earth Science. 647 p., Ed., *Applied Science*, London-New York.

Boyle, J. F. (2001). *Inorganic Geochemical Methods in Palaeolimnology*, Tracking Environmental Change Using Lake Sediments Phyiscal and Geochemical Methods: Ch.5.

Bradley, R. S., and Jones, P. D. (1993). Little Ice Age summer temperature variations: Their nature and relevance to recent global warming trends, *The Holocene*, *3*, 367 − 376.

Bradley, R.S., Vuille, M., Hardy, D., Thompson, L. G. (2003). Low latitute ice cores record Pacific sea surface temperatures, *Geophys. Res. Lett., 30(4)*, 1174, DOI: 10 1029/2002GL016546.

Briffa, K.R., Jones, P.D., Schweingruber F.H., and Osborn, T.J. (1998). Influence of volcanic eruptions on northern hemisphere summer temperature over the past 600 years, *Nature*, *393,* 450–455.

Broecker, W.S. and Olson, I.A. (1961). Lamont Radiocarbon Measurements VIII., *Radiocarbon*, *3*, 176–204.

Brauer, A., Haug, G.H., Dulski, P., Sigman, D.M., Negendank, J.F.W. (2008). An abrupt wind shift in Western Europe at the onset of the Younger Dryas cold period, *Nature Geo*science, *1*, 520–523.

Briffa, K.R. (2000). Annual climate variability in the Holocene: interpreting the message of ancient trees, *Quaternary Science Reviews*, *19*, 87–105.

Burnett, W.C. and Schaeffer, O.A. (1980). Effect of ocean dumping on $^{13}C/^{12}C$ ratios in marine sediments of the New York Bight, *Estuarine and Coastal Marine Science*, *2*, 605 ‑ 611.

Callway J., DeLaune R., and Patrick W. J. (1996). Chernobyl ^{137}Cs used to determine sediment accretion rates at selected northern European coastal wetlands, *Limnol. Oceanogr.*, *41*, 444–450.

Calvert, S. E. and Pedersen, T. F. (1993). Geochemistry of recent oxic and anoxic marine sediments: Implications for the geological record, *Mar. Geol.*, *113*, 67–88.

Calvert, S.E., Thode, H.D., Yeung, D., Karlin, R.E. (1996). A stable isotope study of pyrite formation in the Late Pleistocene and Holocene sediments of the Black Sea, *Geochim. Cosmochim. Acta., 60*, 1261 − 1270.

Carter, M.W. and Moghissi, A.A. (1977). Three Decades of Nuclear Testing, *Health Physics*, **33**, 55–71.

Chapman, P.M., Wang, F., Janssen, C., Persoone, G., Allen, H.E. (1998). Ecotoxicology of metals in aquatic sediments binding and release, bioavailability, risk assessment, and remediation, *Can. J. Fish. Aquat. Sci.*, **55**, 2221–2243.

Chen, J.S., Wei, F.S., Zheng, C.J., Wu, Y.Y., Adriano, D.C. (1991). Background concentrations of elements in soils of China, *Water, Air, Soil Pollut.,* ***57–58***, 699–712.

Cohen, A.S. (2003). Paleolimnology, New York, *Oxford University Press*, 500p.

Cole, J.E., Rind, D., Webb, R.S., Joutel, J., Healy, R. (1999). Climatic controls on interannual variability of precipitation δ^{18}O: Simulated influence of temperature, precipitation amount, and vapour source region, *Journal of Geophysical Research*, ***104***, 14,223–14,235.

Colleta, P., Pentecost, A. and Spiro, B. (2001). Stable isotopes in charophyte instructions: relationships with climate and water chemistry, *Palaeogeography, Palaeoclimatology, Palaeoecology*, ***173***, 9-19.

Croudace, I.W., Rindby, A. and Rothwell, R.G. (2006). ITRAX: description and evaluation of a new X-ray core scanner. In: Rothwell, R.G., (Ed.) New ways of looking at sediment cores and core data, *Geological Society Special Publication*, ***267***, 51-63.

Crusius J., Calvert S.E., Pedersen T.F., and Sage D. (1996). Rhenium and molybdenum enrichments in sediments as indicators of oxic, suboxic and anoxic conditions of deposition, *Earth Planet. Sci. Lett.*, ***145***, 65–79.

Crusius J. and Thomson J. (2000). Comparative behavior of authigenic Re, U, and Mo during reoxidation and subsequent long-term burial in marine sediments, *Geochim. Cosmochim. Acta*, ***64 (13)***, 2233– 2242.

Cullen, H.M. and de Menocal, P.B. (2000). North Atlantic Influence on Tigris-Euprates streamflow, *Int. J. Climatol.*, ***20***, 853-863.

Cuong, D.T., Obbard, J.P. (2006). Metal speciation in coastal marine sediments from Singapore using a modified BCR-sequential extraction procedure, *Appl. Geochem., **21***, 1335–1346.

Çağatay, M. N., Güngör, N., Yılmaz, Y. Z., Sarı, E. (2005). Rapid Changes in the ecological conditions of the Black Sea over the last 3 kyr: Evidence from sediment geochemistry. In: Özerler, M. And Sayın E. (eds.), *The Role of Marine Studies in Ecosystems, ECOSYSTEM 2003*, İzmir, Turkey, pp.85-96.

Çağatay, M.N., Öğretmen, N., Damcı, E., Stochecke, M., Sancar, U., Eriş, K.K., Özeren, S. (2014). Lake level and climate records over the last 90ka from Northern basin of Lake Van, eastern Turkey, *Quaternary Science Review*, ***104***, 97–116.

Çukur, D., Krastel, S., Schmincke, H-U, Sumita, M., Winkelmann, D., Cagatay, M.N., Meydan, A.F., Damcı, E., Stockhecke, M. (2014). Seismic

stratigraphy of Lake Van, eastern Turkey, *Quaternary Science Review*,**104**, 1–22.

Dahl, S.O., Nesje, A. (1994). Holocene glacier fluctuations at Hardangerjøkulen, central-southern Norway: a high resolution composite chronology from lacustrine and terrestrial deposits, *The Holocene, 4*, 269–277.

Dai, J., Song, J., Li, X., Yuan, H., Li, N., Zheng, G. (2007). Environmental changes reflected by sedimentary geochemistry in recent hundred years of Jiaozhou Bay, North China, *Environ. Pollut., 145*, 656–667.

Dalfes, N., Akkemik, Ü., Köse, N., Karaca, M., Kahya, E., Ezber, Y. (2006). Anadolu'nun iklim tarihinin son 500 yılı : Dendroklimatoloji yöntemi ile rökonstrüksiyonlar ve uzay-zaman analizleri, TÜBİTAK, YDABAG 102Y063 nolu proje.

Damcı, E. and Çağatay, M.N. (2015). An automated algorithm for dating annually laminated sediments using X-ray radiographic images, with applications to Lake Van (Turkey), lake Nautajarvi (Finland) and Byfjorden (Sweden), *Quaternary International*, ***1-10***.

Dansgaard, W. (1964). Stable isotopes in precipitation, *Tellus, 16*, 436–468.

Dansgaard, W., Johnsen, S.J., Clausen, H.B., and Langway, C.C. (1971). Climate record revealed by the Camp Century ice core. In: Turekian, K.K., ed. Late Cenozoic Glacial Ages Symposium 1969. New Haven, Connecticut: *Yale University Press*. 37–56.

Dansgaard, W., Johnsen, S.J.,Clausen, H.B., Dahl-Jensen, D.,Gundestrup, N.S., Hammer, C.U., Hvidberg, C.S., Steffensen, J.P., Sveinbjörnsdottir, A.E., Jouzel, J., Bondet, G. (1993). Evidence for general instability of past climate from a 250-kyr ice-core record, *Nature*, **364**, 218–220.

Danulat, E. and Kepme, S. (1992). Nitrogenous waste excretion at extremely alkaline pH: the story of Chalcalburnus tarichi (Cyprinidae), endemic to Lake Van, Eastern Turkey, *Fish Physiol Biochem, 9*, 377–386.

Danulat, E. and Selcuk, B. (1992). Life History and Enviromental Conditions of the Anadromous Chalcalburnus tarichi (Cyprinidae) in the Highly Alkaline Lake Van, Eastern Anatolia Turkey, *Arch. Hidrobiol.*, ***126(1)***, 105-125.

Davison, W. (1993). Iron and manganese in lakes, *Earth Sci. Rev.*, **341**, 119–163.

Dean W., Gardner J., and Anderson R. (1994). Geochemical evidence for enhanced preservation of organic matter in the oxygen minimum zone of the continental margin of northern California during the late Pleistocene, *Paleoceangraphy, 9***,** 47–61.

Dean W., Gardner J. V., and Piper D. Z. (1997). Inorganic geochemical indicators of glacial-interglacial changes in productivity and anoxia on the California continental magrin, *Geochim. Cosmochim. Acta, 61***,** 4507–4518.

Dean W. E., Piper D. Z. and Peterson L. C. (1999). Molybdenum accumulation in Cariaco basin sediment over the past 24 k.y.: A record of water-column anoxia and climate, *Geology, 27***,** 507–510.

Degens, E.T. and Kurtmann, F. (1978). The geology of Lake Van. Ankara, *MTA Press*.

Degens, E. T., Kempe, S., and Spitzy, A. (1984). CO_2: A biogeochemical portrayal. In Hutzinger, O. (Ed.), Handbook of Environmental Chemistry, (Vol. I/C): Berlin (Springer-Verlag), pp. 127-215.

Dominik, J. and Span, D. (1992). The fate of Chernobyl 13'cs in Lake Lugano, *Aquatic Sciences*, *54*, 238–254.

Dural, M., Göksu, M.Z.L., Özak, A.A. (2007). Investigation of heavy metal levels in economically important fish species captured from the Tuzla lagoon, *Food Chem.*, *102*, 415–421.

Eastwood, M. L., Cremel, S. Gehrke, C. Girard, E. and Bertram, A. K. (2008). Ice nucleation on mineral dust particles: Onset conditions, nucleation rates and contact angles, *J. Geophys. Res., 113*, D22203, doi:10.1029/2008JD010639.

Eastwood, W.J., Leng, M.J., Roberts, N., Davis, B. (2007). Holocene climate change in the eastern Mediterranean region: a comparison of stable isotope and pollen data from Lake Gölhisar, southwest Turkey, Journal of Quaternary Science, *22(4),* 327–341

Eddy, J.A. (1976). The Maunder Minimum, *Science*, **192**, 1189–1202.

Ehlers J., Nagorny K., Schmidt P., Stieve B., and Zietlow K. (1993). Storm surge deposits in North Sea salt marshes dated by [134]Cs and ^{137}Cs determination, *J. Coastal Res., 9*, 698–701.

Ertel, J. R. and Hedges, J. I. (1984). The lignin component of humic substances: Distribution among soil and sedimentary humic, fulvic, and base-insoluble fractions, *Geochim. Cosmochim. Acta*, *48*, 2065–2074.

Fischer, G. and Wefer G. (1999). Use of Proxies in Paleoceanography: Examples From the South Atlantic, 735, pp., *Springer-Verlag*, New York.

Fleitmann, D., Cheng, H., Badertscher, S., Edwards, R.L., Mudelsee, M., Göktürk, O.M., Fankhauser, A., Pickering, R., Raible, C.C., Matter, A., Kramers, J., Tüysüz, O. (2009). Timing and climatic impact of Greenland interstadials recorded in stalagmites from northern Turkey, *Geophys. Res. Lett.*, *36*, L197-L207.

Forester, R. M. (1983). Relationship of two lacustrine ostracode species to solute composition and salinity: Implieations for paleohydrochemistry, *Geology*, *11*, 435–438.

Frenzel, P. and Boomer, I. (2005). The use of ostracods from marginal-marine, brackish waters as bioindicators of modern and Quaternary environmental change, *Palaeogeography, Palaeoclimatology, Palaeoecology*, *225*, 68–92.

Gat, J.R., Adar, E., Alpert, P. (2001). Inter- and intra-storm variables of isotope composition of precipitation in southern Israel: are local or large scale factors responsible? In*: Study of Environmental Change Using Isotope Techniques*. IAEA, Vienna.

Gelen, A., Diaz, O., Simon, M.J., Herrera, E., Soto, J., Gomez, J., Rodenas, J., Beltran, J. and Ramirez, M. (2003). ^{210}Pb dating of sediments from Havana Bay, J. Rad.l Nuclear. Chem., *256 (3),* 561-564.

Gessner, F. (1957). Van Gölü. Zur Limnologie des großen Soda-Sees in Ostanatolien (Türkei), *Archiv fuer Hydrobiologie*, *53*, 1–22.

Geary, D.H., Brieske, T.A., Bemis, B.E. (1992). The influence and interaction of temperature, salinity, and upwelling on the stable isotopic profiles of strombid gastropod shells, *Palaios*, *7(1)*, 77–85.

Gevao B., Hamilton-Taylor J., Murdoch C., Jones K. C., Kelly M., and Tabner B. J. (1997). Depositional time trends and remobilization of PCBs in lake sediments, *Environ. Sci. Technol.*, *31*, 3274–3280.

Goldberg, E.D. (1963). Geochronology with ^{210}Pb. [In:] *Radioactive Dating*, International Atomic Energy Agency, Vienna: 121-130.

Goosens, H. (1989). Lipids and their mode of occurrence in bacteria and sediments − II. Lipids in the sediment of a stratified, freshwater lake, *Org. Geochem., 14*, 27–41.

Goñi, M.A., Teixeira, M.J. and Perkey, D.W. (2003). Sources and distribution of organic matter in a river-dominated estuary (Winyah Bay, SC, USA), *Estuar. Coast. Shelf Sci., 57*, 1023-1048.

Göktürk, O.M., Fleitmann, D., Badertscher, S., Cheng, H., Edwards, R.L., Tüysüz, O. (2011). Climate on the Southern Black Sea coast during the Holocene, Quat. Sci. Rev., *30*, 2433–2445.

Guilizzoni, P., Marchetto, A., Lami, A., Cameron, G., Appleby, P., Schnell. N.L., Schnell, O.A., Belis, C.A., Giorgis, A., Guzzi, L. (1996). The environmental history of a mountain lake (Lago Paione Superiore, Central Alps, Italy) for the last c.100 years: a multidisciplinary, paleolimnological study, *Journal of Paleolimnology, 15*, 245–264.

Gulliksen, S., Birks, H.H., Possnert, G., Mangerud, J. (1998). The calendar age of the Younger Dryas–Holocene transition at Kråkenes, western Norway, *The Holocene*, *8*, 249–60.

Güngör, E. and Çağatay, M. N. (2007). Karadeniz'de son 3000 yıldaki ani çevresel değişimler, *İTÜ Dergisi*, *5(4)*, 23–33.

Hakanson, L. (1980). An ecological risk index for aquatic pollution control: a sedimentological approach, *Water Res.*, *14*, 975–1001.

Haroutiunian, R. A. (2006). The historical volcanoes of Armenia and adjacent areas revisited, *Journal of Volcanology and Geothermal Research*, *155*, 334–337.

Harwart, S., Hagedorn, B., Melles, M. et al. (1999). Lithological and biochemical properties in sediments of Lama Lake as indicators for the late Pleistocene and Holocene ecosystem development of the southern Taymyr Peninsula, Central Siberia, *Boreas*, *28*, 167–180.

Hauer, J. (1957). Rotatorien aus dem plankton des Van Sees, *Arch. f. Hydrobiol.*, *53*, 23-29.

Haug, G. H., Hughen, K. A., Sigman, D. M., Peterson, L. C. and Röhl, U., (2001). Southward migration of the Intertropical Convergence Zone through the Holocene, *Science*, *293(5533)*, 1304–1308.

Haug, G.H., Gunter, D., Peterson, L.C., Sigman, D.M., Hughen, K.A., Aeschlimann, B. (2003). Climateand collapse of Maya Civilization, *Science*, *299*, 1731–1735.

Hedges, J. I., Clark, W. A., Quay, P. D., Ricihey, J. E., Devol, A. H. and Santos, U de M. (1986). Compositions and fluxes of particulate organic material in the Amazon River, *Limnol. Oceanogr.*, *31*, 717–738.

Hedges, J. I., Keil, R. G. and Benner, R. (1997). What happens to terrestrial matter in the ocean?, *Org. Geochem.*, *27*, 195–212.

Hilton, J. (1987). A simple model for the interpretation of magnetic records in lacustrine and oceanic sediments, *Quat. Res.*, *27*, 160-166.

Hodell, D.A., Curtis, J.H. and Brenner, M. (1995). Possible role of climate in the collapse of the Classic Maya Civilization, *Nature*, *375*, 391–394.

Holmes, J.A. (1996). Trace-element and stable isotope geochemistry of non-marine ostracod shells in Quaternary palaeoenvironmental reconstruction, *Jornal of Paleolimnology*, *15*, 223-235.

Holmes, R. M., Aminot A., Kerouel, R. Hooker, B. A. and. Peterson, B. J. (1999). A simple and precise method for measuring ammonium in marine and freshwater ecosystems, *Canadian Journal of Fisheries and Aquatic Sciences*, *56*, 1801–1808.

Holzhauser, H., Magny, M., Zumbühl, H.J. (2005). Glacier and lake-level variations in west-central Europe over the last 3500 years, *The Holocene*, *15*, 789–801.

Hosono, T., Su, C.C., Siringan, F., Amano, A., Onodera, S. (2010). Effects of environmental regulations on heavy metal pollution decline in core sediments from Manila Bay, *Mar. Pollut. Bull.*, *60*, 780–785.

Hosono, T., Su, C.C., Delinom, R., Umezawa, Y., Toyota, T., Kaneko, S., Taniguchi, M. (2011). Decline in heavy metal contamination in marine sediments in Jakarta Bay, Indonesia due to increasing environmental regulations, *Estuar. Coast. Shelf Sci.*, *92*, 297–306.

Hughen, K., Overpeck, J., Anderson, R. and Williams, K., (1996). The potential for paleoclimate records from varved Arctic lake sediments: Baffin Island, Eastern Canadian Arctic. In *Paleoclimatology and Paleoceanography From Laminated Sediments*.(ed. A. Kemp),pp. 57-71. Special Publication 116. Geological Society.

Huguet, C., Fietz, S., Stockhecke, M., Sturm, M., Anselmetti, F.S., RosellMelé, A. (2011). Biomarker seasonality study in Lake Van, Turkey, *Org Geochem*, *42*,1289–1298.

Huguet, C., Fietz, S.,, Moraleda, N., Litt, T., Heumann, G., Stockhecke, M., Anselmetti, F.S., and Sturm, M. (2012). A seasonal cycle of terrestrial inputs in Lake Van, Turkey, *Environmental Science and Pollution Research, 19*, 3628–3635.

Hurrel, J. W. (1995). Decadal trends in the North Atlantic Oscillation: Regional temperature and precipitation, *Science*, *269*, 676–679.

Hurrell, J.W., and Van Loon, H. (1997). Decadal variations in climate associated with the North Atlantic Oscillation, *Climate Change*, *36*, 301-326.

IAEA/WMO (2014). Global network of isotopes in precipitation. *The GNIP Database*. Accessible at: http://www.iaea.org/water.

Jacobi, B. (1960). Tore tempel und palaste. *Prisma-Verlag*, Germ.Dem.Rep.

Jansen, J. H. F., Van der Gast, S. J. Kostner, B. and Vaars A. (1992). CORTEX, an XRF-scanner for chemical analyses of sediment cores, *GEOMAR Rep. 15*, GeoMar, Kiel, Germany.

Jones, P. D., Briffa, K. R. Barnett, T. P. and Tett, S. F. B. (1998). High-resolution palaeclimatic records for the last millennium: Interpretation, integration and camparison with General Circulation Model control-run temperatures, *The Holocene*, *8*, 455 – 471.

Jones, P.D., Davies, T.D., Lister, D.H., Slonosky, V., Jónsson, T., Barring, L., Jönsson P., Maheras, P., Kolyva-Machera, F., Barriendos, M., Martin-Vide, J., Rodriguez, R., Alcoforado, M.J., Wanner, H., Pfister, C., Rickli, R., Luterbacher, J., Schüpbach, E., Kaas, E., Schmith, T., Jacobeit, J., and Beck, C. (1999), Monthly mean pressure reconstruction for Europe for the 1780 — 1995 period, *Int. J. Climatol.*, *19*, 347–364.

Jones, M.D., Roberts, N., Leng, M.J., Türkeş, M. (2006). A high-resolution late Holocene isotope record from Turkey and links to North Atlantic and monsoon climate, *Geology*, *34*, 361–364.

Jouzel J., Alley, R.B., Cuffey, K.M., Dansgaard, P., Grootes, P., Hoffmann et al. (1997). Validity of temperature reconstruction from water isotopes in ice cores, *Journal of Geophysical Research*, *102 (C12)*, 26,471–26,487.

Judson, S. (1968). Erosion of the land or what's happening to our continents, *American Scientist*, *56*, 356–374.

Kadıoğlu, M., Sen, Z., Batur, E. (1997). The greatest soda-water lake in the world and how it is influenced by climatic change, *Ann. Geophysicae*, *15*, 1489–1497.

Kanasassanen, P. H. and Jaakkola, T. (1985). Assessment of pollution history from recent sediments in Lake Vanajavesi, southern Finland. I. Selection of representative profiles, their dating and chemostratigraphy, *Ann. Zool. Fennici*, *22*, 13–55.

Karaca, M., Deniz, A., Tayanç, M. (2000). Cyclone Track Variability over Turkey in Association with Region Climate, *International Journal of Climatology*, *20*, 1225–1236.

Kazmierczak, J. and Kempe, S. (2003). Modern terrestrial analogues for the carbonate globules in Martian meteorite ALH84001, Naturwissenchaften, *90*, 167–72.

Kempe, S. (1977). Hydrographie, Warven-Chronologie und Organische Geochemie des Van Sees, Ost-Türkei. Sonderdruck aus Mitteilungen aus dem Geologisch Paläontologischen Institut der Universität Hamburg, *47*, pp. 125–228. Hydrography, varve-chronology and organic geochemistry of Lake Van, east Turkey.

Kempe, S., Degens, E.T. (1978). Lake Van varve record: the past 10,420 years. In: Degens, E.T., Kurtman, F. (Eds.), Geology of Lake Van, *MTA Press*, Ankara, pp. 56–63.

Kempe, S., Khoo, F. and Guryelik, Y. (1978). Hydrography of Lake Van and its drainage are. In : The geology of Lake Van (Degens, E.T. and Kurtman, F., eds.), *MTA Press*, Ankara pp. 30 –44.

Kempe, S., Kazmierczak, J., Landmann, G., Konuk, T., Reimer, A., Lipp, A. (1991). Largest known microbialites discovered in Lake Van, Turkey, *Nature, 349*, 605–608.

Kempe, S., Landmann, G., Müller, G. (2002). A floating varve chronology from the last glacial maximum terrace of Lake Van/Turkey, *Research in deserts and mountains of Africa and Central Asia*, *126*, 97–114.

Keskin, M. (2007). Eastern Anatolia: a hotspot in a collision zone without a mantle plume, *Geological Society of America Special Paper*, *430*, 693–722.

Khoo, F., Degens, E.T. and Lambert, A. (1978). The geology of Lake Van. In: Geochemistry of Lake Van (Degens, E.T. and Kurtman, F., eds), *MTA Pres*, pp 81–91.

Kim, D.C., Sung, J.Y., Park, S.C., Lee, G.H., Choi, J.H., Kim, G.Y., Seo, Y.K and Kim, J.C. (2001). Physical and acoustic properties of shelf sediments, the South Sea of Korea, *Mar. Geol.*, *179*, 39-50.

Kim, C.K., Martin, P., Fajgelj, A. (2008). Quantification of measurement uncertainty in the sequential determination of ^{210}Pb and ^{210}Po by liquid scintillation counting and alpha-particle spectrometry, *Accred Qual Assur.*, *13*, 691–702.

King, J., Banerjee, S. K., Marvin J., and Ozdemir, O. (1982). A comparison of different magnetic methods for determining the relative grain size of magnetite in natural materials: some results from lake sediments, *Earth. Planet. Sci. Lett.*, *59*, 404-419.

Kipfer, R., Aeschbach-Hertig, W., Baur, H., Hofer, M., Imboden, D. M., Signer, P. (1994). Injection of mantle type Helium into Lake Van (Turkey): the clue for quantifying deep water renewal, *Earth and Planet. Sci. Lett.*, *125*, 357–370.

Kirby, M.E., Patterson, W.P., Mullins, H.T., Burnett, A.W. (2002). Post-Younger Dryas climate interval linked to circumpolar vortex variability: isotopic evidence from Fayetteville Green Lake, New York, *Climate Dynamics*, *19*, 321–330.

Krantz, D.E., Kronick, A.T. and Williams, D.F. (1988). A model for interpreting continental-shelf hydrographic processes from the stable isotope and cadmium: calcium profiles of scallop shells, *Palaeogeography, Palaeoclimatology, Palaeoecology*, *64*, 123–140.

Krichak, S.O., Alpert, P., and Dayan, M. (2004). The role of atmospheric processes associated with hurricane Olga in the December 2001 floods in Israel, *J. Hydromet.*, **5**, 1260–1270.

Krishnaswami, S., Lal, D., Martin, J.M. and Meybeck, M. (1971). Geochronology of lake sediments, *Earth and Planetary Science Letters*, **11**, 407-414.

Kutiel, H. and Benaroch, Y. (2002). North Sea − Caspian Pattern (NCP) − an upper level atmospheric teleconnection affecting the Eastern Mediterranean: Identification and definition, Theoretical and Applied Climatology, **71**, 17–28.

Kuzucuoğlu, C., Christol, L., ,Mouralis, D., Doğu, A.F., Akköprü, E., Fort, M., Brunsteın, D., Zorer, H., Fontugne, M., Karabıyıkoğlu, M. (2010). Formation of the Upper Pleistocene terraces of Lake Van (Turkey), *Journal of Quaternary Science*, **25**, 1124–1137.

Kuzucuoğlu, C., Dorfler, W. And Kunesch, S. (2011). Mid- to late-Holocene climate change in central Turkey: The Tecer Lake record, *The Holocene*, **21(1)**, 173–188.

Kwiecien, O., Stockhecke, M., Pickarski, N., Heumann, G., Litt, T., Sturm, M., Anselmetti, F., Kipfer, R., and Haug, G. H. (2014). Dynamics of the last four glacial terminations recorded in Lake Van, Turkey, *Quaternary Sci. Rev.*, **104**, 42–52.

La Fontaine, C.V., Bryson, R.A., Wendland, W.M. (1990). Airstream regions of North Africa and the Mediterranean, *Journal of Climate*, **3**, 366–372.

Lamy F, Arz HW, Bond G, Bahr A, Pätzold J. (2006). Multicentennial-scale hydrological changes in the Black Sea and northern Red Sea during the Holocene and the Arctic/North Atlantic Oscillation, *Paleoceanography*, 21: PA1008, doi:10.1029/2005PA001184.

Landmann, G., Reimer, A., Lemcke, G., Kempe, S. (1996a). Dating Late Glacial abrupt climate changes in the 14.570 yr long continuous varve record of Lake Van, Turkey, *Palaeogeography, Palaeoclimatology, Palaeoecology*, **122**, 107–118.

Landmann, G., Reimer, A. ve Kempe, S. (1996b). Climatically Induced Lake level Changes at Lake Van, Turkey, During The Pleistocene / Holocene Transition, *Global Biochemical Cycles*, **10**, 797–808.

Landmann G, Steinhauser G, Sterba JH, Kempe S, Bichler M. (2011). Geochemical fingerprints by activation analysis of tephra layers in Lake Van sediments, Turkey, *Applied Radiation and Isotopes*, **69**, 929–935.

Lean, J., Beer, J. and Bradley, R.S. (1995). Reconstruction of solar irradiance since 1610: Implications for climate change, *Geophys. Res. Leu.*, **22**, 3195–3198.

Lean, J., and Rind, D. (1999). Evaluating sun-climate relationships since the little ice age, J. *Atmos. Sol.-Terr. Phys.*, **61**, 25–36.

Lemcke, G. (1996). Palaoklimarekonstruktion am Van See (Ostanatolien, Türkei). Dissertation, Swiss Federal Institute of Technology (Zurich), no. 11786, pp 182.

Lemcke, G., and Sturm, M. (1997). $\delta^{18}O$ and trace element measurements as proxy for the reconstruction of climate changes at Lake Van (Turkey): preliminary results. In Dalfes, H.N., Kukla, G. and Weiss, H., editors, Third millennium BC climate change and Old world collapse. *NATO Avanced Study Institutes (ASI) series I*, vol. 49, Berlin: Springer, 653-78.

Leng, M.J., Marshall, J.D. (2004). Palaeoclimate interpretation of stable isotope data from lake sediment archives, *Quaternary Science Reviews*, *23*, 811–831.

Li, H.C., Ku, T.L. (1997). $\delta^{13}C$–$\delta^{18}O$ covariance as a paleohydrological indicator for closed-basin lakes, *Palaeogeography, Palaeoclimatology, Palaeoecology*, *133*, 69–80.

Libby, W. F. (1955). Radiocarbon dating (Second Edition), University of Chicago Press.

Lioubimtseva, E. (2002). Arid environments. In: Shahgedanova, M. (Ed.), Physical Geography of Northern Eurasia, *Oxford University Press*, Oxford 571 pp.

Litt, T., Krastel, S., Sturm, M., Kipfer, R., Oercen, S., Heumann, G., Franz, S. O., Ulgen, U. B., Niessen, F. (2009). 'PALEOVAN', International Continental Scientific Drilling Program (ICDP): site survey results and perspectives, *Quaternary Science Reviews*, *28*, 1555–1567.

Litt, T., Anselmetti, F.S., Çağatay, M.N., Kipfer, R., Krastel, S., Schmincke, H-U. (2011). A 500,000-Year-Long Sediment Archive Drilled in Eastern Anatolia, *Eos., 92*, 477–479.

Litt, T., Anselmetti, F.S., Baumgarten, H., Beer, J., Cagatay, N., Cukur, D.,Damci, E., Glombitza, C., Haug, G., Heumann, G., Kallmeyer, J., Kipfer, R., Krastel, S., Kwiecien, O., Meydan, A.F., Orcen, S., Pickarski, N., Randlett, M., Schmincke, H., Schubert, C.J., Sturm, M., Sumita, M., Stockhecke M.,, Tomonaga, Y., Vigliotti, L., Wonik, T. (2012). The PALEOVAN Scientific Team, 500,000 Years of Environmental History in Eastern Anatolia: The PALEOVAN Drilling Project, *Scientific Drilling*, *14*, 18–29.

Litt, T. and Anselmetti, F.S. (2014). Lake Van Deep Drilling Project PALEOVAN, *Quaternary Science Reviews*, *104*, 1-7.

Litt, T. Pickarski, N., Heumann, G. (2014). A 600,000 Year Long Continental Pollen Record from Lake Van, Eastern Anatolia (Turkey), *Quaternary Science Reviews*, *104*, 30–41.

Löwemark, L., Chen H.F., Yang T.N., Kylander M.,Yu E.F., Hsu Y.W., Lee, T.Q, Song, S.R., Jarvis, S. (2011). Normalizing XRF-scanner data: A cautionary note on the interpretation of high-resolution records from organic-rich lakes, *Journal of Asian Earth Sciences*, *40*, 1250–1256.

Lu, Y., Meyers, P.A., Eadie, B.J., et al. (2010). Carbon cycling in Lake Erie during cultural eutrophication over the last century inferred from the stable carbon isotope composition of sediments, *Journal of Paleolimnology*, *43*, 261–272.

Luterbacher, J., Schmutz, C., Gyalistras, D., Xoplaki, E. and Wanner, H. (1999). Reconstruction of monthly NAO and EU indices back to AD 1675, *Geophys. Res. Lett.*, *26*, 2745 – 2748.

Luterbacher, J. (2000). The Late Maunder Minimum (AD 1675–1715) – Climax of the Little Ice Age in Europe', in Jones, P. D., Davies, T. D., Ogilvie, A. E. J., and Briffa, K. R. (eds.),Climate Impacts: The Last 1000 Years, Climatic Research Unit, University of East Anglia, Norwich, U.K., Kluwer Academic Publishers.

Luterbacher, J. and 33 co-authors (2000). Monthly Mean Pressure Reconstruction for the Late Maunder Minimum Period (AD 1675–1715) Based on Canonical Correlation Analysis, *Int. J. Climatol.*, *20*, 1049–1066.

Mackenzie, F. T., Vink, S., Wollast, R. and Chou, L. (1995). Comparative biogeochemistry of marine saline lakes. In: *Physics and Chemistry of Lakes, 2nd edition*, A. Lerman, D. Imboden, and J. Gat, eds., Springer-Verlag, Berlin, 265-278.

Makaroğlu, Ö., Çağatay M.N. (2015). The radiocarbon reservoir age of Lake Van, Turkey, *Quaternary International*, Doi:10.1016/j.quaint.2015.11.008.

Maunder, E.W. (1922). The prolonged sunspot minimum 1675–1715, *Brit. Astron. Ass. J.* **32**, 140–145.

McKenzie, J.A. (1985). Carbon isotopes and productivity in the lacustrine and marine environment. In Stumm, W. (ed.): *Chemical processes in lakes*, 99–118. John Wiley & Sons, New York.

Mann, M. E., Bradley, R. S. and Hughes, M. K. (1998). Global-scale temperature patterns and climate forcing over the past six centuries, *Nature*, *392*, 779 – 787.

Mann, M. E., Bradley, R. S. and Hughes, M. K. (1999). Northern Hemisphere Temperatures During the Past Millennium: Inferences, Uncertainties, and Limitations, *Geophys. Res. Lett.*, *26*, 759 – 762.

Mann, M. E. (2002). Little Ice Age, Medieval Climatic Optimum, Encyclopedia of Global Environmental Change, Volume 1, The Earth System: Pysical and Chemical Dimensions of Global Environmental Change Ed: Munn T., Wiley J., Ghil M., Vol:1, John Wiley & Sons, Ltd, Chichester, p:544-549.

Matisoff, G. (1995). Effects of biolurbation on solute and particle transport in sediments. In H. Allen [ed.], Metal contaminated aquatic sediments. *Ann Arbor Press*.

Meydan, A.F. (2013). Van Gölü'nde güncel flüvyal çökel girdisi ve gölsel sedimantasyon ilişkisi, *PhD Thesis*, Van.

Meyer, K.M.,Yu, M., Jost, A.B., Kelley, B.M. and Payne, J.L. (2011). $\delta^{13}C$ evidence that high primary productivity delayed recovery from end-

Permian mass extinction, *Earth and Planetary Science Letters*, *302 (3-4)*, 378-384.

Meyers, P.A., Leenheer, M.J., Eadie, B.J. and Maule, S.J. (1984). Organic geochemistry of suspended and settling particulate matter in Lake Michigan. *Geochim. Cosmochim. Acta*, *48*, 443–452.

Meyers, P.A. (1994). Preservation of elemental and isotopic source identification of sedimentary organic matter. *Chem. Geol. 114*: 289–302.

Meyers, P. A. (1997). Organic geochemical proxies of palaeogeographic, paleolimnologic, and paleoclimatic processes. *Org. Geochem. 27*, 213–250.

Meyers, P.A. and Teranes, J.L. (2001). Sediment organic matter. In: Last WM and Smol JP (eds) Tracking Environmental Changes Using Lake Sediment, Vol. 2: Physical and Geochemical Methods. *Dordrecht: Kluwer Academic*, pp. 239–270.

Morillo, J., Usero, J., Gracia, I. (2002). Partitioning of metals in sediments from the Odiel River (Spain). *Environ. Int., 28*, 263–271.

Mülller, P.J. (1977). C/N ratios in Pacific deep-sea sediments: Effect of inorganic ammonium and organic nitrogen compounds sorbed by clays. *Geochim. Cosmochim. Acta, 41*: 765–776.

Muller, R. A. and McDonald, G. J. (2000). Ice Ages and Astronomcal Causes,:Data, spectral analysis and mechanisms, *Praxis Publishing*, UK.

M.T.A. Institute, Ankara, Turkey. (1961). Geological map of the southest Anatolian region. Edited by Cahit Erentöz, prepared and published by the Institute of Mineral Research and Exploration, Ankara, *Turkish Geodetical Survey*. Scale: 1:500,000.

Myrbo, A., Shapley, M. D. (2006). Seasonal water-column dynamics of dissolved inorganic carbon stable isotopic compositions ($\delta^{13}C_{DIC}$) in small hardwater lakes in Minnesota and Montana. *Geochimica et Cosmochimica Acta*,*70* **(11)**, 2699–2714.

Nakai, N., Ohta, T., Fujisawa, H., and Yoshida, M. (1982). Paleoclimatic and sea-level changes deduced from organic carbon isotope ratios, C/N ratios and pyrite contents of cored sediments from Nagoya Harbor, Japan. *The Quaternary Research (Japan Assoc. for Quaternary Res.), 21*, 169–177.

Neale J.W. (1988). Ostracods and palaeosalinity reconstruction. *Ostracoda in the Earth sciences* (eds P. De Decker et al.), 125– 155.

Nesje, A., Dahl, S.O., Andersson, C., Matthews, J.A. (2000). The lacustrine sedimentary sequence in Sygneskardvatnet, western Norway: a continuous, high-resolution record of the Jostedalsbreen ice cap during the Holocene. *Quaternary Science Reviews, 19*, 1047–1065.

Oliver, J.E. (1973). Climate and Man's Environment. Chichester: John Wiley and Sons, 517 pp.

O'Neil, J. R., Clayton, R. N. and Mayeda, T. K. (1969). Oxygen isotope fractionation in divalent metal carbonates, *J. Chem. Phys., 51*, 5547–5558.

Orem, W. H., Burnett, W. C., Landing, W. M., Lyons, W. B. and Showers, W. (1991). Jellyfish Lake, Palau: Early diagenesis of organic matter in sediments of an anoxic marine lake. *Limnol. Oceanogr., 36*, 526– 543.

Palacios-Fest, M.R., Cohen, A.S., Lezzar, K.E., Nahimana, L., and Tanner, B.M. (2005). Paleolimnological investigations of anthropogenic environmental change in Lake Tanganyika: III. Physical stratigraphy and charcoal analysis. *Journal of Paleolimnology. 34*, 139–150.

Peeters, F., Kipfer, R., Achermann, D., Hofer, M., Aeschbach-Hertig, W., Beyerle, U., Imboden, D.M., Rozanski, K., Fröhlich, K. (2000). Analysis of deep-water exchange in the Caspian Sea based on environmental tracers. *Deep-Sea Res,. 47*, 621–654.

Perin, G., Craboledda, L., Lucchese, M., Cirillo, R., Dotta, L., Zanette, M.L., Orio, A.A. (1985). Heavy metal speciation in the sediments of northern Adriatic Sea. A new approach for environmental toxicity determination, in: Lakkas, T.D. (Ed.), *Heavy Metals in the Environment, 2., 454–456.*

Peterson, L. C., Haug, G. H., Hughen K.A.,, and Röhl, U., (2000). Rapid Changes in the Hydrologic Cycle of the Tropical Atlantic During the Last Glacial, *Science 8: 290 (5498)*, 1947-1951.

Peterson, L.C., Haug, G.H. (2006). Variability in the mean latitude of the Atlantic Intertropical Convergence Zone as recorded by riverine input of sediments to the Cariaco Basin (Venezuela), *Palaeogeography, Palaeoclimatology, Palaeoecology, 234*, Issue 1, Pages 97-113.

Pfister, C. (1999). Wetternachhersage. 500 Jahre Klimavariationen und Naturkatastrophen 1496–1995. Haupt: Bern.

Prahl, F. G., Bennett, J. T., and Carpenter, R. (1980). The early diagenesis of aliphatic hydrocarbons and organic matter in sedimentary particulates from Dabob Bay, Washington. *Geochim. Cosmochim., 44*, 1967–1976.

Prahl, F. G., Ertel, J. R., Goni, M. A., Sparrow, M. A. and Eversmeyer, B. (1994). Terrestrial organic carbon contributions to sediments on the Washington margin. Geochim. *Cosmochim. 58*, 3035–3048.

Qiu, Y., Lin, D., Liu, J., Zeng, E.Y. (2011). Bioaccumulation of trace metals in farmed fish from South China and potential risk assessment. *Ecotoxicol. Environ. Saf., 74*, 284–293.

Raicich, F., Pinardi, N., and Navara, A. (2003). Teleconnections between Indian Monsoon and Sahel rainfall and the Mediterranean, *Int. J. Climatol., 23*, 173–186.

Rashid, M. A., and Reinson, G. E. (1979). Organic matter in surficial sediments of the Miramichi Estuary, New Brunswick, Canada. *Estuarine Coastal Shelf Sci., 8*, 23–36.

Raymond, S. B., Hughes, M. K., Diaz, H. F. (2003). Climate in Medieval Time, *Science*, *302*, 404-405.

Reimer, E., Mikolajewics, U. and Winguth, A. (1996) Future ocean uptake of CO_2: interaction between oceancirculation and biology, Clim. Dyn., **12**, 711–721.

Reimer, P.J., Baillie, M.G.L., Bard, E., Bayliss, A., Beck, J.W., Bertrand, C.J.H., Blackwell, P.G., Buck, C.E., Burr, G.S., Kirsten, B.C., Damon, P.E., Edwards, R.L., Fiarbanks, R.G., Friedrich, M., Guilderson, T.P., Hogg, A.G., Hughen, K.A., Kromer, B., McCormac, G., Manning, S., Ramsey, C.B., Reimer, R.W., von der Plicht, J., Weyhenmeyer, C.E. (2004). INTCAL04 Terrestrial radiocarbon age calibration, 0–26 cal kyr BP. *Radiocarbon, 46*, 1029–1058.

Reimer P.J., Baillie, M.G.L., Bard, E., Bayliss, A., Beck, J.W., Blackwell, P.G., Bronk Ramsey, C., Buck, C.E., Burr, G.S., Edwards, R.L., Friedrich, M., Grootes, P.M., Guilderson, T.P., Hajdas, I., Heaton, T.J., Hogg, A.G., Hughen, K.A., Kaiser, K.F., Krome, B., McCormac, F.G., Manning, S.W., Reimer, R.W., Richards, D.A., Southon, J.R., Talamo, S., Turney, C.S.M., van der Plich, J., Weyhenmeyer, C.E. (2009). IntCal09 and Marine09 radiocarbon age calibration curves, 0–50,000 years cal BP. *Radiocarbon 51(4)*, 1111–50.

Reimer, A., Landmann, G., Kempe, S. (2009). Lake Van, Eastern Anatolia, hydrochemistry and history. *Aquat. Geochem., 15*, 195–222.

Ritchie, J.C. and McHenry, J.R., (1990). Application of Radioactive Fallout Cesium-137 for Measuring Soil Erosion and Sediment Accumulation Rates and Patterns: A Review, *Journal of Environmental Quality*, *19*, 215-233.

Roberts, N., Wright, Jr., H.E. (1993). Vegetational, lake level and climatic history of the Near East and Southwest Asia. In: Wright, Jr., H.E., Kutzbach, J.E., Webb, III, T., Ruddiman, W.F., Street-Perrott, F.A., Bartlein, P. (Eds.), *Global Climates since the Last Glacial Maximum*. University of Minnesota Press, St. Paul, MN, pp. 194–220.

Roberts, N., Jones, M.D., Benkaddour, A., Eastwood. W.J., Filippi, M.L., Frogley, M.R., Lamb, H.F., Leng, M.J., Reed, J.M., Stein, M., Stevens, L., Valero-Garcès, B., Zanchetta, G. (2008). Stable isotope records of Late Quaternary climate and hydrology from Mediterranean lakes: the ISOMED synthesis. *Quaternary Science Reviews, 27*, 2426–244.

Roberts, N., Jones, M.D., Benkaddour, A., Eastwood. W.J., Filippi, M.L., Frogley, M.R., Lamb, H.F., Leng, M.J., Reed, J.M., Stein, M., Stevens, L., Valero-Garcès, B., Zanchetta, G., Roberts, N., Brayshaw, D., Kuzucuoğlu, C., Perez, R., Sadori, L. (2011). The mid-Holocene climatic transition in the Mediterranean: Causes and consequences. *Holocene, 21(1)*, 3–13.

Robinson, H.G. (1993). Lithostratigraphic applications for magnetic susceptibility logging of deep-sea sediment cores: examples from ODP Leg 115, In

Hailwood, E.A and Kidd, R.B (Eds.), *High resolution stratigrapy, 70*, Geological Society: London, pp.65-98.

Rosenthal Y., Boyle E. A., Labeyrie L., and Oppo D. (1995). Glacial enrichments of authigenic Cd and U in Subantarctic sediments: A climatic control on the elements' ocean budget? *Paleoceanography,* **10,** 395–413.

Rosenthal, Y., and Boyle E. A. (1993). Factors controlling the fluoride content of planktonic foraminifera: An evaluation of its paleoceanographic applicability. *Geochim. Cosmochim.*, **57:** 335–346.

Rozanski, K., Araguas-Araguas, L., Gonfiantini, R. (1992). Relation between long-term trends of oxygen-18 isotope composition of precipitation and climate. *Science, 258*, 981–985.

Ruiz, F., Abad, M., Bodergat, A.M., Carbonel, P., Rodrı´guez-La´zaro, J., Gonza´lez-Regalado, M.L., Toscano, A., Garcı´a, E.X., Prenda, J. (2013). Freshwater ostracods as environmental tracers. *Int. J. Environ. Sci. Technol., 10*, 1115–1128.

Sandgren, P. and Snowball, I. (1996). Late Weichselian shore-line displacement on the Kullen Peninsula in NW Scania documented by the mineral magnetic, geochemical and biostratigraphical analyses of lake sediments—preliminary results. *GFF, 118*, A69–A70.

Savage, C., Leavitt, P. R. and Elmgren, R. (2004). Distribution and retention of sewage nitrogen in surface sediments of a coastal bay. *Limnol. Oceanogr., 49,* 1503–1511.

Schilman, B., Ayalon, A., Bar-Matthews, M., Kagan, E.J. and Almogi-Labin, A. (2002). Sea-land paleoclimate correlation in the Eastern Mediterranean region during the late Holocene. *Israel Journal of Earth Sciences, 51*, 181–190

.**Schöll, M.** (1978). Some chemical and isotopic data of core material of Lake Van. In Geology of Lake Van edited by E.T. Degens and F. Kurtman, *M.T.A. Press*, Ankara, Turkey.

Schwalb, A. (2003). Lacustrine ostracodes as stable isotope recorders of late-glacial and Holocene environmental dynamics and climate. *Journal of Paleolimnology, 29*, 265–351.

Schweizer, G. (1975). Untersuchungen zur Physiogeographie von Ostanatolien und Nordwestiran. Geomorphologische, klima und hydrogeographische Studien im Vansee und Rezaiyehsee-Gebiet. *Tübinger Geographische Studien 60, 9*.

Sen, Z., Kadıoğlu, M. and Batur, E. (1999). Cluster regression model and level fluctuation features of Van Lake, Turkey. *Ann. Geophysicae, 17*, 273–279.

Sieger, R. (1888). Die Schwankungen der hocharmenisehen Seen Seit 1880 im Vergleich mit einigen Verwandten Erscheinungen. Mitt. K.K. *Geogr. Ges*., 95-1155.

Singer, S. F. and Avery, D. T. (2007). "Chap 16". Unstoppable Global Warming: Every 1,500 Years. *Rowman and Littlefield*, p. 221, ISBN 9780742551176.

Singh, K., Mohan, D., Singh, V., Malik, A. (2005). Studies on distribution and fractionation of heavy metals in Gomti river sediments − a tributary of the Ganges, India, *J. Hydrol., 312*, 14–27.

Sima, O., Arnold, D., Dovlete, C., (2001). GESPECOR—a versatile tool in gamma-ray spectrometry. *J. Radioanal. Nucl. Chem. 248 (2)*, 359–364.

Smith, J.T. (2001). Why should we believe 210Pb sediment geochronologies ?. *J. Environ. Radioact., 55*, 121 − 3.

Soulet, G., Ménot, G., Lericolais, G., Bard, E. (2011). A revised calendar age for the last reconnection of the Black Sea to the global ocean. *Quaternary Science Reviews, 30*, 1019–1026.

Stein, M., Migowski, C., Bookman, R., Lazar, B. (2004). Temporal changes in the radiocarbon reservoir age in the Dead Sea. *Radiocarbon 46(2)*:649–55.

Stable isotope records of Late Quaternary climate and hydrology from Mediterranean lakes: the ISOMED synthesis. Quaternary Science Reviews 27, 2426–2441.

Stevens, L.R., Wright, H.E., Jr., E., Ito, E. (2001). Proposed changes in seasonality of climate during the Lateglacial and Holocene at Lake Zeribar, Iran. *The Holocene, 11(6)*, 747−756.

Stevens, L.R., Stone, J.R., Campbell, J., Fritz, S.C. (2006). A 2200-yr record of hydrologic variability from Foy Lake, Montana, USA, inferred from diatom and geochemical data. *Quat Res, 65*, 264–274.

Stockhecke, M. Anselmetti, F.S., Meydan, A.F. Odermatt, D., Sturm,M. (2012). The annual particle cycle in Lake Van (Turkey). *Palaeogeography, Palaeoclimatology, Palaeoecology*, 333–334, 148–159.

Stockhecke, M., Kwiecien, O., Vigliotti, L., Anselmetti, F., Beer, J., Cagatay, N., Channell, J.E.T., Kipfer, R., Litt, T., Pickarski, N., Sturm, M. (2014). Chronostratigraphy of the 600,000 Year Old Continental Record of Lake Van (Turkey). *Quat. Sci. Rev., 104*, 8–17.

Stuiver, M. and Reimer, P. J. (1993). Extended ^{14}C data base and revised CALIB 3.0 ^{14}C age calibration program. In Stuiver, M., Long, A. and Kra, R. S., eds., Calibration 1993. *Radiocarbon, 35(1)*, 215-230.

Stuiver M. and Braziunas, T.F. (1993). ^{14}C ages of marine samples to 10,000 BC, Radiocarbon, **35(1)**, 137-189.

Stumm, W., ed. (1987). Aquatic Surface chemistry. *John Wiley & Sons. (Interscience)* New York.

Spörer, F.W.G. (1887), Über die Periodizität der Sonnenflecken seit dem Jahre 1618, vornehmlich in Bezug auf die heliographische Breite derselben, and Hinweis auf eine erhebliche Störung dieser Periodizität während eines langen Zeitraumes, Vjschr. *Astron. Ges. Leipzig, 22*: 323–329.

Sumita, M., Schmincke, H.-U. (2013). Impact of volcanism on the evolution of Lake Van II: Temporal evolution of explosive volcanism of Nemrut Volcano (eastern Anatolia) during the past ca. 0.4 Ma. *Journal of Volcanology Geothermal Research, 253*, 15–34.

Şengör, A., Özeren, S., Genç, T., Zor, E. (2003). East Anatolian high plateau as a mantle supported, north-south shortened domal structure. *Geophysical Research Letters, 30*, 24.

Talbot, M.R. (1990). A review of the palaeohydrological interpretation of carbon and oxygen isotopic ratios in primary lacustrine carbonates. *Chemical Geology, 80*, 261–279.

Talbot, M. R. and Johannessen, T. (1992). A high resolution palaeoclimatic record for the last 27,500 years in tropical West Africa from the carbon and nitrogen isotopic composition of lacustrine organic matter. *Earth Planet. Sci. Lett., 10*, 23–37

Tarutani, T., Clayton, R.N., Mayeda, T.K. (1969). The effect of polymorphism and magnesium substitution on oxygen isotope fractionation between calcium carbonate and water. *Geochim. Cosmochim., 33*, 897–996.

Teranes, J.L. and Bernasconi, S.M., 2005. Factors controlling δ^{13}C values of sedimentary carbon in hypertrophic Baldeggersee Switzerland, and implications for interpreting isotope excursions in lake sedimentary records. Limnology and Oceanography 50: 914–922.

Tkachuk, R. D. (1983). The Little Ice Age. *Geoscience Research Institute*, *v. 10, issue 2*, p. 56-65.

Thiel, V., Jenisch, A., Landman, G., Reimer, A., Michaelis, W. (1997), Unusual distributions of long-chain alkenones and tetrahymanol from the highly alkaline Lake Van, Turkey. *Geochimica et Cosmochimica Acta, 61*, 10**,** 2053-2064.

Thomson, J., N. C. Higgs, R. R. S. Wilson, I. W. Croudace, de Lange G. J., and van Santvoort P. J. M. (1995). Redistribution and geochemical behaviour of redox-sensitive elements around S1, the most recent eastern Mediterranean sapropel, *Geochim. Cosmochim.*, *59*, 3487 – 3501.

Thompson, R. and Oldfield, F. (1986). Environmental Magnetism. London: Allen and Unwin.

Thomson, J., Croudace, I.W., Rothwell, R.G. (2006). A geochemical application of the ITRAX scanner to a sediment core containing eastern Mediterranean sapropel units. In: Rothwell, R.G. (Ed.), *New Techniques in Sediment Core Analysis*. Geological Society, London, Special Publications 267.

Thornton, S. F. and McManus, J., (1994). Application of organic carbon and nitrogen stable isotope and C/ N ratios as source indicators of organic matter provenance in estuarine systems: evidence from the Tay Estuary, Scotland. *Estuarine Coastal Shelf Sci.*, *38*, 219–233.

Tkachuk, R. D. (1983). The Little Ice Age. *Geoscience Research Institute, 10*, issue 2, p. 56–65.

Tokieda, T., Narita, H., Harada, K., Tsunogai, S. (1994). Sequential and rapid determination of Po-210, Bi-210 and Pb-210 in natural waters. *Talanta, 41*, 2079–2085.

Todd, P.A., Ong, X., Chou, L.M. (2010). Impacts of pollution on marine life in Southeast Asia. Biodivers. *Conserv*. *19*, 1063–1082.

Tomonaga, Y., Berennwald, M.S.,Meydan, A.F., and Kipfer, R. (2014). Noble geses in the sediments of Lake Van- solute transport and palaeoenvironmental reconstruction. *Quat. Sci Rev.,104*, 117-126.

Trimble, S. W. (1975).Denudation studies: Can we assume stream steady state?, *Science*, *188*, 1207–1208.

Türkeş, M. (1996). Spatial and temporal analysis of annual rainfall variations in Turkey. *International Journal of Climatololgy, 16*, 1057–1076.

Türkeş, M., Erlat E. (2003). Precipitation changes and variability in Turkey linked to the North Atlantic Oscillation during the period 1930-2000. *International Journal Climatology, 23*, 1771–1796.

Türkeş, M., Erlat E. (2009). Winter mean temperature variability in Turkey associated with the North Atlantic oscillation Meteorol. *Atmos. Phys*., *105*, 211–25.

Tütken, T., Vennemann, T.W., Janz, H. and Heizmann, H.E.P. (2006). Palaeoenvironment and palaeoclimate of the Middle Miocene lake in the Steinheim basin, SW Germany, a reconstruction from C, O, and Sr isotopes of fossil remains, Palaeogeography, Palaeoclimatology, Palaeoecology, *241*, 457–91.

Vajda, N., LaRosa, J., Zeisler, R., Danesi, P. and Kis-Benedek, Gy. (1997). A novel technique for the simultaneous determination of ^{210}Pb and ^{210}Po using a crown ether. *J. Environ. Radioactiv., (37/ 3)*, 355–372.

Valeton, I., (1978). A morphological and petrological study the terraces around Lake Van, Turkey. In: Degens, E.T. and Kurtman, F. (eds.): Geology of Lake Van. *MTA Publications, 169*, 64–80.

Van Zeist, W. and Woldring, H. (1978). A Postglacial pollen diagram from Lake Van in East Anatolia. *Review of Palaeobotany and Palynology, 26*, 249–76.

Vigliotti, L., Channell, J. E. T., and Stockhecke, M., (2014). Paleomagnetism of Lake Van sediments: chronology and paleoenvironment since 350 ka, *Quaternary Sci. Rev., 104*, 18–29.

Von Grafenstein, U., Erlernkeuser, H., Trimborn, P. (1999). Oxygen and carbon isotopes in modern fresh-water ostracod valves: assessing vital offsets and autecological effects of interest for palaeoclimate studies. *Palaeogeogr. Palaeoclimatol. Palaeoecol., (148 (1–3)*, 133–152.

Wagner, B. and Melles, M. (2002). Holocene environmental history of western Ymer Ø, East Greenland, inferred from lake sediments. *Quat. Intern*., *89*, 165–176.

Walker, M.J.C. (2005). Quaternary Dating Methods, John Wiley & Sons Ltd, Chichester. ch.2.

Wanner, H., Pfister, C., Brázdil, R., Frich, P., Frydendahl, K., Jónsson, T., Kington, J., Rosenørn, S., Wishman, E. (1995). Wintertime European circulation patterns during the Late Maunder Minimum cooling period (1675–1704). *Theoretical and Applied Climatology, 51*, 167–175.

Wanner, H., Holzhauser, H. P., Pfister, C., and Zumbühl, H. (2000). Interannual to Century Scale Climate Variability in the European Alps, *Erdkunde, 54*, 62–69.

Weaver, P.P.E., Schultheis, P.J. (1990). Current methods for obtaininig, logging and splitting marine sediment cores, *Marine Geophysical Researches, 12*, 85-100.

Wefer, G., and Berger, W.H. (1991). Isotope paleontology: growth and compo sition of extant calcareous species, *Mar. Geol., 100,*:207-248.

Wefer, G., Berger, W. H., Bijma, J. and Fischer, G. (1999). Clues to Ocean History: a Brief Overview of Proxies. In: Fischer, G. Wefer, G (Eds.). *Use of Proxies in Paleoceanography: Examples from the South Atlantic*. Springer-Verlag Berlin Heidelberg, p. 1- 68

Wetzel, J.E. (2001). A Production Methods for Freshwater Prawn in Illinois Ponds. *Rural Enterprise and Alternative Development Initiative Report.,10*, 13 pp.

Wick, L., Lemcke, G., Sturm, M. (2003). Evidence of Lateglacial and Holocene climatic change and human impact in eastern Anatolia: high resolution pollen, charcoal, isotopic and geochemical records from the laminated sediments of Lake Van, Turkey. *The Holocene, 13*, 665–675.

Wigley, T.M.L., Farmer, G. (1982). Climate of the Eastern Mediterranean and the near east. In: Bintliff, J.L., et al. (Eds.), *Paleoclimates, Paleoenvironments and Human Communities in the Eastern Mediterranean Region in Later Prehistory*, pp. 3-37.

Wong, H.K. and Degens, E.T. (1978). The bathymetry of Lake Van, eastern Turkey. (Ed. Degens ve Kurtman)., *MTA Yayınları, 169*, 6-11. Ankara.

Wong, H. K., and Finckh, P. (1978). Shallow structures in Lake Van, pp. 20–27, in the Geology of Lake Van, Ed. Degen and Kurtman, *The Mineral Research and Exploration Institute of Turkey*, Rep. 169.

Wong, K., Wong, P.P.K., Chu, L.M. (2001). Heavy metal concentrations in marine fishes collected from fish culture sites in Hong Kong. Arch. Environ. Con. Tox. 40, 60–69.

Xia, J., Haskell, B.J., Engstrom, D.R., Ito, E. (1997a). Holocene climate reconstructions from tandem trace-element and stable-isotope composition of ostracodes from Coldwater Lake, North Dakota, USA. *J Paleolimnol, 17,*: 85–100.

Xia, J., Ito, E., Engstrom, D.R. (1997b). Geochemistry of ostracode calcite: Part 1. An experimental determination of oxygen isotope fractionation. *Geochim Cosmochim., 61*, 377–382.

Xu, H., Ai, L., Tan, L. et al. (2006). Stable isotopes in bulk carbonates and organic matter in recent sediments of Lake Qinghai and their climatic implications. *Chemical Geology, 235*, 262–275.

Yarincik, K.M., Murray, R.W., Peterson L.C. (2000). Climatically sensitive eolian and hemipelagic deposition in the Cariaco Basin, Venezuela, over the past 578,000 years: results from Al/Ti and K/Al, *Paleoceanography, 15 (2)*, pp. 210–228.

Yıldız, N., Yener, G., (2010). Dating of the Sediment Accumulation Rate, Radioactive and Heavy Metal Pollution in the Van Lake. *Ekoloji, 19(77)*, 80-87.

Zeng, F.R., Mao, Y., Cheng, W.D., Wu, F.B., Zhang, G.P. (2008). Genotypic and environmental variation in chromium, cadmium and lead concentrations in rice. *Environ. Pollut., 153*, 309-314.

Zhang, W., **Yu, L., Hutchinson, S.M., Xu, S., Chen, Z., Gao, X.** (2001). China's Yangtze Estuary: I. Geomorphic influence on heavy metal accumulation in intertidal sediments, *Geomorphology, 41*, 195–205.

Zhang, Y., Chen, Y., Meng, A., Li, Q., Cheng, H. (2008). Experimental and thermodynamic investigation on transfer of cadmium influenced by sulfur and chlorine during municipal solid waste (MSW) incineration. *J. Hazard. Mater., 152*, 309–319.

Zhou, A.F., Chen, F.H., Wang, Z.L., Yang, M.L., Qiang, M.R., Zhang, J.W. (2009). Temporal change of radiocarbon reservoir effect in Sugan Lake, northwest China during the late Holocene., *Radiocarbon, 51*, 529–535.

Ziv, B., Saaroni, H., and Alpert, P. (2004). The factors governing the summer regime of the eastern Mediterranean, *Int. J. Climatol., 24*, 1859–1871.

CURRICULUM VITAE

Name Surname: Funda BARLAS ŞİMŞEK

Place and Date of Birth: Ankara 06.12.1976

Address: Çekmece Nuclear Research and Training Center Yarımurgaz Mah.

Nükleer Araştırma Merkezi Yolu, 34303, Küçükçekmece İSTANBUL

E-Mail: funda.simsek@taek.gov.tr

B.Sc.: Middle East Technical University, Physics

M.Sc.: Muğla University, Physics

Professional Experience and Rewards:

2002-2005, Research Assistant, Muğla University.

2005-…, Researcher, Çekmece Nuclear Research and Training Center.

List of Publications and Patents:

ICRM 2013, Uncertaınty Budget In Trıtıum Measurements For The LSC Method, 17-21 June 2013, Antwerp, Belgium

LSC 2013-Advances in Liquid Scintillation Spectrometry "Geochronology of Lake Sediments from ^{210}Pb with Double Energetic Window Method by LSC" 18-22 March 2013. Barcelona, Spain.

EGU General Assembly 2012 "Late Holocene High Resolution Multi-proxy Climate and Environmental Records from Lake Van, Eastern Turkey" 22-27 April 2012. Vienna, Austria.

V. Eurasian Conference on Nuclear Science and Its Application "Comparison Of Performance Parameters For Different Types Of Liquid Scintillation Cocktails" 14-17 Ekim 2008. Ankara, Türkiye.

IV. Eurasian Conference on Nuclear Science and Its Application, "The Radiological Effects of Yatagan Coal-Fired Power Plant at Different Conditions" 31 Ekim-3 Kasım 2006. Bakü, Azarbeycan.

World Year of Physics 2005- Turkish physical Society 23nd International Physics Congress, "Radiation Dose Calculations At Different Atmospheric Stability Categories for Yatagan Coal-Fired Power Plant." 13-16 Eylül 2005. Muğla -Turkey

III. Eurasian Conference on Nuclear Science and Its Application," Radiological Effects of Yatagan Coal-Fired Power Plant." 5-8 Ekim 2004. Taşkent, Özbekistan.

PUBLICATIONS/PRESENTATIONS ON THE THESIS

Barlas Simsek, F., Çağatay, M.N.**,** 2014. Geochronology of Lake Sediments Using ^{210}Pb with Double Energetic Window Method by LSC: An Application to Lake Van, *Applied Radiation and Isotopes*, **93**, 126–133.

Barlas Simsek, F., Çağatay, M.N.**,** 2013. Geochronology of Lake Sediments from ^{210}Pb with Double Energetic Window Method by LSC, *Advances in Liquid Scintillation Spectrometry* , March 18-22, Barcelona, Spain.

Barlas Simsek, F., Çağatay, M.N., 2012. Late Holocene High Resolution Multi-proxy Climate and Environmental Records from Lake Van, Eastern Turkey, *EGU General Assembly* 2012, April 22-27, Vienna, Austria.